Design, synthesis and anticancer activity of amide derivatives of substituted 3-methyl-benzofuran-2-carboxylic acid

Jayashree V. Patil, Shweta Umar, Rina Soni, Shubhangi S. Soman & Suresh Balakrishnan

View supplementary material ⬚

Published online: 23 Dec 2022.

Submit your article to this journal ⬚

Article views: 192

View related articles ⬚

View Crossmark data ⬚

Taylor & Francis
Taylor & Francis Group

Check for updates

Design, synthesis and anticancer activity of amide derivatives of substituted 3-methyl-benzofuran-2-carboxylic acid
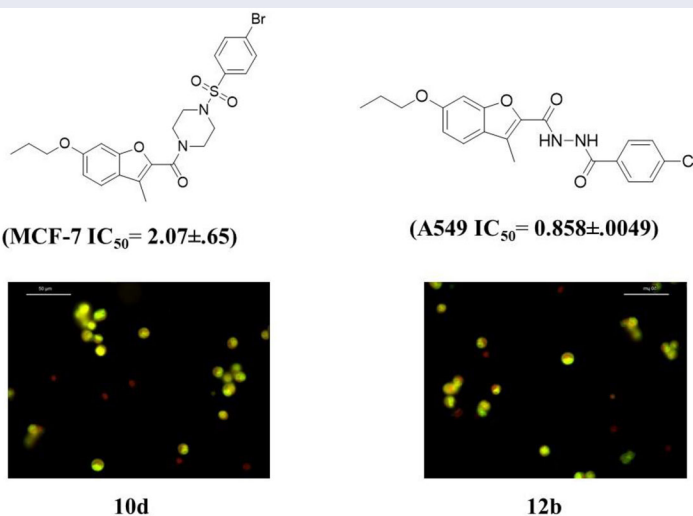
Jayashree V. Patil[a]*, Shweta Umar[b]*, Rina Soni[a], Shubhangi S. Soman[a], and Suresh Balakrishnan[b]

[a]Department of Chemistry, The M.S. University of Baroda, Vadodara, India; [b]Department of Zoology, Faculty of Science, The M.S. University of Baroda, Vadodara, India

ABSTRACT

We have designed and synthesized amide derivatives of substituted 3-methyl-benzofuran-2-carboxylic acid with aryl sulfonamide piperazines, aryl hydrazides and aryl hydrazines. All the synthesized compounds were screened for their anticancer activity against lungs cancer cell line (A549) and breast cancer cell line (MCF7) using MTT assay. Compound **12b** showed excellent activity against lungs cancer cell line (A549) with IC_{50} value of 0.858 μM and compound 10d showed good activity against breast cancer cell line (MCF7) with IC_{50} value of 2.07 μM. Hence, compounds **10d** and **12b** were studied further for their mechanism of cytotoxicity by using EtBr/AO and LDH assay in respective cell lines. The cytostatic potential of compound **10d** and **12b** was uncurtail by Trypan blue exclusion assay and active involvement of ROS was quantified using DCFH-DA dye. The drug-likeliness and toxicity predictions were done using in-silico-based SwissADME and ProTox-II webserver, which confirmed negligible toxicity (Class IV).

GRAPHICAL ABSTRACT

(MCF-7 IC_{50} = 2.07±.65)

(A549 IC_{50} = 0.858±.0049)

10d

12b

CONTACT Shubhangi S. Soman ✉ shubhangiss@rediffmail.com 💬 Department of Chemistry, The M.S. University of Baroda, Vadodara, India.
*Both the authors have contributed equally.

📄 Supplemental data for this article can be accessed online at https://doi.org/10.1080/00397911.2022.2160648

Introduction

Cancer is a large family of diseases resulting from uncontrolled cell growth, which remains one of the most potentially life threatening diseases worldwide.[1] Despite the availability of a multitude of anticancer drugs, none of them can kill cancer cells without hurting healthy normal cells. As a result, medicinal chemists are increasingly focused on the development of new anticancer drugs and more selective cancer therapy procedures.

Benzofuran is one of the important heterocyclic compounds having natural as well as synthetic compounds, which shows variety of biological activities. In nature, several benzofuran ring systems with diverse substituents at the C-2 position can be found. There are number of well-known natural compounds with benzofuran ring having various applications. Natural benzofurans have a wide range of physiological, pharmacological, and poisonous effects. There are well-known natural benzofuran compounds, the most acknowledged benzofurans are *amiodarone, ailanthoidol* and *bufuralol. Ailanthoidol* is a neolignan with a 2-arylbenzofuran skeleton. It has been reported that benzofuran derivatives possess a variety of biological activities such as Antimicrobial,[2] Antifungal,[3] Anti-inflammatory,[4] Antioxidant,[5] Antiviral agent.[6]

During last few decades, benzofuran carboxylic acid derivatives have been reported having potent anticancer activity with low side effects and better solubility for therapeutic applications. Benzofuran derivatives exhibited antitumor activities at different stages of cancer formation through various mechanisms, for example blocking cell cycle, inducing cell apoptosis, modulating estrogen receptor.[7] Literature search reveals that benzofuran carboxamide derivatives showed anticancer activity.[8]

There are few reports of synthetic benzofuran derivatives as an anticancer agent against breast cancer cell line(MCF-7) and lungs cancer cell line(A549). Sandra et al. reported novel heterocyclic derivatives of benzofuran-2-carboxamides containing compound **1** (Figure 1), having good anticancer activity with IC_{50} value 7 μM against MCF-7 cell line and induced apoptosis.[9] Further modifications were made by various researchers to enhance activity of benzofuran. Qi-dong *et al.* reported compounds **2** and **3** (Figure 1) exhibited excellent cytotoxicity against many cancer cell lines, including MCF-7 and A549 with IC_{50} values 2.39 μM and 3.08 μM respectively.[10] The research is ongoing on the development of new active anticancer compounds by changing the position of the substituent attached to the benzofuran. Recently Mohammad et al. reported compound **4** (Figure 1) as potential anticancer agent toward A549 cell lines, the target benzofuran-based derivatives efficiently inhibited the growth of A549 cell lines with IC_{50} value 3.69 μM and also further investigated for their effects on the cell cycle progression and apoptosis in A549 cell line.[11]

The pharmacological properties and applications of benzofuran derivatives can be tuned by varying type and position of substitution on furan ring. Due to potential applications of benzofuran derivatives and as a part of our continuous efforts to design and develop novel derivatives for anticancer activity,[12,13] we report herein synthesis of various amide derivatives of substituted 3-methyl benzofuran carboxylic acid and studied them for their anticancer activity, cytotoxicity and drug likeness (Figure 1).
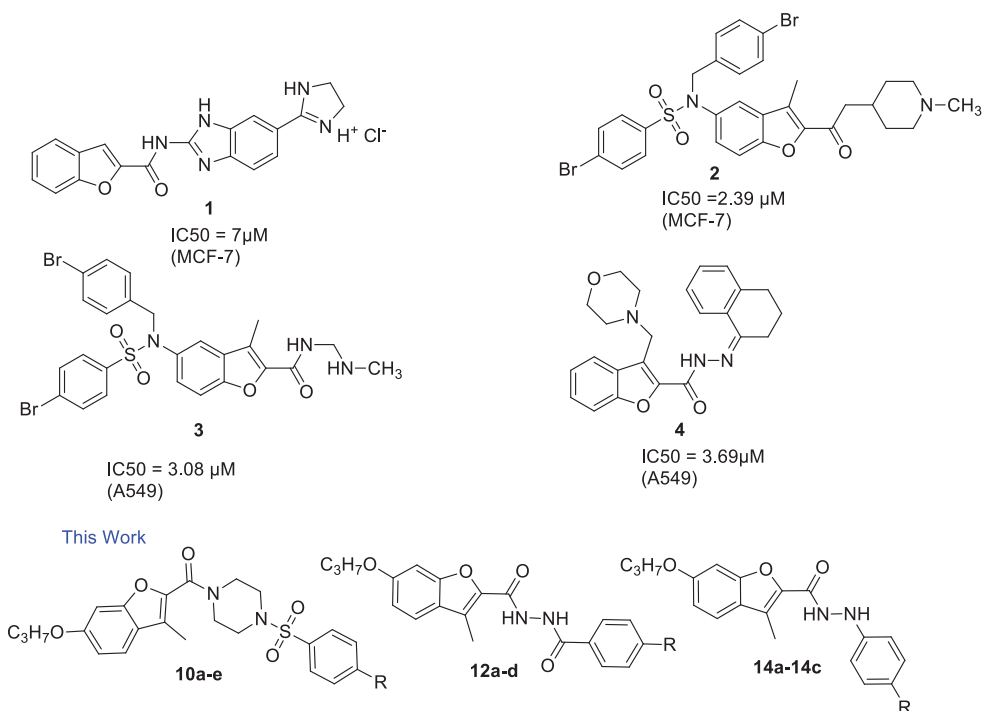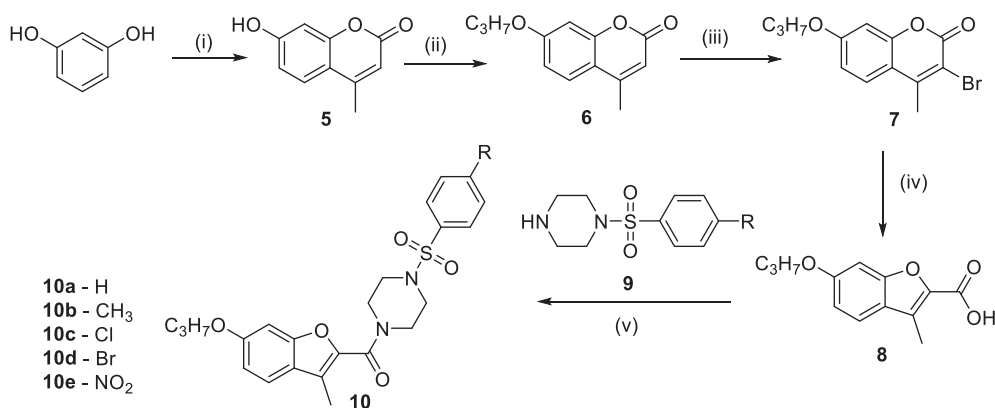
Figure 1. Benzofuran derivatives with anticancer activity.

Results and discussion

Chemistry

In search of some novel compounds with potent anticancer activity, compounds **10a–e** have been synthesized from 3-methyl-6-propoxybenzofuran-2-carboxylic acid **8**. Compound **8** synthesized in four steps starting with 7-Hydroxy-4-methyl coumarin **5** was prepared via Pechmann condensation of resorcinol with ethyl acetoacetate in presence of conc. H_2SO_4. Compound **5** was O-alkylated using propyl bromide in presence of K_2CO_3 and DMF with pinch of KI to give 7-propoxy-4-methylcoumarin **6** (Scheme 1). Bromination of compound **6** was carried out by using bromine in glacial acetic acid at room temperature to give 3-bromo-4-methyl-7-propoxy coumarin **7**. Compound **7** was refluxed with 10% ethanolic KOH for 3 hours to give 6-propoxy-3-methyl benzofuran-2 carboxylic acid **8** via Perkin rearrangement. Compound **8** on reaction with different arylsulfonamide piperazines derivatives using EDC.HCl, HOBT and TEA in dichloromethane gave final compounds **10a–e**. All the synthesized compounds were characterized by different spectral techniques such as ^{1}H-NMR, ^{13}C-NMR, IR, ESI-MS and CHN analysis.

In general, the IR spectra of compounds **10a–e** exhibited two strong bands in the range of 2840–3060 cm^{-1} for –CH stretching of propyl chain, and at 1611–1670 cm^{-1} for amide carbonyl stretching frequency. In ^{1}H-NMR spectrum of compound **10b**, the triplet for –CH$_3$ of propyl chain is observed at δ 1.08, the multiplet for CH$_2$– of propyl chain is observed at δ 1.84. The singlet for three protons of methyl on furan ring is observed at δ 2.41. The triplet for two methylene protons is observed at δ 3.9.
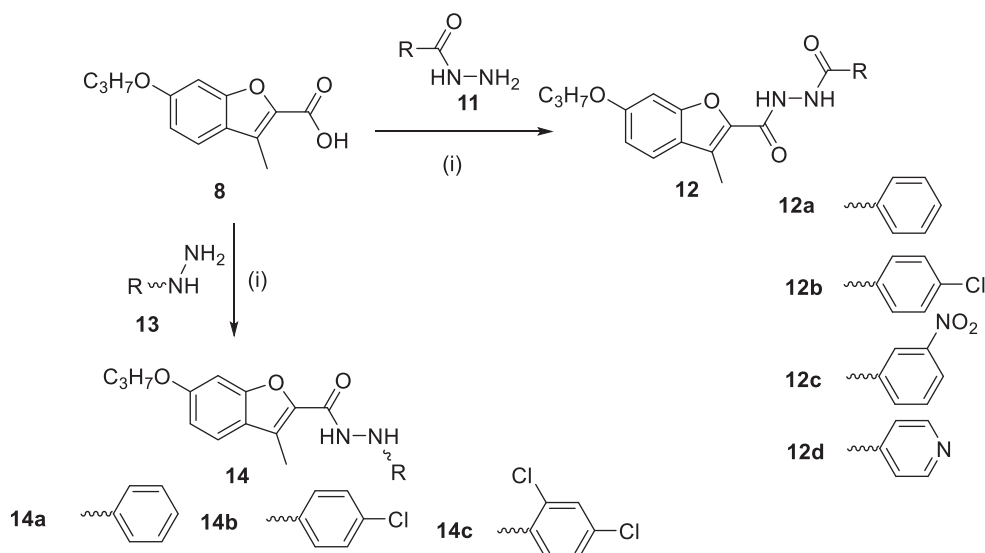
Reaction conditions:(i) Ethyl acetoacetate, conc.H_2SO_4, rt 5-6 hr (ii) C_3H_7Br, K_2CO_3, KI, DMF, rt, 8-10hr; (iii) Br_2 in glacial acetic acid, rt 8-12 hr; (iv) 10% ethanolic KOH, reflux 3 hr (v) compound **9**, EDC.HCl, HOBT, TEA, DCM 6 hr.

Scheme 1. Benzofuran derivatives **10a–e**.

All aromatic protons observed in the range of δ 7.09–7.67. In ^{13}C-NMR of compound **10b** the $-CH_3$ carbons observed at δ 9.25 and 22.51, the methylene carbons observed at δ 10.93 and 70.06 ppm. All the aromatic carbons observed between δ 113.5–161.0 ppm along with amide carbonyl carbon observed at δ 160.89. The ESI-Mass spectrum of compound **10b** showed $[M + H]^+$ peak at 457.10. In general, for ^{1}H-NMR of compounds **10a–e** the triplet, multiplet for $-CH_3-CH_2$ are observed in the range of δ 1.07–1.11 and δ 1.77–1.85 respectively. Singlet for three protons of methyl group attached to aromatic furan ring is observed in the range of δ 2.40–2.41 ppm, methylene protons which are attached to oxygen are observed in the range of δ 3.89–3.99, all aromatic protons observed in the range of δ 6.91–8.44 ppm. In ^{13}C-NMR spectra of compounds **10a–e**, the methyl carbons observed at δ9.25 and 22.51 and methylene carbons are observed at δ10.93, and δ 70.06 ppm, all aromatic carbons are observed in the range of δ 113.00–161.05 ppm along with amide carbonyl carbon is observed at δ 160.89.

Compound **8** (3-methyl-6-propoxy benzofuran 2-carboxylic acid) was reacted with various substituted aryl hydrazides **11** in presence of EDC.HCl, HOBT, TEA in DCM to give corresponding (Scheme 2) different substituted dihydrazides derivatives of furan carboxylic acid **12a–d**. In another variation, benzofuran carboxylic acid 8 was reacted with different substituted aryl hydrazines **13** under similar reaction conditions to give compounds **14a–c** (Scheme 2). The structures of all the compounds were confirmed by its IR, ^{1}H-NMR, ^{13}C-NMR, ESI-Mass spectra.

In IR spectra of **12a–d**, band for –NH stretching was observed from 3200 to 3450 cm^{-1}, while –CH stretching of propyl chain was observed around 2840–3060 cm^{-1}. The amide carbonyl band was observed at 1622–1675 cm^{-1}. In the ^{1}H-NMR spectrum of **12b** the CH_3 protons of propyl chain are observed as triplet at δ 1.03 and CH_2 protons as multiplet at δ 1.84 and $-CH_2$ protons as triplet at δ 4.06. The methyl protons of furan ring are observed at δ 2.50–2.55. All aromatic protons were observed in range of δ 6.94–10.65 ppm along with two –NH protons appeared at δ 10.50 and 10.62 ppm respectively, which was confirmed by D2O exchange study. In ^{13}C-NMR spectrum of compound **12b** showed two methyl carbons at δ 9.24 and 22.46,

Reaction conditions:(i) compound **11/13** , EDC.HCl, HOBT, TEA, DCM 6 hr.

Scheme 2. Benzofuran derivatives **12a–d** and **14a–c**.

CH_2 carbon at δ 10.93 and $-CH_2$ attached to oxygen atom at δ 70.04 ppm. All aromatic carbons were observed in the range of δ 96.04–165.25 along with amide carbonyl carbon observed at δ 165.25 ppm respectively. The ESI-Mass of **12b** showed $[M^+]$ peak at 386.60

In IR spectra of compounds **14a–c**, three bands are observed for $-NH$ stretching frequencies and -CH stretching of propyl chain at 3058, 3010 and 2854 cm^{-1} respectively. The amide carbonyl stretching frequency observed at 1650–1673 cm^{-1}. In ^{1}H-NMR spectrum of **14c** the CH_3-CH_2-protons of propyl chain are observed as triplet and multiplet at δ 1.11, δ 1.90 respectively and The triplet for two methylene protons observed at δ 4.01 which is attached to oxygen, the $-CH_3$ protons of furan methyl are observed as singlet at δ 2.58 all aromatic protons observed in the range of δ 6.58–8.32. In ^{13}C-NMR spectrum of compound **14c** showed two methyl carbons at δ 9.01 and δ 22.50 two $-CH_2$ carbons at δ 10.57, and 70.09 ppm respectively. All aromatic carbons are observed in the range of δ 96.05–160.30 with amide carbonyl carbons are observed at δ 160.3 The ESI-Mass of compound **14c** showed $[M^+]$ peak at 393.00.

Biological evaluation

Anticancer activity by MTT assay

Benzofuran carboxamide derivatives **10a–e**, **12a–d** and **14a–c** were screened for their anticancer activity against A549 (lungs cancer cell line), MCF-7 (breast cancer cell line) using MTT assay (Table 1). In benzofuran carboxamide derivatives with arylsulfonamide piperazines, compound **10a** showed poor activity against both tested cell lines. Addition of methyl group on arylsulphonamide piperazine part, compound **10b** showed good activity with IC_{50} values of 3.08 ± .003 μM and 4.9 ± .0239 μM against

Table 1. Anticancer activity against A549 (lungs cancer cell line), MCF-7 (breast cancer cell line) for compounds **10a–e**, **12a–d** and **14a–c**.

	IC_{50} μM^a	
Compound	A549	MCF7
10a	16.77 ± .034	10.22 ± .045
10b	3.08 ± .003	4.9 ± .0239
10c	8.97 ± .092	2.74 ± .026
10d	1.504 ± .056	**2.07 ± 0.65**
10e	1.04 ± .006	4.391 ± .032
12a	16.41 ± .401	13.45 ± .25
12b	**0.858 ± .0049**	7.756 ± 1.03
12c	9.07 ± 0.21	7.49 ± .042
12d	22.61 ± .96	4.86 ± 0.72
14a	3.66 ± .073	9.34 ± .019
14b	1.822 ± .029	4.19 ± 1.27
14c	1.86 ± .023	23.1 ± 1.02
Fluorouracil	11.13 ± 0.083	45.04 ± 1.02

$^a IC_{50}$ values were determined based on MTT assay using GraphPad Prism software.The bold values indicate lowest IC50 values against the particular cell lines.

A549 and MCF7 cell lines respectively. On replacing methyl group with chloro in compound **10c**, resulted in drop of activity against A549 cell lines, however against MCF7 activity was found to be better. Bromo analogue compound **10d** showed very good activity against both the cell lines with IC_{50} values 1.504 ± .056 μM and 2.07 ± 0.65 μM against A549 and MCF7 cell lines respectively. On replacing halogen with electron withdrawing group nitro in compound **10e**, resulted in very good activity against A549 cell line with IC_{50} values 1.04 ± .006 μM as compared to standard drug, however anticancer activity was slightly dropped against MCF7 cell line.

In another variation substituted benzofuran carboxylic acid derivative was reacted with substituted aryl hydrazides to give compounds **12a–d**. In these particular derivatives, compound **12a** without any substitution on aryl ring showed moderate activity against both the tested cell lines as compared to that of standard drug. Compound **12b** with chloro substituent on aryl hydrazide part showed very good activity with IC_{50} values 0.858 ± .0049 μM, however activity against MCF7 cell line remained moderate. On replacing chloro with nitro group in compound **12c** resulted in drop of activity against A549 cell line, while activity against MCF7 cell line almost remained same. Compound **12d** with pyridine ring exhibited poor activity against A549 cell line but there was improvement in activity against MCF7 cell line.

Compounds **14b** with chloro and **14c** with dichloro substituents, showed very good activity against A549 cell line with IC_{50} values 1.822 ± .029 and 1.86 ± .023 μM respectively as compared to compound **14a** without any substituent on aryl hydrazine. Against MCF7 cell line, only compound **14b** showed good activity with IC_{50} value 4.19 ± 1.27 μM compared to standard drug.

Out of all the screened compounds, compound **12b** with IC_{50} values 0.858 ± .0049 μM against A549 cell line and compound **10d** with IC_{50} values 2.07 ± .065 μM against MCF7 cell line were selected for further study for LDH assay, Trypan blue assay and ROS activity.
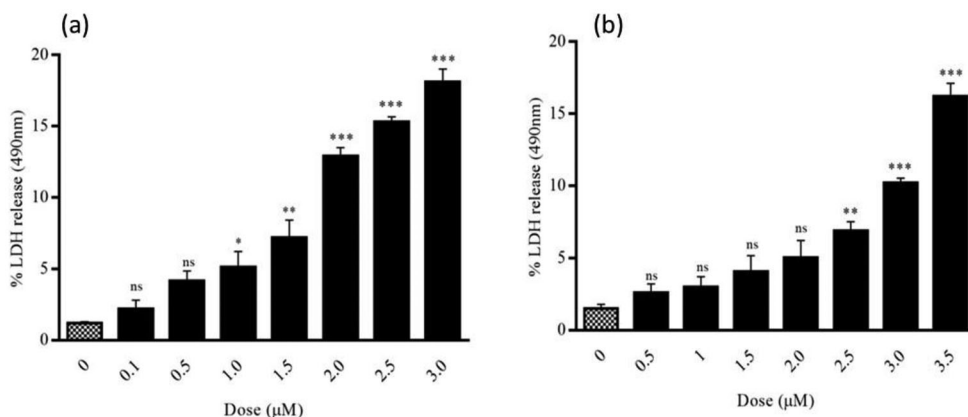
Figure 2. In LDH assayIn LDH assay (a)–(b): Representation of cytosolic enzyme LDH (a) activity of LDH in A549 cell line (b) activity of LDH in MCF-7 cell line. Cells were treated with 0.1, 0.5, 1.0, 1.5, 2.0, 2.5, 3.0 μM concentrations of compound **12b** and 0.1, 0.5, 1.0, 1.5, 2.0, 2.5, 3.0, 3.5 μM concentrations of compound **10d**. Graph was plotted against LDH release versus dose. (***$p \leq$ .001, **$p <$ .01 significance one-way ANOVA (Tukey–Kramer). ANOVA: analysis of variance; LDH: lactic dehydrogenase.

LDH assay

There are many mechanisms by which an anticancer compound exerts its effect on cancer cell *in vitro*. Apoptosis and necrosis are the most acknowledged mechanisms. To understand the mode of cytotoxicity of compounds **12b** and **10d** in A549 and MCF-7 cancer cell lines LDH Assay was performed (Figure 2).

At lower concentration of both compounds (IC$_{50}$), the LDH release was very low which revealed that at this concentration the prevalent mechanism of cytotoxicity was apoptosis. At increased concentration of compounds, the LDH release increases significantly, at higher concentration treated cells changed its fate toward the necrosis from apoptosis. However, the preferred mechanism of cytotoxicity for compounds **12b** and **10d** is apoptosis at IC$_{50}$ concentration.

Ethidium bromide/acridine orange staining assay

For A549 cell line and MCF7 cell line, further experimental confirmation is required to explain the effect of compound **12b** and compound **10d** on cancer cell lines respectively. In order to reaffirm the findings of LDH assay, the EtBr/AO staining assay was performed with compound **12b** and compound **10d**.

Acridine orange is a vital dye that stains both live and dead cells however, ethidium bromide stains only the cells that have lost their membrane integrity. EtBr/AO dye stains, necrotic cells red, live cells green, early apoptotic cell's nuclei green but with visible condensation whereas, late apoptotic cell's nuclei orange with condensation and fragmentation. Cells were treated with IC$_{50}$ concentration of compound **10d**, compound **12b** and it was found that most of the cells of A549 cell line (Figure 3a–c) were under late apoptosis, there were no cells under necrosis whereas, in MCF- 7 cell line (Figure 3d–f) most of the cells were under early apoptosis with few under necrosis. Number of
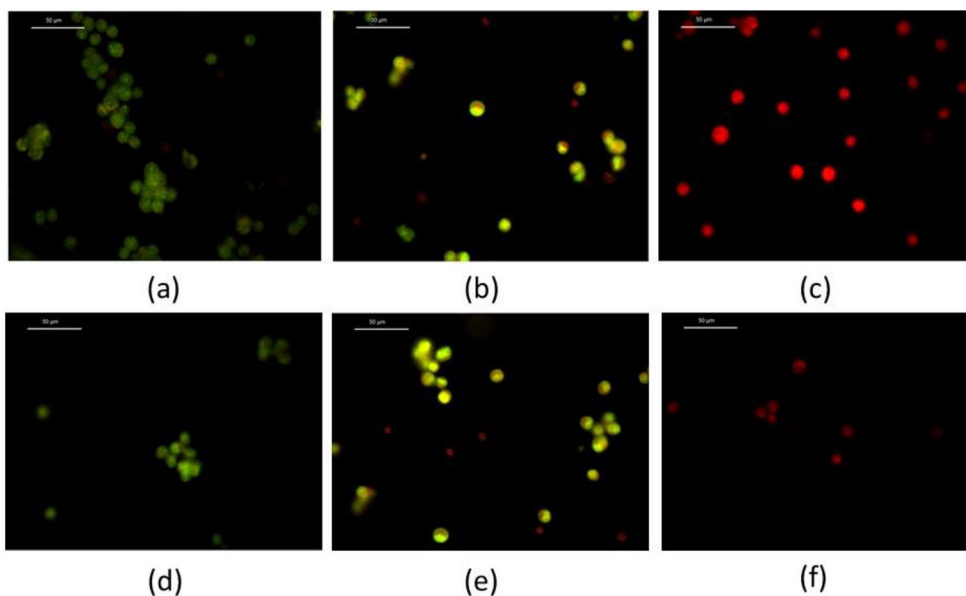
Figure 3. EtBr/AO assay: EtBr/AO assay was performed with A549 cell line (a–c) for compound **12b** and MCF-7 (d–f) for compound **10d**. (a–c) For compound **12b**, (a–c) images represent control, IC_{50} conc. of compound **12b** treated and positive control in A549 cell line. Images (d–f) represent control, IC_{50} conc. of compound **10d** treated and positive control in MCF-7 cell line.

the cells under apoptosis and necrosis was negligible in control cell lines. Which confirmed the LDH assay finding that compound **10d** and compound **12b** exhibits cytotoxic activity in both cell lines via apoptosis.

Trypan blue

To confirm, that loss of percentage viability was either due to cell death or due to cell proliferation inhibition effect of compound **10d** and **12b**, Trypan blue assay was performed in both A549 and MCF-7 cell lines. The percentage cell death at IC_{50} concentration for compound **10d** is 45% ± 2.68% in MCF-7 cell line and for compound **12b** it was approx. 36% ± 3% in A549 cell line and (Figure 4), from this it can be construed that compound **10d** cytotoxic toward the MCF-7 whereas it might be cytotoxic or cytostatic toward A549 cell line, while compound **12b** is cytotoxic toward A549 cell line and it might be cytostatic or cytotoxic toward MCF-7 cell line.

DCFH-DA assay

Most of the chemotherapeutics, elevates ROS beyond the threshold limit to exert cytotoxicity to cancer cell.[14] The elevated ROS play a vital role in induction of apoptosis via caspase 8 dependent and Fas-associated cell death[15] as well via p53 dependent pathway. Ramsey and Sharpless[16] reported that P^{53} is a redox-sensitive transcription factor that senses the increased ROS and initiates the apoptotic death in cancer cells Hence, herein, we investigated the ROS concentration in compound **12b** and 10d in
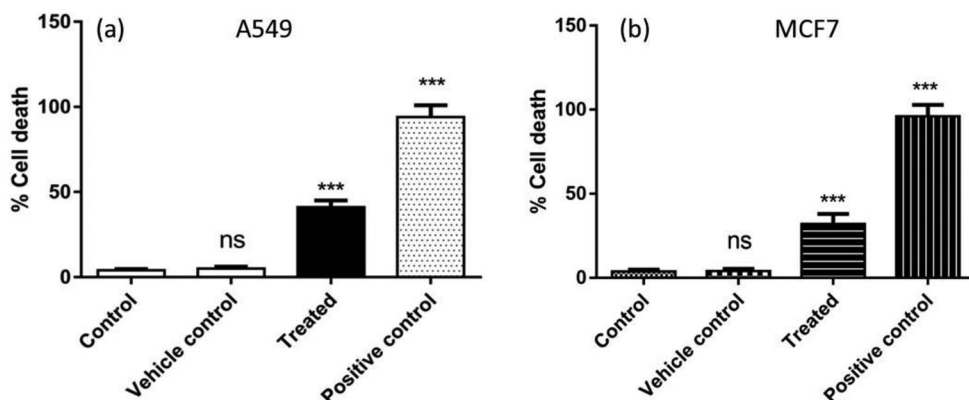
Figure 4. Trypan blue assay, the pecentage of cell death of A549 and MCF-7 cell line treated with DMF, with IC50 concentration of compounds **12b** and **10d** with positive control was plotted. Data were represented as mean ± SD from three independent experiments.
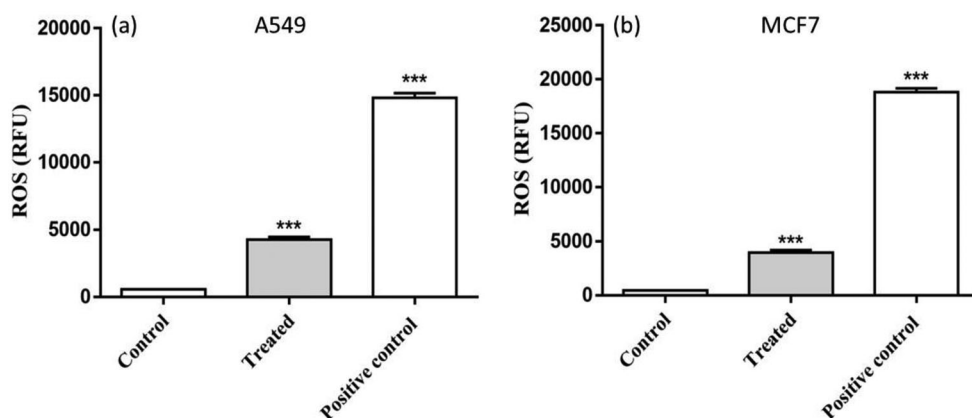

Figure 5. Estimation of intracellular reactive oxygen species level by using DCFH-DA for compound **12b** in A549 (a) and **10d** in MCF-7 (b) respectively. (***$p \leq .001$).

A549 and MCF-7 cell line respectively. The result vividly confirmed the increased ROS level in both cell lines at IC_{50} concentration (Figure 5).

DFT calculation

DFT calculations were carried out to explore conformational behavior of the two most active compounds **10d** and **12b**. The ground state geometries of these compounds were optimized by applying the B3LYP method 6-31 G(d) basis set in gas phase. Initially **10d** and **12b** compounds were optimized by applying the B3LYP method and 6-31 F(d) basis set in gas phase. Ground state geometries of compounds **10d** and **12b** were optimized. The predicted plot of frontier molecular orbitals (FMOs) HOMO (highest occupied) and LUMO (lowest unoccupied) molecular orbitals are shown in Figure 6.

For benzofuran carboxamide containing piperazine moiety **10d,** the LUMO shows electron density on phenyl ring attached to piperazine sulfonamide, while in HOMO of
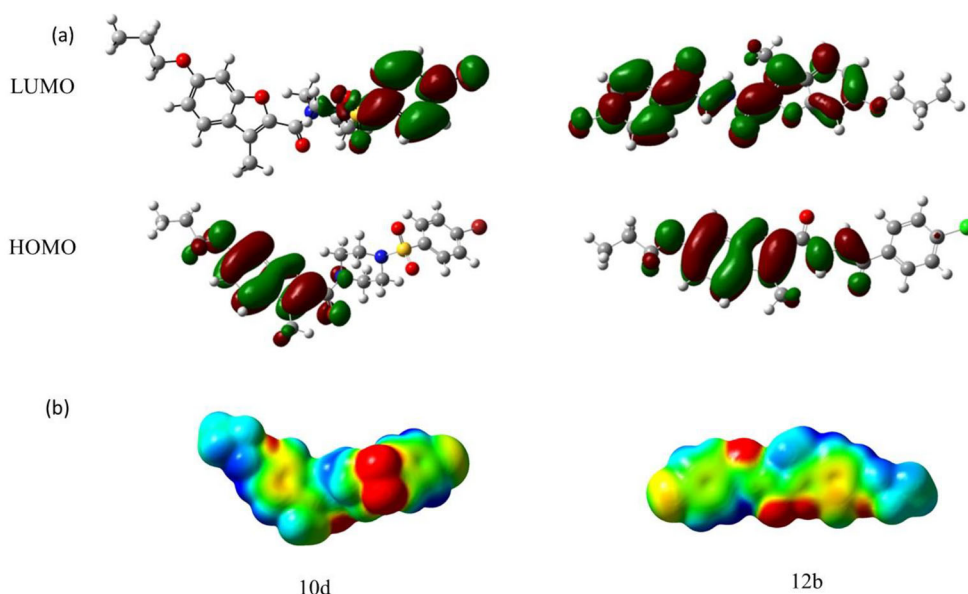
Figure 6. DFT calculation data for compound **10d** and **12b** (a) frontiers molecular orbitals (HOMO and LUMO) diagram obtained from calculation at B3LYP/6-31G (d, p) level, (b) shows the molecular electrostatic potential maps (MEP) of compounds **10d** and **12b**.

10d it is observed that the electron density is shifted on benzofuran ring from piperazine sulfonamide ring contributing negligible by propyl chain. In **12b** LUMO shows the electron density is distributed on the whole molecule that is benzofuran as well as phenyl hydrazide ring (Figure 6) contributing negligible to propyl chain, while the HOMO showed shifting electron density from phenyl ring of hydrazide to the benzofuran carboxamide. For compound **12b** the highest occupied molecular orbitals (HOMO) are localized on benzofuran carboxamide core. Figure 6b shows molecular electrostatic potential maps (MEP) of compounds **10d** and **12b**, thus support the highest activity of these two compounds.

In-silico based ADME and toxicity study

The drug-likeliness of compounds was predicted using SwissADME. (Table 2) To be a drug-like candidate, the compounds should follow Lipinski's Rule of Five (clogP $\leq$ 5, molecular weight $\leq$ 500, the number of hydrogen bond acceptors $\leq$ 10 and donor $\leq$ 5) which predict lipophilicity, critical molecular weight and chemical structure, and probability of crossing the blood-brain barrier (BBB). The compound violating more than one of these rules will be poor in terms of bioavailability and not be orally active, hence, cannot be used as drug without modification.[17] The compound **12b** was satisfying all four criteria of good drug candidate *viz.,* Molecular weight 386.83 g/mol; octanol/water partition coefficient *viz.,* 4.03 (logP$_{o/w}$ less than 5), the number of hydrogen donor *viz.,* 2 and the number of hydrogen acceptor *viz.,* 4. In addition, GI absorption, Blood brain barrier permeability is also predicted which are again under acceptable limit (GI absorption is high, BBB permeability not present and moderately soluble). Similarly, the **10d**

Table 2. ADMET properties of compounds **12b** and **10d**.

ADMET properties	12b	10d
M.W (g/mol)	386.83	521.42
No of H-donor group	2	0
No of H-acceptor	4	6
logP$_{o/w}$	4.03	3.98
GI absorption	High	High
BBB permeability	No	No
Log S	Moderately soluble	Moderately soluble
LD50	1000 mg/kg	1000 mg/kg
Hepatotoxicity (dilli)	Moderate active	Inactive
Carcinogenicity	Inactive	Inactive
Immunotoxicity	Inactive	Inactive
Mutagenicity	Inactive	Inactive

was analyzed and showed M.W. of 521.42 g/mol, slightly higher than the accepted limit with no H donor group, 6-H acceptor group and with logP$_{o/w}$ 3.98. The allowed violation of rule of five is one, hence the compound was still a good drug candidate for further study. The compound also showed a high GI absorption as well as negligible BBB permeability however moderate solubility require further consideration. The toxicity of compounds was predicted using ProTox-II webserver developed by Drwal et al.,[18] the parameters such as rat oral acute toxicity with special reference to median lethal dose (LD$_{50}$) as mg/kg, organ toxicity especially hepatotoxicity, immunotoxicity, genetic toxicity endpoints especially cytotoxicity, mutagenicity and carcinogenicity, were predicted for both the compounds. The LD$_{50}$ for compound **10d** and **12b** was 1000 mg/kg hence, classified to class IV (300 $\leq$ LD50 $\leq$ 2000). According to GHS class I is the most toxic and class VI is nontoxic.[18] However, the IC$_{50}$ concentration of compounds was found to be very less than LD$_{50}$ hence, it will not pose any toxicity if given orally. The derivative **12b** was showing moderate hepatotoxicity, however, carcinogenicity, immunotoxicity and mutagenicity was not observed. In the compound **10d** there was no Hepatotoxicity, no carcinogenicity, no immunotoxicity and no mutagenicity observed. Hence, both the compounds can be taken further as anticancer drug candidates for detailed analysis.

Conclusion

In conclusion, a series of substituted amide derivatives of substituted benzofuran carboxylic acid were synthesized and evaluated for their anticancer activity against A549 and MCF-7 cell lines. Based on MTT assay, compound **10d** has shown very good selectivity for MCF-7 breast cancer cell line and compound **12b** shows excellent activity against A549 lungs cancer cell line. The cytotoxic studies of compounds **12b** and **10d** have shown the apoptosis in both A549 and MCF- 7 cell lines using LDH assay, Trypan blue assay and the EtBr/AO assay. The increased level of ROS concentration in compounds **12b** and **10d** in A549 and MCF-7 cell line at IC$_{50}$ value confirmed apoptosis. The *In-silico* based ADME and toxicity study of **12b** and **10d** compounds indicated that both compounds showed drug-likeliness and can be studied further in detail as anticancer drug.

Experimental

General chemistry

Reagent grade chemicals and solvents were purchased from commercial suppliers and used after purification. TLC has been performed on silica gel F254 plates (Merck). For column chromatographic purification Acme's silica gel (60–120 mesh) was used. Melting points were measured in open capillary tubes, using a Rolex melting point apparatus. IR spectra were recorded as KBr pellets on Perkin Elmer RX 1 spectrometer. ^1H NMR and ^{13}C NMR spectral data were recorded on Advance Bruker 400 spectrometer (400 MHz) with $CDCl_3$ or DMSO-d_6 as solvent and TMS as internal standard. J values are in Hz. Mass spectra were determined by ESI-MS, using a Shimadzu LCMS 2020 apparatus. Elemental analyses were recorded on Thermosinnigan Flash 11–12 series EA. 4-methyl-7-propoxy-2H-chromen-2-one, 3-bromo-4-methyl-7-propoxy-2H-chromen-2-one, 3-methyl-6-propoxybenzofuran-2-carboxylic acid and substituted phenyl piperazine and substituted benzofuran carboxamide derivatives were prepared according to literature method.[2,19–21]

Preparation of 3-methyl-6-propoxybenzofuran-2-carboxylic acid (8)

A solution of compound 7 (23.64 mmol, 10.0 eq) in 10% ethanolic KOH (100 mL) was reflux for 3 h in an oil bath. The completion reaction was checked by TLC. After completion of the reaction excess ethanol was distilled under reduced pressure and the reaction mixture was poured into crushed ice. The solution was acidified to pH 2 to give solid. The solid separated out was filtered and washed with cold water. The solid was dissolved in saturated solution of $NaHCO_3$ and filtered to remove insoluble impurity of starting material. The filtrate was acidified using conc. HCl to pH 2 to give solid. The solid separated out was filtered, washed with cold water, dried and recrystallized from ethanol to give compound 8 as light brown solid.

General procedure for preparation of compounds 10a-e/12a-d/14a-c

Compound 8 (0.90 mmol, 1.0 eq), EDC.HCl (1.35 mmol, 1.5 eq) and HOBT (0.9 mmol, 1 eq) in DCM (15 mL) were stirred at room temperature for 10 min then added Substituted phenyl piperazine sulfonamide 9/substituted hyrdazides 11/aryl hydrazines 13 in the mixture of compound 8 and TEA (1.8 mmol, 2.0 eq) added to the same reaction mixture at 0–5 °C. The resultant mixture was brought to room temperature and stirred for 6 h. After the reaction completion, consumption of both the starting materials was confirmed by TLC. Reaction mixture was washed with water (3×40 mL), $NaHCO_3$ solution (2×10 mL), brine solution. The organic layer was separated, dried over anhy. Na_2SO_4, filtered and evaporated on rotavapor to give crude compound. The crude solid was purified by column chromatography over silica gel using DCM:MeOH (9:1–7:3). The pure compounds isolated from column purification were triturated in pet. ether, filtered and dried to give solid.

Characterization data for compounds 10a, 12a and 14a

(3-Methyl-6-propoxybenzofuran-2-yl) (4-(phenylsulfonyl) piperazin-1-yl) methanone 10a

White Solid; Yield: 88%; M.P: 124–126 °C; IR (KBr) 2970, 2928, 2865, 1888, 1632, 1608, 1494, 1450, 1431, 1387, 1347, 1327, 1297, 1276, 1236, 1214, 1166, 1113, 1097, 1067, 1048, 1001, 982, 961, 934, 890, 854, 821, 759, 744 cm^{-1}; ^{1}H-NMR (400 MHz, CDCl$_3$): δ 1.07 (t, $J = 7.2$ Hz, 3H), 1.81–1.90 (m, 2H), 2.41 (s, 3H), 3.13 (br s, 4H), 3.89 (br s, 4H), 3.97 (t, $J = 6.4$ Hz, 2H), 6.91–6.95 (m, 2H), 7.43 (d, $J = 9.2$ Hz, 1H), 7.56–7.60 (m, 2H), 7.64–7.68 (m, 1H), 7.77–7.79 (m, 2H); ^{13}C-NMR (100 MHz, CDCl$_3$): δ ppm 9.26, 10.55, 22.50, 45.44, 46.27, 70.06, 96.06, 113.33, 120.88, 122.13, 125.32, 129.31, 133.25, 135.35, 154.56, 159.56, 160.95; Anal. calc. for C$_{23}$H$_{26}$N$_2$O$_5$S C,62.42; H,5.92; N,6.33; S,7.25; found: C,62.35; H,5.77; N,6.23; S,7.15; ESI-MS: 442.95[M$^+$].

N′-Benzoyl-3-methyl-6-propoxybenzofuran-2-carbohydrazide 12a

White Solid; Yield: 86%; M.P:160–162 °C; IR (KBr) 3213, 2966, 2309, 1632, 1604, 1514, 1491, 1381, 1268, 1247, 1166, 1146, 1125, 1096, 1075, 981, 818, 771 cm^{-1}; ^{1}H-NMR (400 MHz, CDCl$_3$): δ 1.02 (t, $J = 7.4$ Hz,3H), 1.76–1.82 (m, 2H), 2.53 (s, 3H), 4.04 (t, $J = 6.8$ Hz, 2H), 7.00(dd, $J = 8.4$ Hz, 2.0 Hz, 2H), 7.15 (d, $J = 2.0$ Hz, 1H), 7.53–7.57 (m,2H), 7.61–7.67 (m, 2H), 7.93–7.95 (m, 2H), 10.47 (br s, 2H); ^{13}C-NMR (100 MHz, CDCl$_3$): δ ppm 9.24, 10.91, 22.45, 70.03, 96.62, 113.67, 122.06, 122.49, 123.30, 127.96, 129.00, 132.38, 132.97, 141.63, 154.70, 159.48, 159.90, 166.28; Anal. calc. for C$_{20}$H$_{20}$N$_2$O$_4$; C,68.17; H,5.72; N,7.95; found: C,68.09; H,5.57; N,7.89; ESI-MS: 353.00 [M + H]$^+$.

3-Methyl-N′-phenyl-6-propoxybenzofuran-2-carbohydrazide 14a

White solid; Yield: 90%; M.P: 120–122 °C; IR (KBr) 3222, 2967, 2932, 2875, 2854, 1655, 1603, 1494, 1469, 1432, 1391, 1379, 1356, 1345, 1317, 1282, 1271, 1235, 1161, 1133, 1121, 1083, 1070, 1059, 980, 945, 908, 884, 825, 816, 751, 692, 636 cm^{-1}; ^{1}H-NMR (400 MHz, CDCl$_3$): δ 1.11 (t, $J = 7.4$ Hz, 3H), 1.85–1.94 (m, 2H), 2.60 (s, 3H), 4.01 (t, $J = 6.4$ Hz, 2H), 6.29 (d, $J = 4.0$ Hz, 1H), 6.93–7.00 (m, 1H), 7.26–7.30 (m, 2H), 7.51 (d, $J = 8.8$ Hz, 1H), 8.27 (s, 1H); ^{13}C-NMR (100 MHz, CDCl$_3$): δ ppm 9.01, 10.58, 22.52, 70.10, 96.10, 113.47, 113.74, 121.33, 121.42, 122.60, 124.84, 129.28, 140.62, 148.17, 154.84, 160.13, 160.44; Anal. calc. for C$_{19}$H$_{20}$N$_2$O$_3$; C,70.35; H,6.21; N,8.64; found: C,70.24; H,6.13; N,8.58; ESI-MS: 324.90 [M$^+$].

Biological activity screening

MTT assay

The half minimal inhibitory concentration was evaluated using MTT [3-(4,5-dimethylthiazol-2-yl)-2,5-diphenyltetrazolium bromide] assay as per standard prot^{oc}ol, used previously in Durgapal et al.[22] Cells were plated in a 96-well plate (1×10^4 cells/well) and incubated overnight in DMEM media supplemented with 10% FBS. Each compound was added in 0.5, 1, 10, 25, 50, 75, 100 μM conc. and incubated further for 48 h. 20 μl

of MTT solution (5 mg/mL in PBS) was added and plate was further incubated for 4 hours. Supernatant solution was removed and the blue formazan was dissolved in 100 μl of acidified isopropanol. The absorbance was measured using microplate reader at 570 nm (Metertech Σ960) Cell viability (%) = (average absorbance of treated groups/ average absorbance of control group) × 100%. IC$_{50}$ values were calculated using Graph Pad Prism.

Trypan blue

Cells per well (5×10^5) were seeded in 12 well plate and kept overnight for attachment. Next day, the respective cells were treated with IC$_{50}$ conc. of compounds (**12b** and **10d**), DMF and TritonX-100 and were incubated for 48 h. DMF treated cells were taken as vehicle control and TritonX-100 as a positive control. Following incubation, the supernatant was removed and adherent cells were collected. The cells were diluted with 0.4% trypan blue (1:1 ratio) and immediately counted on hemocytometer. Each experiment was performed in triplicates. Result expressed as percentage cell death.[23]

LDH assay

Lactate dehydrogenase enzyme remains in cytoplasm, however during necrosis due to plasma membrane damage it leaches out. Cells were plated on 96 well plate (1×104 cells/well) for 24 h in DMEM media without phenol red, then compounds **12b** and **10d** were added in the 0.5, 1, 10, 25, 50, 75, 100 μM concentration range. Subsequently, they were incubated for 48 h. Assay was performed according to the manufacture's instruction (Pierce LDH Cytotoxicity Assay, Thermo Scientific,USA). Absorbance was measured at 490 nm in a microplate reader and percentage cytotoxicity was calculated.

Ethidium bromide/acridine orange staining assay

Morphological changes due to apoptosis and necrosis were visualized using EtBr/AO staining technique. Respective cells were treated with IC$_{50}$ concentration of compound **12b** and **10d** for 48 h. Triton-X 100 was used as positive control. Post-treatment, Cells were stained with EtBr and AO solution (100 μg/mL in 1:1 ratio). Cells to stain ratio was maintained as 1:25 μl. 10 μl of cell suspension was placed on microscopic slide and images were taken using Leica DM 2500 fluorescence microscope fitted with Leica EZ camera.

DCFH-DA assay

Dichlorodihydrofluorescein diacetate (DCFH-DA) staining was done to quantitate the intracellular ROS level in post treatment of derivative in both the cell line (A549 and MCF-7). For ROS estimation using Fluorimetry, 5×10^5 cells/well were seeded in 6 well plates overnight. The next day, the respective cells were treated with the IC$_{50}$ conc. of compound **12b** and **10d** and incubated for 48 h. Following incubation, the experiment was performed as per the protocol described earlier in Umar *et al.*[24]

Computational method

On a computer with a Pentium IV CPU and Gaussian 09 software, all computations for the analyzed derivatives were completed. DFT/B3LYP methods were used in the computations with the 6-31 G (d, p) basis set. Without imposing any molecular symmetry restrictions, the geometries were optimized by minimizing the energies with respect to all geometrical parameters. The optimized geometries' structures have been depicted using GaussView. The same level of theory was also applied to frequency computations. In the geometry optimization processes, all structures were shown to be stationary points by the frequency calculations, and none of the vibrational analyses.

In-silico-based ADME and toxicity study

The drug-likeliness prediction of compounds was done using Lipinski rule of five or criteria of four [25] retrieved from webserver tool SwissADME [26]. The structures of compounds **12b** and **10d** were converted to canonical SMILES format and uploaded to SwissADME prediction (http://www.swissadme.ch). The Toxicity prediction of compound was done using ProTox-II[18] using chemical structure of the compound. The oral toxicity, the organ toxicity and toxicity end-point (hepatotoxicity, cytotoxicity, carcinogenicity, mutagenicity and immunotoxicity) were predicted using ProTox-II. The compounds are given different toxicity classes, depending on their LD_{50} (mg/kg), which are defined according to the globally harmonized system of classification in labeling of chemicals (GHS).

Full experimental detail, ^{1}H-NMR and ^{13}C-NMR spectra, this material can be found via the "Supplementary Content" section of this article's webpage.
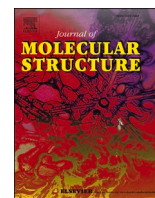
ORCID

Suresh Balakrishnan 🔟 http://orcid.org/0000-0002-6559-022X

References

[1] Khan, Z.; Bisen, P. S. Oncoapoptotic Signaling and Deregulated Target Genes in Cancers: Special Reference to Oral Cancer. *Biochim. Biophys. Acta* **2013**, *1836*, 123–145. DOI: 10. 1016/j.bbcan.2013.04.002.

[2] Soni, J. N.; Soman, S. S. Synthesis and Antimicrobial Evaluation of Amide Derivatives of Benzodifuran-2-Carboxylic Acid. *Eur. J. Med. Chem.* **2014**, *75*, 77–81. DOI: 10.1016/j.ejmech.2014.01.026.

[3] Kawasaki, K. I.; Masubuchi, M.; Morikami, K.; Sogabe, S.; Aoyama, T.; Ebiike, H.; Niizuma, S.; Hayase, M.; Fujii, T.; Sakata, K.; et al. Design and Synthesis of Novel Benzofurans as a New Class of Antifungal Agents Targeting Fungal N-Myristoyltransferase. Part 3. *Bioorganic Med. Chem. Lett.* **2003**, *13*, 87–91. DOI: 10.1016/S0960-894X(02)00844-2.

[4] Yadav, P.; Singh, P.; Tewari, A. K. Design, Synthesis, Docking and Anti-Inflammatory Evaluation of Novel Series of Benzofuran Based Prodrugs. *Bioorg. Med. Chem. Lett.* **2014**, *24*, 2251–2255. DOI: 10.1016/j.bmcl.2014.03.087.

[5] Chand, K.; Hiremathad, A.; Singh, M.; Santos, M. A.; Keri.; R. S.; Rajeshwari. A Review on Antioxidant Potential of Bioactive Heterocycle Benzofuran: Natural and Synthetic Derivatives. *Pharmacol. Rep.* **2017**, *69*, 281–295. DOI: 10.1016/j.pharep.2016.11.007.

[6] Khanam, H.; Shamsuzzaman. Bioactive Benzofuran Derivatives: A Review. *Eur. J. Med. Chem.* **2015**, *97*, 483–504. DOI: 10.1016/j.ejmech.2014.11.039.

[7] Li, X. Y.; He, B. F.; Luo, H. J.; Huang, N. Y.; Deng, W. Q. 3-Acyl-5-Hydroxybenzofuran Derivatives as Potential Anti-Estrogen Breast Cancer Agents: A Combined Experimental and Theoretical Investigation. *Bioorg. Med. Chem. Lett.* **2013**, *23*, 4617–4621. DOI: 10.1016/j.bmcl.2013.06.022.

[8] Choi, M.; Jo, H.; Park, H.-J.; Sateesh Kumar, A.; Lee, J.; Yun, J.; Kim, Y.; Han, S.-B.; Jung, J.-K.; Cho, J.; et al. Design, Synthesis, and Biological Evaluation of Benzofuran- and 2,3-Dihydrobenzofuran-2-Carboxylic Acid N-(Substituted)Phenylamide Derivatives as Anticancer Agents and Inhibitors of NF-KB. *Bioorg. Med. Chem. Lett.* **2015**, *25*, 2545–2549. DOI: 10.1016/j.bmcl.2015.04.050.

[9] Hranjec, M.; Sović, I.; Ratkaj, I.; Pavlović, G.; Ilić, N.; Valjalo, L.; Pavelić, K.; Kraljević Pavelić, S.; Karminski-Zamola, G. Antiproliferative Potency of Novel Benzofuran-2-Carboxamides on Tumour Cell Lines: Cell Death Mechanisms and Determination of Crystal Structure. *Eur. J. Med. Chem.* **2013**, *59*, 111–119. DOI: 10.1016/j.ejmech.2012.11.009.

[10] Xu, X. l.; Yang, Y. r.; Mo, X. f.; Wei, J. l.; Zhang, X. j.; You, Q. d Design, Synthesis, and Evaluation of Benzofuran Derivatives as Novel Anti-Pancreatic Carcinoma Agents via Interfering the Hypoxia Environment by Targeting HIF-1α Pathway. *Eur. J. Med. Chem.* **2017**, *137*, 45–62. DOI: 10.1016/j.ejmech.2017.05.042.

[11] Al-Sanea, M. M.; Al-Ansary, G. H.; Elsayed, Z. M.; Maklad, R. M.; Elkaeed, E. B.; Abdelgawad, M. A.; Bukhari, S. N. A.; Abdel-Aziz, M. M.; Suliman, H.; Eldehna, W. M. Development of 3-Methyl/3-(Morpholinomethyl)Benzofuran Derivatives as Novel Antitumor Agents towards Non-Small Cell Lung Cancer Cells. *J. Enzyme Inhib. Med. Chem.* **2021**, *36*, 987–999. DOI: 10.1080/14756366.2021.1915302.

[12] Karandikar, S.; Soni, R.; Soman, S. S.; Umar, S.; Suresh, B. 1,2-Benzisoxazole-3-Acetamide Derivatives as Dual Agents for DPP-IV Inhibition and Anticancer Activity. *Synth. Commun.* **2018**, *48*, 2877–2887. DOI: 10.1080/00397911.2018.1508723.

[13] Durgapal, S. D.; Soman, S. S. Evaluation of Novel Coumarin-Proline Sulfonamide Hybrids as Anticancer and Antidiabetic Agents. *Synth. Commun.* **2019**, *49*, 2869-2883. DOI: 10.1080/00397911.2019.1647439.

[14] Trachootham, D.; Zhou, Y.; Zhang, H.; Demizu, Y.; Chen, Z.; Pelicano, H.; Chiao, P. J.; Achanta, G.; Arlinghaus, R. B.; Liu, J.; Huang, P. Selective Killing of Oncogenically Transformed Cells through a ROS-Mediated Mechanism by β-Phenylethyl Isothiocyanate. *Cancer Cell* **2006**, *10*, 241–252. DOI: 10.1016/j.ccr.2006.08.009.

[15] Reinehr, R.; Becker, S.; Eberle, A.; Grether-Beck, S.; Häussinger, D. Involvement of NADPH Oxidase Isoforms and Src Family Kinases in CD95-Dependent Hepatocyte Apoptosis. *J. Biol. Chem.* **2005**, *280*, 27179–27194. DOI: 10.1074/jbc.M414361200.

[16] Ramsey, M. R.; Sharpless, N. E. ROS as a Tumour Suppressor? *Nat. Cell. Biol.* **2006**, *8*, 1213–1215. DOI: 10.1038/ncb1106-1213.

[17] Sakkiah, S.; Lee, K. W. Pharmacophore-Based Virtual Screening and Density Functional Theory Approach to Identifying Novel Butyrylcholinesterase Inhibitors. *Acta Pharmacol. Sin.* **2012**, *33*, 964–978. DOI: 10.1038/aps.2012.21.

[18] Drwal, M. N.; Banerjee, P.; Dunkel, M.; Wettig, M. R.; Preissner, R. ProTox: A Web Server for the In Silico Prediction of Rodent Oral Toxicity. *Nucleic Acids Res.* **2014**, *42*, 3–8. DOI: 10.1093/nar/gku401.

[19] Hayakawa, I.; Shioya, R.; Agatsuma, T.; Furukawa, H.; Naruto, S.; Sugano, Y. 4-Hydroxy-3-Methyl-6-Phenylbenzofuran-2-Carboxylic Acid Ethyl Ester Derivatives as Potent Anti-Tumor Agents. *Bioorg. Med. Chem. Lett.* **2004**, *14*, 455–458. DOI: 10.1016/j.bmcl.2003.10.039.

[20] He, J.; Tang, X. M.; Liu, T. T.; Peng, F.; Zhou, Q.; Liu, L. W.; He, M.; Xue, W. Synthesis and Antibacterial Activity of Novel Myricetin Derivatives Containing Sulfonylpiperazine. *Chem. Pap.* **2021**, *75*, 1021–1027. DOI: 10.1007/s11696-020-01363-3.

[21] Mao, Z. W.; Zheng, X.; Lin, Y. P.; Hu, C. Y.; Wang, X. L.; Wan, C. P.; Rao, G. X. Design, Synthesis and Anticancer Activity of Novel Hybrid Compounds between Benzofuran and N-Aryl Piperazine. *Bioorg. Med. Chem. Lett.* **2016**, *26*, 3421–3424. DOI: 10.1016/j.bmcl.2016.06.055.

[22] Durgapal, S. D.; Soni, R.; Umar, S.; Suresh, B.; Soman, S. S. Anticancer Activity and DNA Binding Studies of Novel 3,7-Disubstituted Benzopyrones. *ChemistrySelect* **2017**, *2*, 147–153. DOI: 10.1002/slct.201601361.

[23] Elkady, A. I. Crude Alkaloid Extract of Rhazya Stricta Inhibits Cell Growth and Sensitizes Human Lung Cancer Cells to Cisplatin through Induction of Apoptosis. *Genet. Mol. Biol.* **2013**, *36*, 12–21. DOI: 10.1590/S1415-47572013005000009.

[24] Umar, S.; Soni, R.; Durgapal, S. D.; Soman, S.; Balakrishnan, S. A Synthetic Coumarin Derivative (4-Flourophenylacetamide-Acetyl Coumarin) Impedes Cell Cycle at G0/G1 Stage, Induces Apoptosis, and Inhibits Metastasis via ROS-Mediated P53 and AKT Signaling Pathways in A549 Cells. *J. Biochem. Mol. Toxicol.* **2020**, *34*, e22553. DOI: 10.1002/jbt.22553.

[25] Lipinski, C. A. Lead- and Drug-like Compounds: The Rule-of-Five Revolution. *Drug Discov. Today Technol.* **2004**, *1*, 337–341. DOI: 10.1016/j.ddtec.2004.11.007.

[26] Daina, A.; Blatter, M. C.; Baillie Gerritsen, V.; Palagi, P. M.; Marek, D.; Xenarios, I.; Schwede, T.; Michielin, O.; Zoete, V. Drug Design Workshop: A Web-Based Educational Tool to Introduce Computer-Aided Drug Design to the General Public. *J. Chem. Educ.* **2017**, *94*, 335–344. DOI: 10.1021/acs.jchemed.6b00596.

Design of unsymmetric coumarin chalcone derivatives with tunable self-assembling behavior

Jayashree V. Patil [#], Rina Soni [#], Ashish Nandawana , Shubhangi S. Soman [*]

Department of Chemistry, Faculty of Science, The M. S. University of Baroda, Vadodara - 390002, India

ARTICLE INFO

ABSTRACT

Unsymmetric coumarin chalcone derivatives were designed with unsymmetric alkoxy chain on both terminal of the molecules to find their effect on the overall mesomorphic properties. In the first homologous series, compounds with fixed octyloxy chain on chalcone end and varied alkoxy chain length at coumarin end of the molecule (n = 10,12,14,16,18) have been analyzed for their mesomorphic properties. In this series, all the Compounds showed stable enantiotropic SmC mesophase. In the second homologous series, compounds with fixed octyloxy chain on coumarin end and varied alkoxy chain length at chalcone end (n = 10,12,14,16,18) have been studied for their mesomorphic properties. In the second homologues series, compounds (n = 10,12) exhibited monotropic nematic mesophase. For higher analogues (n = 16,18), enantiotropic SmA mesophase was observed. Further, the powder X-ray diffraction analysis of the three compounds from both the series at 112 °C showed diffraction pattern quite close to identified mesophase type. To understand effect of variation of terminal chain, DFT theoretical study was carried out for both different series and tried to understand correlation between mesomorphic properties and structural parameters.

1. Introduction

The structure of small rod like molecules is extremely important for mesomorphic properties and small variations in structure of these molecules also show different liquid crystalline phases [1–3]. Design of such material have rigid core containing two or more aromatic or heterocyclic rings attached through different linking groups such as azo, amido, ester, imine, chalcone etc. and terminal flexible alkyl chain [4–9]. Along with aromatic core, type of central linkage and length of terminal flexible chain have significant effect on thermal stability along with mesophase type and stability range [10–12]. Chalcone central linkage can induce dipole within the core of the molecule, similar to ester, azo, amido or imino linkages hence many thermotropic liquid crystalline compounds with chalcone linkage have been synthesized and investigated [13–19]. Chalcone linkage provides linearity in the structure as well as good thermal stability, which has significant impact on mesophase type. While variation of flexible terminal alkyl/alkoxy chain in the main core of the molecule has effect on the both physical as well as thermal properties of the molecules including melting point, phase transition temperature, mesophase type, dielectric anisotropy, dipole

moment and polarizability. Recently, coumarin containing liquid crystal compounds are designed and explored as liquid crystalline materials due to several advantageous properties associated with it such as molecular stability, photo-physical properties and low energy non-covalent intermolecular interactions [20–25].

Symmetric and non-symmetric molecules along with variation of different linkages have been prepared and studied for their mesomorphic properties [26–38]. Recently, Ahmed et al. have reported non symmetrical homologues series 1a containing Schiff base and ester linkages having two terminal alkoxy groups. All the compounds were studied for their mesophase behavior and compared with azo series 1b (Fig. 1) [27,28]. Compounds have shown dimorphic Smectic A and Nematic phases having more stability when substituted with higher alkoxy chain. Mohammad A. T. and Mustafa H. K. have reported two series 2a and 2b as unsymmetrical coumarin derivatives attached with chalcone via ether linkage (Fig. 1) [30]. Compounds from both the series showed interesting mesomorphic properties. Thus, when there is a change in the terminal alkyl/alkoxy group, the overall rigidity of the molecules will be affected and hence the linearity will be changed as well as in intermolecular interactions. Overall, the mesogenic planar

ring, central linkages and terminal alkyl chains are important in development of new compounds

In our previous work, we have also carried out synthesis of coumarin derivatives 3 and 4 with unsymmetrical terminal alkoxy chain (Fig. 1) [37–39]. It was observed that mesophase type and stability are easily affected on varying the alkoxy group at one of terminal of the molecules. In this direction, DFT calculations can be used to evaluate crucial parameters of molecules including geometry, the frontier molecular orbitals energy, molecular electrostatic map and energy gap. The DFT calculation is one of the tool for correlation of such parameters with experimental properties of liquid crystalline compounds [40–42].

As a part of our work on the design and study of liquid crystalline compounds based on coumarin containing chalcone linkages, earlier our group has reported coumarin-chalcone derivatives with symmetric chain at both terminal of the molecule showed dimorphic properties with octyloxy chain, while lower analogues showed nematic mesophase transitions and higher analogues showed enantitropic SmA mesophase [23]. In this particular class, all the compounds have showed fair stability of coumarin ring and chaclone central linkages in rigid core.

We have selected coumain chalcone derivatives to study effect of different alkoxy chains at both ends (Fig. 2). As unsymmetric terminal alkoxy groups would result in change of polarizability of chalcone linkage as well as that of the whole molecule and hence overall effect on mesomorphic properties and stability of the molecules. Further, compounds were studied for DFT calculations to obtain the various geometrical parameters, which can be further use to correlate the observed mesomorphic properties and estimated theoretical simulations. (Scheme 1)

2. Results and discussion

2.1. Chemistry

Chalcone derivative 9 was prepared by condensation of compound 7 with 4-octyloxy benzaldehyde 8 using pyrrolidine and acetic acid by refluxing for 36 h in ethanol. Alkylation Compound 9 was carried out using different n-bromo alkanes and anhyd. K_2CO_3 using *N, N*-dimethylformamide (DMF) as solvent at 70–72 °C to form compounds 10a-e. In second variation, first compound 7 was reacted with n-octyl bromide in presence of anhyd. K_2CO_3 and pinch of KI in DMF to form 11. Further, 11 on reaction with 4-hydroxy benzaldehyde 12 and catalytic amount pyrrolidine (2–3 drops) and acetic acid in solvent ethyl alcohol by refluxing for 36 h to give chalcone derivative 13. Compound 13 was reacted with n-alkyl bromides in presence of anhyd. K_2CO_3 in dry DMF at 70–72 °C to give compounds 14a-e. All the compounds 10a-e and 14a-e were analyzed by using various spectral studies like IR, ^{1}H NMR, ^{13}C NMR, ESI-MS and CHN analysis.

In IR spectra, all compounds 10a-e and 14a-e showed alkyl chain C—H stretching as two bands in the range 3096–2838 cm^{-1}. The stretching frequency of lactone coumarin was obsved at 1735–1715

cm^{-1} and chalcone carbonyl was found to be at 1665–1648 cm^{-1} for all the compounds. ^{1}H NMR of compound 10b showed methyl groups as multiplet at δ 0.87–0.90 ppm and methylene groups observed at δ 1.27–1.82, while –OCH$_2$ protons of both terminal alkyl chain was observed at δ 4.01 and 4.05 as triplet. Aromatic protons of compound 10b were observed at δ 6.84–7.93 ppm including chalcone linkage protons as two doublets at δ 7.80 and 7.91 having coupling constant value for trans protons. In ^{13}C NMR of 10b methyl group carbons at both end observed at δ 14.14and 14.15 ppm, methylene group carbons of two alkoxy chain were observed between δ 22.68–31.90 ppm, alkoxy chain carbon next to oxygen at δ 68.17and 69.01 ppm. Aromatic carbons of compounds 10b were appeared from δ 100.68 to 161.46 ppm, while carbonyl carbon of lactone ring was appeared at δ 164.68 ppm and chalcone carbonyl carbon at δ 186.29 ppm. All the compounds 10a-e and 14a-e have shown similar pattern in ^{1}H NMR and ^{13}C NMR analysis as variation were done at only chain length of terminal alkyl group at coumarin side and chalcone side of the compounds. Further all the compounds were analyzed by CHN analysis and ESI-MS analysis.

2.2. Mesomorphic properties

Compounds 10a-e and 14a-e were analysed using polarizing optical microscope for mesophase identification and optical textures. For POM analysis, thin film of compound was studied at the rate of 10 °C/min during 1st cooling and 2nd heating cycle and textures formed were identified. Further, all the compounds were analysed using differential scanning calorimetry (DSC) to calculate thermograms in heating and cooling scan at the rate of 10 °C/min. DSC curves have shown clear transition temperatures, while good mesophase textures were obtained from POM analysis for all the studied compounds for multiple heating and cooling cycles (Table 1).

2.3. Polarizing optical microscopy (POM) study

Chalcone derivatives of coumarin with successive increase of alkyl group at two sides of the molecules were studied earlier from our group and compounds with octyloxy group showed stable SmA and nematic mesophase during heating and cooling cycle respectively. Hence, octyloxy chain length was selected to explore the effect of change in alkyl group of two sides of the coumarin chalcone molecules. In the first homologous series, compounds 10a-e have been analyzed for their mesomorphic properties with octyloxy chain on chalcone end and varied alkoxy chain length $n = 10,12,14,16,18$ at coumarin end of the molecule. In this series, compound 10a with decyloxy chain exhibited nematic mesophase only in cooling cycle, while enantiotropic SmC mesophase (Fig. 3a-b). On changing the decyloxy with higher alkoxy chain length, compounds 10b-e showed enantiotropic SmC mesophase (Fig. 3c).

In second homologous series, compounds 14a-e have been analyzed for their mesomorphic properties and varied alkoxy chain length $n =$
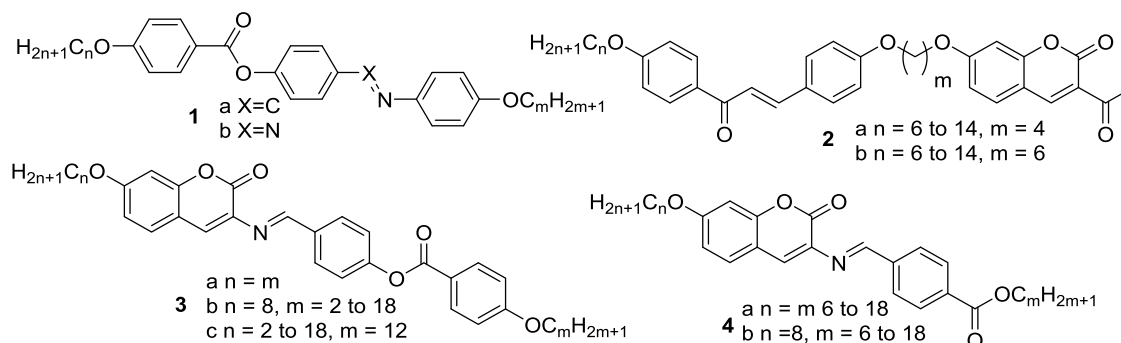

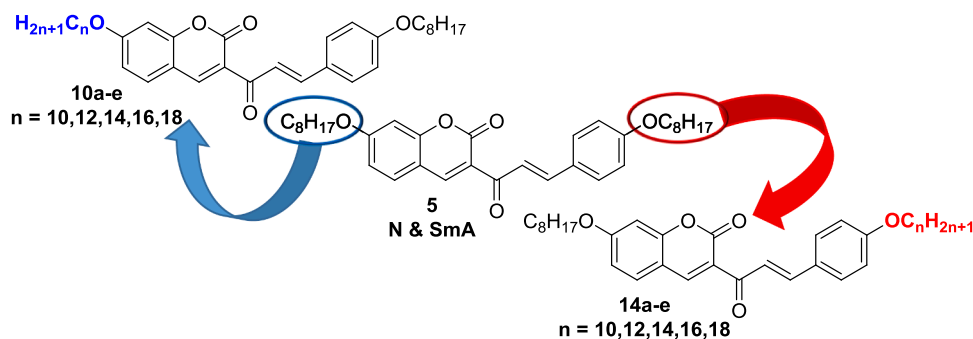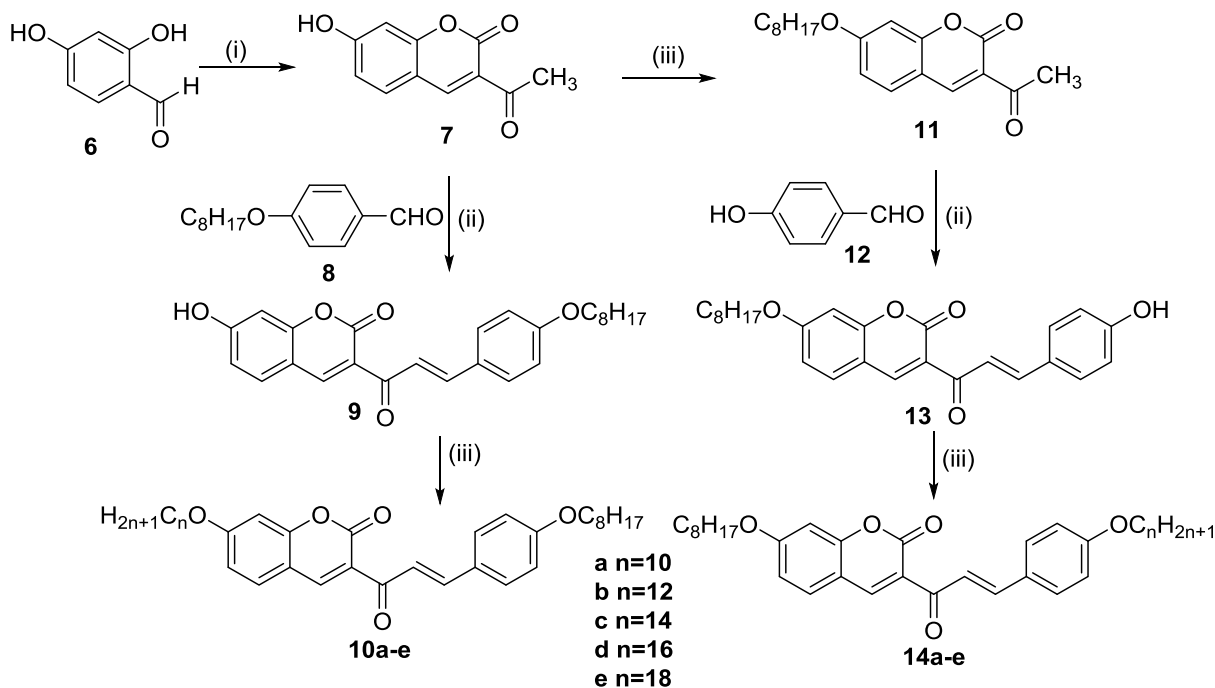Fig. 1. Thermotropic mesomorphic unsymmetric derivatives.

Fig. 2. Unsymmetric coumarin chalcone derivatives.

Reagents and condition : (i) EAA, pyridine, piperidine, reflux, 14 h; (ii) compound **8/9**, pyrrolidine, acetic acid, ethanol, reflux, 36 h; (iii) alkyl bromide, DMF, anhy. K₂CO₃, KI, reflux, 24 h.

Scheme 1. Synthesis of compounds 10a-e and 14a-e.

10,12,14,16,18 at chalcone end of the molecule. In this series, monotropic nematic mesophase was observed from compounds 14a-b with decyloxy and dodecyloxy chain length respectively (Fig. 3d). Compound 14c with tetradecyloxy exhibited enantiotropic nematic mesophase (Fig. 3e). While both the compounds 14d and 14e showed enantiotropic SmA mesophase (Fig. 3f).

2.4. Differential scanning calorimetry study (DSC)

Unsymmetic coumarin chalcone derivatives 10a-e and 14a-e have been analyzed for transition temperatures and associated enthalpy values using DSC during both heating scan and cooling scan (Table 1). In first homologous series with octyloxy chain at chalcone end of the molecules, compound 10a showed two endothermic transition on heating cycle associated with Cr-SmC and SmC-Iso at 111.5 °C & 127.5 °C respectively, while three exothermic transitions during cooling cycle associated with Iso-N, N-SmC and SmC–Cr at 124.1 °C, 118.9 °C & 76.9 °C respectively. Compounds 10b to 10e showed enantiotropic liquid crystalline properties with two endothermic transitions during heating cycle related to Cr-SmC and SmC-Iso, while two exothermic transitions during cooling cycle (Table 1, Fig. 4a).

In second homologous series, the variation of alkoxy group at chalcone terminal of the molecules, compounds 14a-b showed only endotherms for Cr-Iso transitions at 110.1 °C & 121.2 °C respectively on heating cycle, while two exotherms associated with Iso-N & N—Cr during cooling cycle (Table 1 & Fig. 4b). Compound 14c-e exhibited enantiotropic liquid crystalline properties. Compound 14c showed two endotherms 110.4 °C for Cr-N & 117.7 °C for N-Iso transitions respectively and two exotherms 114.3 °C for Iso-N & 91.2 °C for N—Cr transitions. Compound 14d exhibited two endotherms related to Cr-SmA (109.1 °C) and SmA-Iso (117.4 °C) while heating and two exotherms associated to Iso-SmA (114.3 °C) and SmA-Cr (90.3 °C) phase during cooling cycle (Table 1, Fig. 4c).

Further, graph for alkoxy chain length vs the temperature of mesophase transitions were plotted (Fig. 5). Typical mesophases such as nematic, SmA and SmC phases were observed for newly prepared mesogens. The clearing temperature was increased in both the series with increase in alkoxy chain length and then decreased with the increase of chain length (Fig. 5). Compounds 14a-e showed low clearing temperature as compared to that for compounds 10a-e. Compound 5 has shown both nematic and SmA mesophase transitions. On changing octyloxy to decyloxy chain length on coumarin end of the molecule, it

Table 1

Mesophase assignments, transition temperature °C of compounds 10a-e and 14a-e as determined by POM and DSC.

Compd	n	2nd heating process[a] Temp °C (ΔH KJmol^{-1})	1st cooling process[a] Temp °C (ΔH KJmol^{-1})
10a	10	Cr 111.5(−22.83) SmC 127.5(−1.89) Iso	Iso 124.1(1.99) N 118.9(0.38) SmC 76.9(16.38) Cr
10b	12	Cr 109.4(−17.85) SmC 130.7(−2.13) Iso	Iso 123.6(1.91) SmC 78.2(15.37) Cr
10c	14	Cr 100.0(−44.83) SmC 135.0(−2.40) Iso	Iso 129.1(3.48) SmC 81.3(17.08) Cr
10d	16	Cr 104.8(−64.49) SmC 129.2(−4.06) Iso	Iso 124.2(4.14) SmC 78.0 (22.81) Cr
10e	18	Cr 93.5(−18.09) SmC 106.6 (−8.15) Iso	Iso 103.6*SmC 82.2(16.12)Cr
14a	10	Cr 110.1(−33.04) Iso	Iso 108.9(0.65) N 76.7(14.32) Cr
14b	12	Cr 121.2(−54.81) Iso	Iso 115.7(68.13) N 81.6(18.95) Cr
14c	14	Cr 110.4(−27.81) N 117.7 (−1.24) Iso	Iso 114.3(2.05) N 91.2(29.78) Cr
14d	16	Cr 109.1(−25.40) SmA 117.4(−1.28) Iso	Iso 114.3(2.26) SmA 90.3(30.55) Cr
14e	18	Cr 113.1(−35.24) SmA 120.30(2.05) Iso	Iso 117.2(2.68) SmA 98.8(40.85) Cr

[a] Cr: Crystalline state; N: Nematic; SmA: Smectic A; SmC: Smectic C; Iso: Isotropic state;.

* Mesophase transition temperature observed in POM study.

resulted in molecules to show Iso-N and N-SmC mesophase transitions, while higher analogues showed only Iso-SmC transitions due to increase of intermolecular forces with increase chain length to result in layered packing. While, on changing octyloxy with decyloxy chain length on chalcone end of the molecules, it resulted in loss of SmA mesophase transition and exhibited Iso-N phase transition only. Similarly, compounds with dodecyloxy and tetradecyloxy chain length exhibited Iso-N phase transition as a result of change in shape anisotropy as well as less intermolecular interactions between the mesogenic units. While, higher analogues have shown enantiotropic Iso-SmA phase transition.

2.5. X-ray diffraction studies

Unsymmetric coumarin chalcone derivatives 10d, 14a and 14d were studied for powder X-ray diffraction analysis to study the identification of mesophase (Fig. 6). The powder XRD analysis of compound 10d at 112 °C showed two peaks. First sharp reflection was observed in the small angle regime (layer spacing 36.2 Å) and second broad hump in the wide-angle region (layer spacing 4.4 Å) (Fig. 6a). Similar set of two

peaks were observed for compound 14a, however sharp reflection peak was found to be with very low intensity when compared with compound 10d corresponding to more liquid like nature (Fig. 6b). While compound 14d showed the sharp reflection peak with layer spacing of 41.6 Å and the broad hump in the wide-angle region (layer spacing 4.3 Å) (Fig. 6c). The SmA and SmC mesophases can be easily distinguished based on their powder XRD pattern at small-angle region. The peak in small angle region appeared with very low intensity in compound 14a with nematic mesophase as compared to that in compounds 10d and 14d At the same time diffused broad halo around 4.3–4.4 Å was found to be almost similar for all the compounds as originated as a result of liquid like nature of alkoxy terminal. For compounds 10d and 14d, tilt angle was calculated using the formula tilt angle $\theta = \cos^{-1}$ (d/L), (where L is molecular length was obtained by DFT optimized structure). The tilt angles were found to be 40.0° and 28.5° respectively for compounds 10d and 14d which further confirms tilted SmC mesophase of compound 10d, while the orthogonal Smectic-A mesophase of 14d Bragg's diffraction equation was used to calculate the inter layer distances from the 2θ values.

2.6. DFT calculations

The DFT calculations were investigated for 10a-e and 14a-e in order to develop correlation between the observed mesomorphic properties and theoretical geometrical parameters. All the DFT optimization of compounds were done using B3LYP method at 6–311 G (d,p) basis set. All the optimized structures have shown good stability and the frequency for all the compounds were calculated using the same basis set to calculate various parameters (Supporting Information SI, Fig.S1). The estimated optimized structures of compounds 10d and 14d are shown in Fig. 7. Compound 5 was also selected and optimized using same basis set to find a comparative study. All the compounds have shown planar structures (Fig. 7), which could be one of the factor to align the molecules in parallel pattern to give more ordered mesophase. Compound 5 showed nematic and SmA mesophase. In the first series with octyloxy chain on chalcone end, compounds aspect ratio was increased with increase in alkoxy chain length on coumarin end of the molecule, however clearing temperatures were initially increased (for n = 10,12,14,) and then decreased (for n = 16,18). Similar variation of alkoxy chain length on chalcone end of the molecules showed random behavior for clearing temperature with respect to increase in aspect ratio.

The HOMO, LUMO and ΔE values of the studied compound were calculated by the B3LYP/6–311G(d,p) method. The frontier molecular orbitals (FMOs) have been calculated for the compounds 5, 10d and 14d
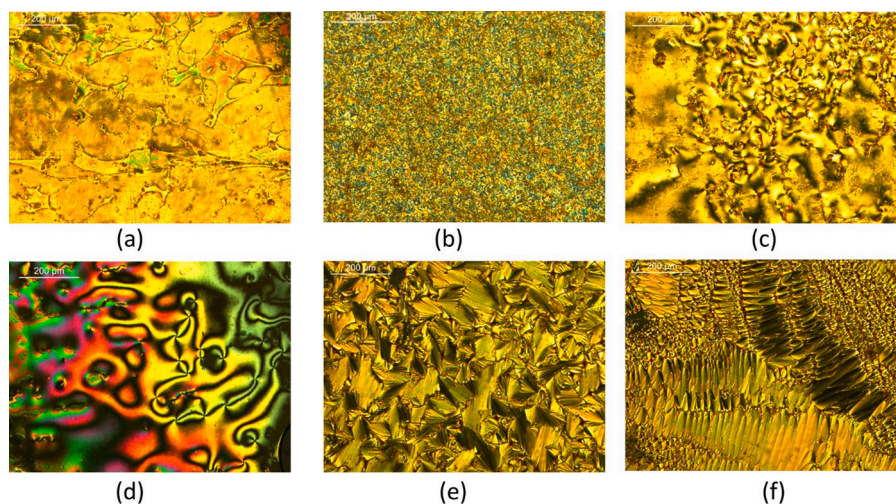

Fig. 3. Liquid crystal phase transition (a) nematic marble for compound 10a on cooling (b) SmC broken fan texture 10d (c) nematic marble for compound 14a (d) nematic schlieren texture for compound 14c (e) SmA focal conic for compound 14d in cooling cycle (f) SmA focal conic for compound 14d in heating cycle.
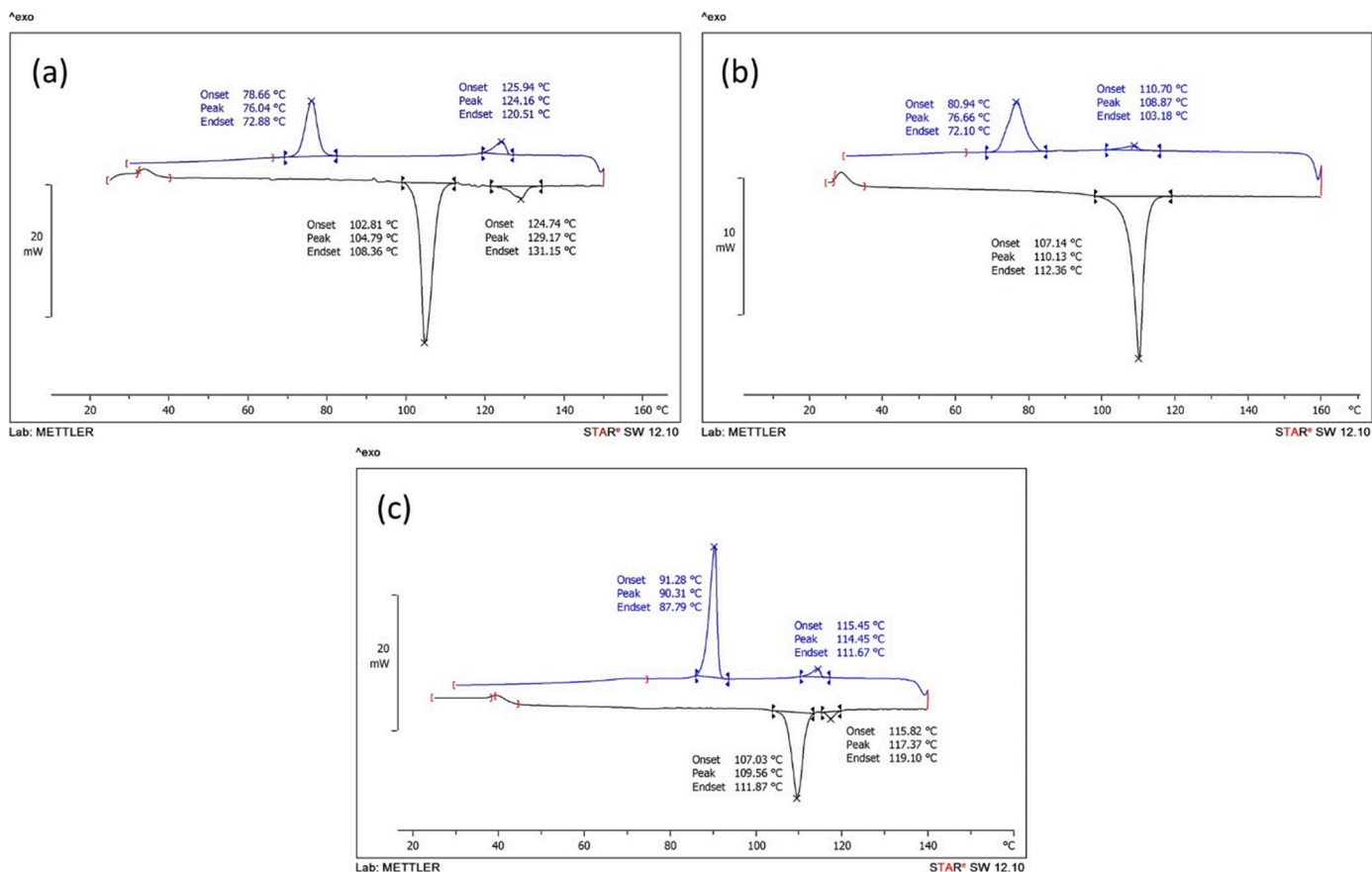
Fig. 4. DSC plot in both heating and cooling cycles (at the rate of 10 °C/min.) along with transition temperatures (a) compound 10d (b) compound 14a (c) compound 14d
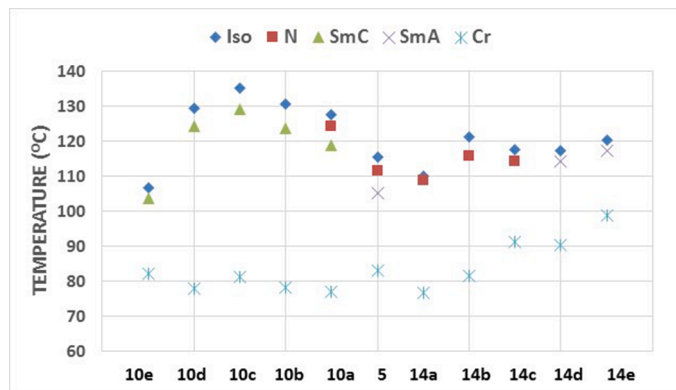

Fig. 5. Effect of chain length variation on both end of the molecules on transition temperatures of compounds 5, 10a-e and 14a-e.

(Fig. 8). For all the compounds, HOMO are mainly located on chalcone and attached aromatic ring, while LUMO are mainly located on coumarin ring, chalcone group and aromatic ring (SI, Fig. S2). Some of the valuable parameters of liquid crystalline compounds can be calculated from energy gap such as global softness and chemical hardness (SI, Table S1). The ΔE value of molecule can be used to find the chemical reactivity and stability of it. With high ΔE is less polarizable and is generally associated with a low chemical reactivity and high kinetic stability and vice versa. Interestingly the all the studied compounds 5, 10a-e and 14a-e, ΔE values were found to be almost identical (SI, Table S1). Hence, other parameters such as chemical hardness (η, 0.06 eV) and softness (S, 16.66 eV^{-1}) were found to be quite same throughout

the variation of terminal alkoxy chain length on both end of the molecules (SI, Table S1).

The molecular electrostatic potential (MEP) of molecules can provide overall electron density distribution over the molecules as well as possible molecular interaction which will further affect overall dipole moment and polarizability of molecules (Table 2 and Fig. 9). The MEP maps were calculated to locate charge distribution by using the same basis sets (SI, Fig. S3) to explore the possible intra- and intermolecular interactions sites on the molecule. For all the studied compounds, electron deficient centers are mainly localized on chalcone or coumarin part (red color region), while the electron rich regions are located on both terminal alkoxy chains (Blue color region)

For compounds 10a-e, dipole moments as well as polarizability were found to increase with successive variation in alkoxy chain at coumarin end (Table 2). On varying alkoxy chain length on coumarin ring has resulted in enhancement of the head-tail interaction to give SmC mesophase and overall very good stability was observed on varying alkoxy chain length (Fig. 9). However, on varying alkoxy chain length on chalcone end, dipole moment was decreased on increasing the alkoxy chain length for compounds 14a-d and again increased for compound 14e. In this series, compounds 14a-b exhibited monotropic nematic mesophase, while compound 14c showed enantiotropic nematic mesophase (Table 2). At the same time nematic mesophase stability was initially increased with increase in alkoxy chain on chalcone end and then decreased (Fig. 9). On the other hand, enantiotropic SmA mesophase was observed for compounds 14d-e. At the same time polarizability was found to be increasing initially for compounds 14a-e except that it is decreased for compound 14d with increase in alkoxy chain on chalcone end.
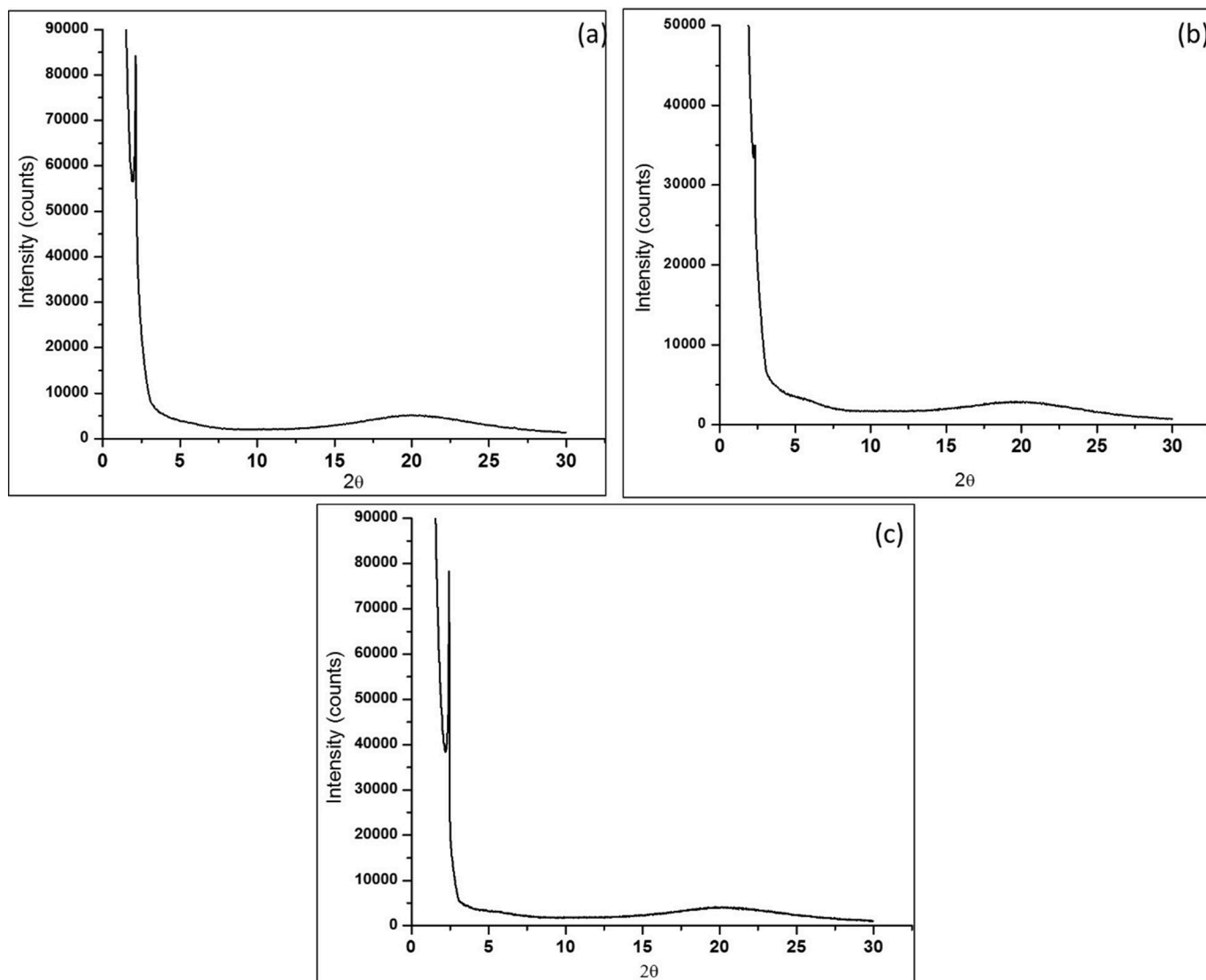
Fig. 6. Powder X-ray diffraction analysis at 112 °C (a) compound 10d (b) compound 14a and (c) compound 14d (the scattering intensity (in counts) vs the scattering angle, 2θ).
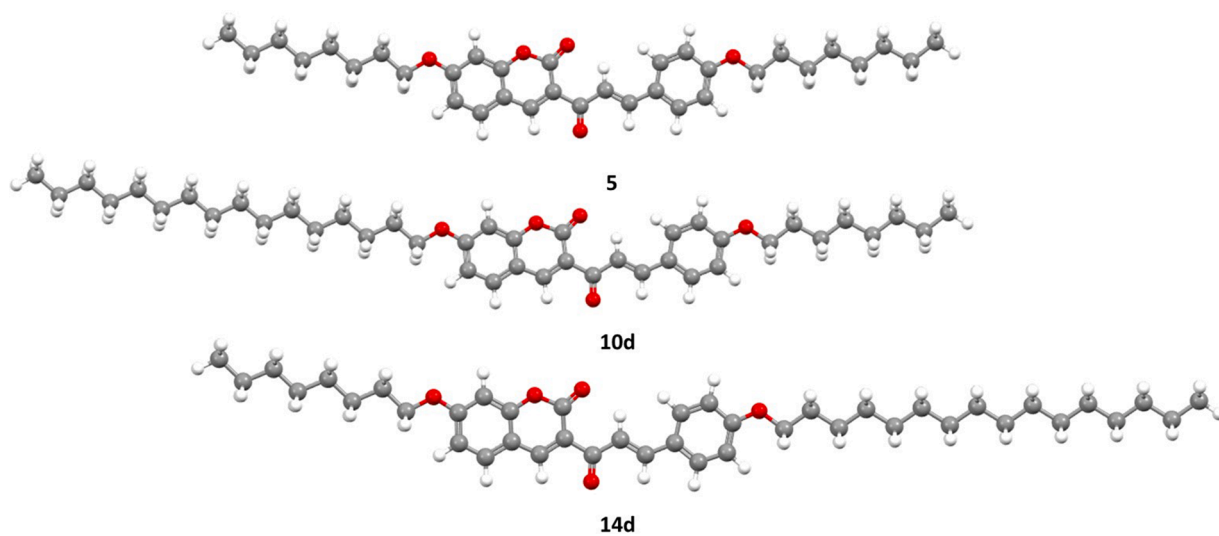

Fig. 7. Calculated molecular geometry of the compounds 5, 10d and 14d (Colour online).
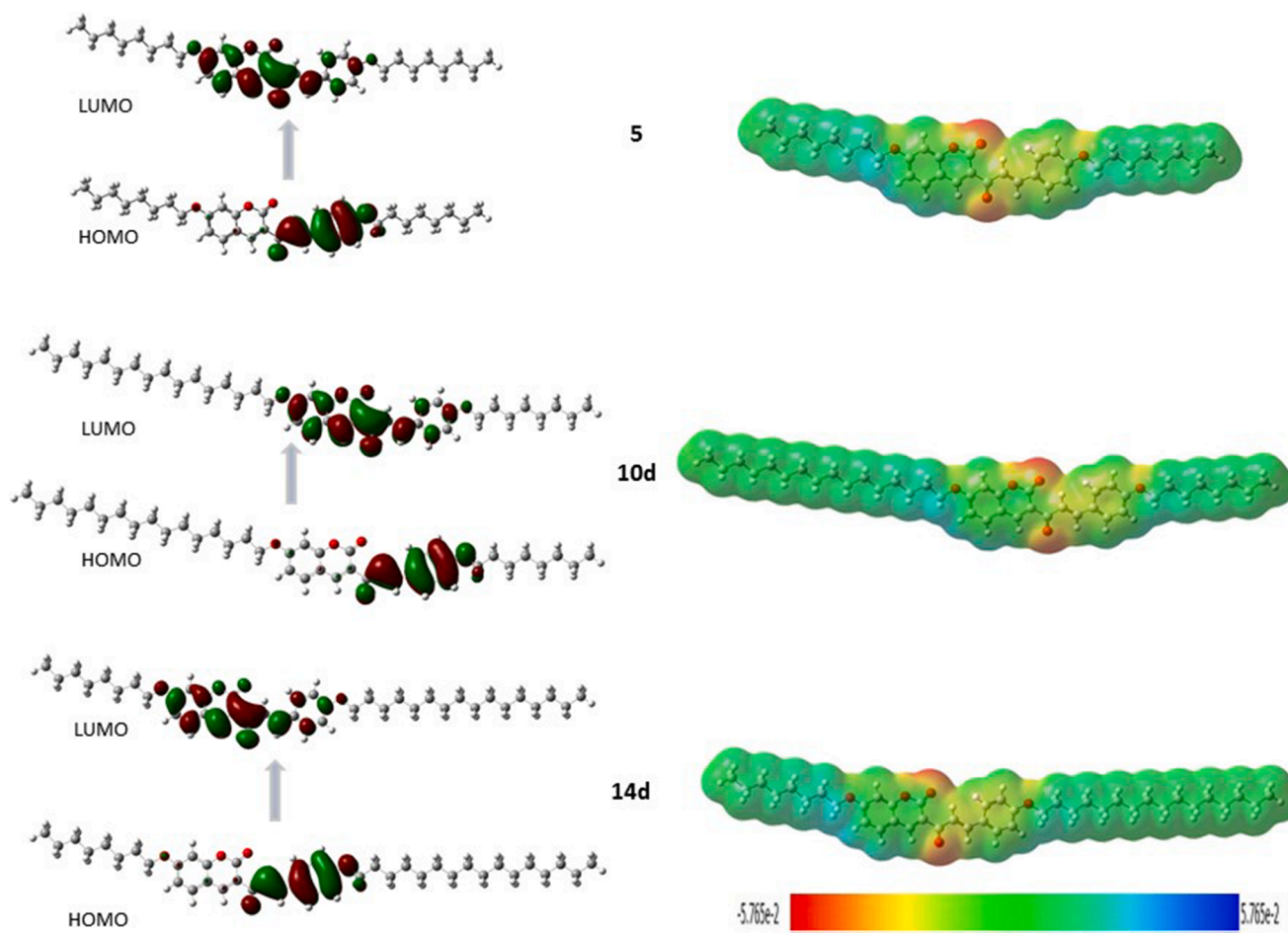
Fig. 8. Frontier Molecular orbitals (FMOs) and Molecular electrostatic potentials (MEP) for the prepared compounds 5, 10a-e and 14a-e.

Table 2
Mesomorphic parameters in cooling cycle (°C), dipole moment (Debye), polarizability α (Bohr³), aspect ratio of the studied compounds 5, 10a-e and 14a-e.

| Compd | ΔT_{Cr} | ΔT_{SmA} | ΔT_{SmC} | ΔT_N | Dipole moment | Polariza-bility | Dimension (Å) | | Aspect ratio |
							Length L	WidthD	L/D
5	28.5	22.0	–	6.4	3.158	518.128	37.062	5.60	6.62
10a	47.2	–	42.0	5.2	3.181	543.335	39.615	5.70	6.95
10b	45.4	–	45,4	–	3.189	568.362	42.164	6.01	7.02
10c	47.8	–	47.8	–	3.208	593.197	44.718	6.26	7.14
10d	46.2	–	46.2	–	3.212	617.997	47.276	6.47	7.31
10e	21.4	–	21.4	–	3.215	642.763	49.834	6.65	7.49
14a	32.2	–	–	32.2	3.141	543.347	39.622	5.74	6.91
14b	34.1	–	–	34.1	3.131	568.321	42.183	5.87	7.19
14c	23.1	–	–	23.1	3.127	593.195	44.742	5.99	7.47
14d	24.0	24.0	–	–	2.948	565.386	47.304	6.10	7.75
14e	18.4	18.4	–	–	3.121	642.834	49.866	6.22	8.02

3. Conclusion

Unsymmetric Coumarin chalcone derivatives were designed with various alkoxy chain at both terminal end of the molecule. All the compounds 10a-e and 14a-e were synthesized and fully characterized. In the first homologous series with octyloxy chain on chalcone end, compounds were prepared with varied alkoxy chain on coumarin terminal of the molecule. Compound 10a has shown SmC and Nematic phases while compounds 10b-e have shown enantiotropic stable SmC mesophase. In the second series with octyloxy chain on coumarin end, compounds were prepared with varied alkoxy chain on chalcone terminal of the molecule. In this particular series, compounds 14a-b have shown monotropic nematic mesophases, while compound 14d-e have shown

enantiotropic SmA mesophases. Types of mesophases were also confirmed from the powder X-ray diffraction analysis at 112 °C and diffraction patterns were found to be in close agreement to those identified by using POM. To understand this difference between the assembling behaviors of molecules with variation of terminal alkoxy chain in both the series, the geometrical and electronic parameters were calculated from the optimized DFT structures and compared with compound 5. For both the series, parameters such as band gap, chemical hardness and softness were found to be almost unchanged. While dipole moments and polarizability were found to be affected by variation of alkoxy chain length at both ends of the molecules. Variation of alkoxy chain length at chalcone end of the molecules have shown effect on dipole moment and total polarizability, which was also observed in mesomorphic behavior
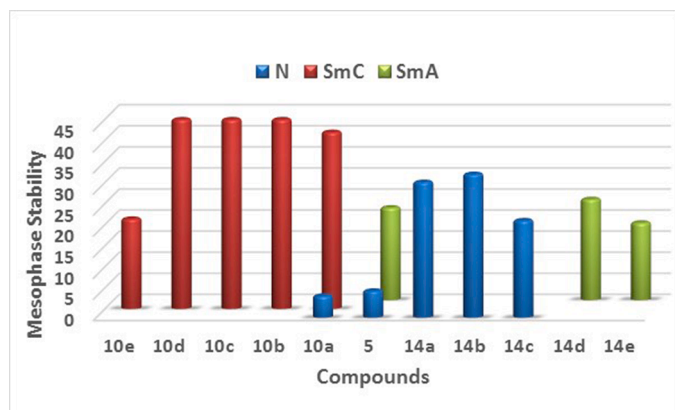
Fig. 9. The relation between the variation of chain length in compounds and N, SmC and SmA mesophase range.

in the series.

3.1. Experimental

3.1.1. Materials and methods

All the chemicals and solvents were purchased from commercial supplier and used after purification. For thin-layer chromatography analysis, silica gel F254 plates (Merck & Co., Kenilworth, NJ, USA) were used. Avra's silica gel (60–120 mesh) was used for column chromatographic purification. All the reactions were carried out in normal atmosphere. Melting points (M.P.) were measured in open capillary tubes and were uncorrected. IR spectra were recorded as KBr pellets on Bruker spectrometer. ^{1}H NMR and ^{13}C-NMR spectral data were recorded on Avance Bruker Neo 400 spectrometer (400 MHz) with CDCl₃ or DMSO-d₆ as solvent and *J* values in Hz. Liquid crystalline properties were studied using Polarizing Optical Microscope (POM) LEICA DM 2500P (Wien, Austria) attached with CAMERA-LEICA-DFC 295 and Heating Pod- LINKA 19. The textures of the compounds were observed by using polarized light with a crossed polarizer at angle of 45° and 10x magnification with the sample in thin film sandwiched between a glass slide and cover. Differential scanning calorimetry (DSC) analysis were carried out during heating and cooling cycles at the rate of 10.0 °C /min by using DSC-822, Mettler Toledo (Greifensee, Switzerland) having STARe software.

3.1.2. Synthesis of (E)−7-hydroxy-3-(3-(4-(octyloxy)phenyl)acryloyl)−2H-chromen-2-one (9)

To a solution of 3-acetyl-7-hydroxy coumarin 7 (5.0 g, 24.50 mmol, 1.0 eq) in ethanol (15 ml), 4-octyloxy benzaldehyde 8 (6.30 g, 26.96 mmol, 1.1 eq) was added followed by catalytic amount of pyrrolidine and acetic acid. The reaction mixture was refluxed at 78–80 °C for 36 hrs. The progress of reaction was monitored by TLC. The reaction mixture was cooled to room temperature and solvent were evaporated on rotavapor. The residue were poured into ice cold water to give crude product. The crude product was filtered, washed with water, and dried. The crude product was purified by column chromatography using pet ether:ethyl acetate (9:1 to 6:4) to give pure compound 82%Yield, M.P.: 168–170 °C; ESI-MS: 421.2 $[M + H]^+$.

3.1.3. Synthesis of alkoxy chromen-2-one chalcone derivatives 10a-e

To a solution of compound 9 (200 mg, 0.476 mmol, 1.0 eq) in DMF (15 mL) was added anhydrous K₂CO₃ (262 mg, 1.90 mmol, 4.0 eq), n-alkyl bromide (2.0 eq) and pinch of KI. The resulting mixture was heated at 70–72 °C for 14–16 hrs and monitored by TLC. On completion of reaction, reaction mixture was cooled to room temperature and poured into ice cold water to give crude product. The crude product was filtered, dried and recrystallized from ethanol to give pure compound as a yellow

solid.

3.1.4. (E)−7-(decyloxy)−3-(3-(4-(octyloxy)phenyl)acryloyl)−2H-chromen-2-one 10a

Yield:88%; M.P.: 128–130 °C; IR (KBr): 2923, 2853, 1731, 1654, 1599, 1564, 1510, 1472, 1422, 1395, 1342, 1303, 1265, 1185, 1168, 1144, 1072, 1011, 986, 953, 850, 832, 803, 775, 721, 640 cm^{-1}; ^{1}H NMR (400 MHz, CDCl₃): δ ppm 0.90–0.92 (m, 6H), 1.29–1.36 (m, 20H), 1.46–1.47 (m, 4H), 1.77–1.87 (m, 4H), 4.00 (t, *J* = 6.4 Hz, 2H), 4.06 (t, *J* = 6.4 Hz, 2H), 6.84–6.93 (m, 4H), 7.55 (d, *J* = 8.8 Hz, 1H), 7.63 (d, *J* = 8.8 Hz, 2H), 7.84 (d, *J* = 16.0 Hz, 1H), 7.92 (d, *J* = 16.0 Hz, 1H), 8.59 (s, 1H); ^{13}C NMR (100 MHz, CDCl₃): δ ppm 14.14, 14.15, 22.68, 22.70, 25.93, 26.02, 28.90, 29.17, 29.25, 29.33, 29.36, 29.55, 31.82, 31.90, 68.17, 69.01, 100.68, 112.26, 114.18, 114.82, 121.34, 121.68, 127.54,130.74, 131.22, 144.61, 148.38, 157.63, 159.95, 161.45, 164.68, 186.29; ESI-MS: 561.4 $[M + H]^+$; Anal. Calc. for C₃₆H₄₈O₅; C, 77.11; H, 8.63; found: C, 77.23; H, 8.71%.

Characterization data for compounds 10b-10e are provided in supporting information.

3.1.5. Synthesis of 3-acetyl-7-(octyloxy)−2H-chromen-2-one 11

To a solution of 3-acetyl-7-hydroxy coumarin 7 (5.0 g, 24.48 mmol, 1.0 eq) in DMF (50 ml) was added anhydrous K₂CO₃ (5.06 g, 36.72 mmol, 1.5 eq) followed by octyl bromide (4.67 ml, 26.92 mmol, 1.1 eq) and pinch of KI. The resulting mixture was heated at 70–72 °C for 14–16 hrs and r monitored by TLC. The reaction mixture was cooled to room temperature and poured into ice-cold water to give crude compound. The crude compounds was filtered, dried and recrystallized from ethanol to give compound 11. Yield: 72%, M.P. 110–112 °C.

3.1.6. Synthesis of (E)−3-(3-(4-hydroxyphenyl)acryloyl)−7-(octyloxy)−2H-chromen-2-one 13

To 11 in ethanol was added 4-hydroxy benzaldehyde 12 along with small amount of pyrrolidine and acetic acid. The reaction mixture was heated for 48 hrs. The completion of reaction was checked by TLC. The reaction mixture was cooled to room temperature and solvent was evaporated on rotavapour, then poured into ice. The product obtained was filtered, washed with cold water and dried. The crude product was purified by column chromatography using pet ether: ethyl acetate (9:1 to 6:4) to give pure compound 13 as a yellow solid.

Yield: 72%; M.P.: 148–150 °C; IR (KBr): 3289, 3043, 2916, 2852, 1700, 1653, 1593, 1570, 1513, 1447, 1376, 1357, 1277, 1247, 1193, 1166, 1084, 1019, 997, 827, 778, 754, 713, 649, 595, 570, 529 cm^{-1}; ^{1}H NMR (400 MHz, CDCl₃): δ ppm 0.86 (t, *J* = 6.4 Hz, 3H), 1.25–1.28 (m, 8H), 1.37–1.40 (m, 2H), 1.71–1.75 (m, 2H), 4.10 (t, 6.4 Hz, 2H), 6.84 (d, *J* = 8.8 Hz, 2H), 7.00 (dd, *J* = 8.8 Hz & 2.4 Hz, 1H), 7.06 (d, *J* = 2.4 Hz, 1H), 7.58–7.66 (m, 4H), 7.84 (d, 8.8 Hz, 1H), 8.65 (s, 1H), 10.17 (s, 1H); ^{13}C NMR (400 MHz, CDCl₃): δ ppm 14.45, 22.56, 25.87, 28.83, 29.14, 29.16, 31.71, 39.30, 39.51, 39.72, 39.93, 40.14, 40.35, 40.55, 69.11, 101.10, 112.43, 114.21, 116.44, 121.61, 121.80, 126.08, 131.27, 132.29, 144.44, 148.08, 157.35, 159.43, 160.76, 164.49, 186.63; ESI-MS: $[M + H]^+$ 421.2.

3.1.7. Synthesis of (E)−3-(3-(4-n-alkoxyphenyl)acryloyl)−7-(octyloxy)−2H-chromen-2-one 14a-e

To a solution of compound 13 (200 mg, 0.476 mmol, 1.0 eq) in DMF (10 mL) was added anhydrous K₂CO₃ (1.5 eq) followed by alkyl bromide (1.1 eq) and pinch of KI. The reaction mixture was heated at 70–72 °C for 16–18 hrs and monitored by TLC. On completion of the reaction, mixture was cooled to room temperature and poured into ice cold water to give crude product. The crude product was filtered, dried and recrystallized from ethanol to give compound as a yellow solid.

3.1.8. (E)−3-(3-(4-(decyloxy)phenyl)acryloyl)−7-(octyloxy)−2H-chromen-2-one 14a

Yield: 82.70%; M.P.: 110–112 °C; IR (KBr): 2922, 2850, 1725, 1654,

1597, 1568, 1546, 1506, 1467, 1426, 1377, 1356, 1289, 1250, 1211, 1168, 1117, 1063, 1015, 984, 957, 905, 841, 822, 775, 721, 642, 593, 574cm^{-1}; ^{1}H NMR (400 MHz, CDCl$_3$): δ ppm 0.91–0.93 (m, 6H), 1.29–1.37 (m, 20H), 1.44–1.51 (m, 4H), 1.78–1.88 (m, 4H), 4.01 (t, J = 6.8 Hz, 2H), 4.07 (t, J = 6.4 Hz, 2H), 6.85 (d, J = 2.0 Hz, 1H), 6.85–6.94 (m, 3H), 7.57 (d, J = 8.8 Hz, 1H), 7.65 (d, J = 8.8 Hz, 2H), 7.85 (d, J = 16.0 Hz, 1H), 7.93 (d, J = 16.0 Hz, 1H), 8.60 (s, 1H); ^{13}C NMR (100 MHz, CDCl$_3$): δ ppm 14.14, 14.16, 22.67, 22.71, 25.94, 26.02, 28.90, 29.17, 29.22, 29.30, 29.34, 29.40, 29.58, 31.80, 31.91, 68.18, 69.01, 100.68, 112.26, 114.19, 114.83, 121.34, 121.68, 127.54, 130.75, 131.22, 144.64, 148.40, 157.63, 159.97, 161.46, 164.69, 186.31; ESI-MS: 561.4 [$M + H$]$^+$; Anal. Calc. for C$_{36}$H$_{48}$O$_5$; C, 77.11; H, 8.63; found: C, 77.27; H, 8.69%.

Characterization data for compounds 14b-14e are provided in supporting information.

CRediT authorship contribution statement

Jayashree V. Patil: Investigation, Methodology, Formal analysis, Writing – original draft. **Rina Soni:** Conceptualization, Formal analysis, Writing – original draft. **Ashish Nandawana:** Investigation, Methodology. **Shubhangi S. Soman:** Conceptualization, Supervision, Writing – review & editing.

Declaration of Competing Interest

The authors declare that they have no known competing financial interests or personal relationships that could have appeared to influence the work reported in this paper.

Data availability

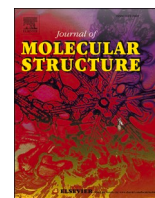No data was used for the research described in the article.

Supplementary materials

Supplementary material associated with this article can be found, in the online version, at doi:10.1016/j.molstruc.2023.135739.

References

[1] G.W. Gray, Handbook of Liquid Crystals, Fundamentals, Wiley, Germany, 1998.
[2] Handbook of Liquid Crystals, 8 Volume Set. (2014). Germany: Wiley.
[3] D. Andrienko, Introduction to liquid crystals, J. Mol. Liq. 267 (2018) 520–541, https://doi.org/10.1016/j.molliq.2018.01.175.
[4] G.H. Brown, J.W. Doane, V.D. Neff, Structure Phys. Propert. Liquid Crystals, 1970, https://doi.org/10.1080/10408437008243422.
[5] J. Wyart, G.W. Gray, Molecular structure and the properties of liquid crystals by, Acta Crystallogr. 16 (1963), https://doi.org/10.1107/s0365110x63000657, 235-235.
[6] V. Novotna, V. Hamplova, A. Bubnov, M. Kaspar, M. Glogarova, N. Kapernaum, S. Bezner, F. Giesselmann, First photoresponsive liquid-crystalline materials with small layer shrinkage at the transition to the ferroelectric phase, J. Mater. Chem. 19 (2009) 3992–3997, https://doi.org/10.1039/B821738F.
[7] A. Poryvai, A. Bubnov, D. Pociecha, J. Svoboda, M. Kohout, The effect of the length of terminal n-alkyl carboxylate chain on self-assembling and photosensitive properties of chiral lactic acid derivatives, J. Mol. Liq. 275 (2019) 829–838, https://doi.org/10.1016/j.molliq.2018.11.058.

[8] A. Bubnov, M. Cigl, N. Sedláčková, D. Pociecha, Z. Böhmová, V. Hamplová, Self-assembling behaviour of new functional photosensitive cinnamoyl-based reactive mesogens, Liq. Cryst. 47 (2020) 2276–2291, https://doi.org/10.1080/02678292.2020.1783586.
[9] B. Barman, B. Das, M.K. Das, V. Hamplová, A. Bubnov, Effect of molecular structure on dielectric and electro-optic properties of chiral liquid crystals based on lactic acid derivatives, J. Mol. Liq. 283 (2019) 472–481, https://doi.org/10.1016/j.molliq.2019.03.071.
[10] M. Kohout, A. Bubnov, J. Šturala, V. Novotná, J. Svoboda, Effect of alkyl chain length in the terminal ester group on mesomorphic properties of new chiral lactic acid derivatives, Liq. Cryst. 43 (2016) 1472–1485, https://doi.org/10.1080/02678292.2016.1185170.
[11] A. Bubnov, C. Vacek, M. Czerwiński, T. Vojtylová, W. Piecek, V. Hamplová, Design of polar self-assembling lactic acid derivatives possessing submicrometre helical pitch, Beilstein J. Nanotechnol. 9 (2018) 333–341, https://doi.org/10.3762/bjnano.9.33.
[12] Y.S.K. Reddy, N.P. Lobob, T. Narasimhaswamy, Effect of alkyl chain and linking units on mesophase transitions and molecular order of rod-like thiophene mesogens: ^{13}C NMR investigation, New J. Chem. 42 (2018) 598–612, https://doi.org/10.1039/C7NJ03525J.
[13] H.T. Srinivasa, A.K.T. Mohammad, Influence of terminally attached branched alkyloxy chains on the mesophase behaviour of calamitic liquid crystals, Phase Transitions 94 (2021) 256–269, https://doi.org/10.1080/01411594.2021.1931202.
[14] N.K. Chudgar, S.N. Shah, New fluorescent mesogens with a chalcone central linkage, Liq. Cryst. 4 (1989) 661–668, https://doi.org/10.1080/02678298908033201.
[15] B.T. Thaker, P.H. Patel, A.D. Vansadiya, J.B. Kanojiya, Substitution effects on the liquid crystalline properties of thermotropic liquid crystals containing schiff base chalcone linkages, Mol. Cryst. Liq. Cryst. 515 (2009) 135–147, https://doi.org/10.1080/15421400903291533.
[16] E.A. Bakr, M.H.A. Al-Jumaili, Synthesis and liquid crystalline properties of new chalcone derivatives central linkages, Mol. Cryst. Liq. Cryst. 710 (2020) 40–48, https://doi.org/10.1080/15421406.2020.1848254.
[17] H.T. Srinivasa, H.N. Harishkumar, B.S. Palakshamurthy, New coumarin carboxylates having trifluoromethyl, diethylamino and morpholino terminal groups: synthesis and mesomorphic characterisations, J. Mol. Struct. 1131 (2017) 97–102, https://doi.org/10.1016/j.molstruc.2016.11.047.
[18] O. Stamatoiu, A. Bubnov, I. Tărcomnicu, M. Iovu, Synthesis and spectral characterisation of new amido-ether Schiff bases, J. Mol. Struct. 886 (2008) 187–196, https://doi.org/10.1016/j.molstruc.2007.11.025.
[19] A. Bubnov, V. Novotna, V. Hamplova, M. Kašpar, M. Glogarova, Effect of multilactate chiral part of liquid crystalline molecule on mesomorphic behaviour, J. Mol. Struct. 892 (2008) 151–157, https://doi.org/10.1016/j.molstruc.2008.05.016.
[20] J.P. Van Meter, B.H. Klanderman, Mesomorphic Properties of Some Phenyl Benzoate Derivatives, Mol Cryst Liq Cryst 22 (1973) 271–284, https://doi.org/10.1080/15421407308083350.
[21] A.A. Merlo, A. Tavares, S. Khan, M.J. Leite Santos, S.R. Teixeira, Liquid-crystalline coumarin derivatives: contribution to the tailoring of metal-free sensitizers for solar cells, Liq. Cryst. 45 (2018) 310–322, https://doi.org/10.1080/02678292.2017.1324644.
[22] A.T. Mohammad, M.H. Al-Mohammedi, M.Z. Ghdhayeb, S.M. Husain Al-Majidi, Coumarin dimers of benzidine and phenylenediamine cores: synthesis, characterisation and mesomorphic properties, Liq. Cryst. 47 (2020) 414–422, https://doi.org/10.1080/02678292.2019.1655806.
[23] S.D. Durgapal, R. Soni, S.S. Soman, A.K. Prajapati, Synthesis and mesomorphic properties of coumarin derivatives with chalcone and imine linkages, J. Mol. Liq. 297 (2020), 111920, https://doi.org/10.1016/j.molliq.2019.111920.
[24] P. Shah, R. Soni, S.S. Soman, Synthesis and mesomorphic properties of bis ester derivatives of coumarin containing chalcone linkage, J. Mol. Liq. 335 (2021), 116178, https://doi.org/10.1016/j.molliq.2021.116178.
[25] A.E. Blatch, G.R. Luckhurst, The liquid crystal properties of symmetric and non-symmetric dimers based on the azobenzene mesogenic group, Liq. Cryst. 27 (2000) 775–787, https://doi.org/10.1080/026782900202264.
[26] M.G. Reddy, N.P. Lobo, T. Narasimhaswamy, Structural assignment and molecular order of three-ring mesogen by 13C NMR spectroscopy in mesophase, Liq. Cryst. 43 (2016) 896–909, https://doi.org/10.1080/02678292.2016.1148208.
[27] H.A. Ahmed, M.M. Naoum, G.R. Saad, Effect of alkoxy-chain length proportionation on the mesophase behaviour of terminally di-substituted phenylazo phenyl benzoates, Liq. Cryst. 40 (2013) 914–921, https://doi.org/10.1080/02678292.2013.788739.
[28] H.A. Ahmed, M. Hagar, G.R. Saad, Impact of the proportionation of dialkoxy chain length on the mesophase behaviour of Schiff base/ester liquid crystals; experimental and theoretical study, Liq. Cryst. 46 (2019) 1611–1620, https://doi.org/10.1080/02678292.2019.1590743.
[29] S.Z. Mohammady, D.M. Aldhayan, M.A. Alshammri, A.K. Alshammari, M. Alazmi, K.D. Katariya, M. Jaremko, M. Hagar, Polar Alkoxy Group and Pyridyl Effects on the Mesomorphic Behavior of New Non-Symmetrical Schiff Base Liquid Crystals. Symmetry 13 (2021) 1832, https://doi.org/10.3390/sym13101832.
[30] A.K.T. Mohammad, H.K. Mustafa, Unsymmetrical Coumarin based dimeric liquid crystals: synthesis, Characterization, Mesomorphic investigation, Photoluminescence and Thermal conductivity, Liq. Cryst. 49 (2022) 354–365, https://doi.org/10.1080/02678292.2021.1970835.

[31] M. Hagar, H.A. Ahmed, T.H. El-Sayed, R. Alnoman, Mesophase behavior and DFT conformational analysis of new symmetrical diester chalcone liquid crystals, J. Mol. Liq. 285 (2019) 96–105, https://doi.org/10.1016/j.molliq.2019.04.083.

[32] J. Godzwon, M.J. Sienkowska, Z. Galewski, Liquid crystalline polymorphism of 4-alkyloxybenzylidene-4'- alkyloxyanilines and entropie effects of their phase transitions, Acta Phys. Pol. A. 113 (2008) 1145–1154, https://doi.org/10.12693/APhysPolA.113.1145.

[33] M. Amela-Cortés, B. Heinrîch, B. Donnio, K.E. Evans, C.W. Smith, D.W. Bruce, Unsymmetric main-chain liquid crystal elastomers with tuneable phase behaviour: synthesis and mesomorphism, J. Mater. Chem. 21 (2011) 8427–8435, https://doi.org/10.1039/c0jm03691a.

[34] J.W. Goodby, Smectic polymorphism and molecular shape - the orthogonal phases, Mol. Cryst. Liq. Cryst. 75 (1981) 179–199, https://doi.org/10.1080/00268948108073613.

[35] J.W. Goodby, I.M. Saez, S.J. Cowling, J.S. Gasowska, R.A. MacDonald, S. Sia, P. Watson, K.J. Toyne, M. Hird, R.A. Lewis, S.-.E. Lee, V. Vaschenko, Molecular complexity and the control of self-organising processe, Liq. Cryst. 36 (2009) 567–605, https://doi.org/10.1080/02678290903146060.

[36] J.W. Goodby, R.J. Mandle, E.J. Davis, T. Zhong, S.J. Cowling, What makes a liquid crystal? The effect of free volume on soft matter, Liq. Cryst. 42 (2015) 593–622, https://doi.org/10.1080/02678292.2015.1030348.

[37] K.D. Katariya, K.J. Nakum, R. Soni, S.S. Soman, M. Hagaar, Coumarin Schiff base-esters liquid crystals with symmetrical and unsymmetrical alkoxy chains: synthesis,

mesomorphic properties and DFT approach, J. Mol. Liq. 357 (2022), 119073, https://doi.org/10.1016/j.molliq.2022.119073.

[38] K.D. Katariya, R. Soni, K.J. Nakum, S.S. Soman, M. Hagaar, Coumarin derivatives containing Schiff base and ester mesogenic core: synthesis, mesomorphic behaviour and DFT calculations, J. Mol. Struct. 1262 (2022), 133043, https://doi.org/10.1016/j.molstruc. 2022.133043.

[39] R. Soni, K.D. Katariya, K.J. Nakum, S.S. Soman, S. Nada, M. Hagaar, Synthesis, mesomorphic properties and DFT calculations of new coumarin Schiff base-ester liquid crystals, , Liq. Cryst. (2022), https://doi.org/10.1080/02678292.2022.2145378.

[40] H.A. Ahmed, M. Hagar, T.H. El-Sayed, R.B. Alnoman, Schiff base/ester liquid crystals with different lateral substituents: mesophase behaviour and DFT calculations, Liq. Cryst. 46 (2019) 1–11, https://doi.org/10.1080/02678292.2019.1566581.

[41] M. Hagar, H.A. Ahmed, O.A. Alhaddad, Experimental and theoretical approaches of molecular geometry and mesophase behaviour relationship of laterally substituted azopyridines, Liq. Cryst. 46 (2019) 1440–1451, https://doi.org/10.1080/02678292.2019.1581290.

[42] K.D. Katariya, K.J. Nakum, M. Hagar, New fluorinated azo/Schiff base liquid crystals: synthesis, characterisation, mesomorphic study and DFT calculations, Liq. Cryst. 49 (2022) 312–326, https://doi.org/10.1080/02678292.2021.1963493.

ELSEVIER

Check for updates

Studies in synthesis of 6-aminocoumarin Schiff base derivatives as mesogens and their DFT approach

Jayashree V. Patil, Rina Soni, Aditya B. Nair, Shubhangi S. Soman[*]

[a] *Department of Chemistry, Faculty of Science, The M. S. University of Baroda, Vadodara 390 002, India*

ABSTRACT

In first series, 6-amino coumarin Schiff base derivatives 10a-g were synthesized with alkoxy chain $n = 6–18$ and studied for their mesomorphic properties. In this series, compounds 10b with $n = 8$ showed monotropic nematic mesophase, while enantiotropic smectic A mesophase for higher analogues compounds 10c-g (with $n = 10–18$) was observed. In another series of Schiff base derivatives 12a-h additional ester linkage was introduced at the aldehyde end and were studied for their mesomorphic behavior. In second series, compounds 12a-c (with $n = 4–8$) showed enantiotropic nematic mesophase with very good thermal stability. Higher analogues of the second series with $n = 12–18$ showed stable enantiotropic smectic A mesophase. Compounds of both series were studied by DFT calculations. Different electronic parameters such as dipole moment, polarizability, molecular electrostatic potentials, frontier molecular orbitals, and thermodynamic variables were calculated and compared with the observed mesomorphic trends in both the studied series. Further, electronic parameters of compounds 10b and 12c and that of reference compound 4 were calculated and discussed to understand the effect of the removal of a hydroxyl group on the ortho position of the aldehyde part.

1. Introduction

Liquid crystals contain a variety of intriguing and practical qualities that make them suitable for use in various devices. The use of liquid crystals in various devices depends on a variety of features such as optical and dielectric anisotropy, birefringence behavior, etc. [1–3]. Compounds having liquid crystalline phases are created at certain transition temperatures by a combination of morphological structural components [4]. At a specific temperature range, a class of materials known as thermotropic liquid crystals exhibits both liquid-like and crystalline-like characteristics. These substances often consist of elongated or rod-like molecules that are capable of aligning themselves in an orderly manner to produce liquid crystal phases [5,6]. Temperature has a major role on the behavior of thermotropic liquid crystals. Thermotropic liquid crystals are used in a variety of products, such as displays, sensors and optical equipment. For instance, they are frequently employed in the production of liquid crystal displays (LCDs), where they enable the capacity to transit between various polarization states and so produce various colors [7–10]. Liquid crystal materials utilized in liquid crystal devices have hard rod-like molecules as their core molecular structure, functionalized with one or two flexible hydrocarbon tails. An

extended, rigid structure that is extremely anisotropic appears to be the primary requirement for liquid crystalline behavior [11–13].

Synthetic coumarin derivatives are well-studied for their biological and pharmacological applications [14–20]. Coumarin derivatives have shown very distinctive photophysical characteristics and have been explored for their material applications such as fluorescent sensors, effective colorimetric sensor, laser dyes and organic light-emitting diodes (OLEDs) [7,8,21–23]. Recently, several new thermotropic compounds have been designed containing coumarin as a heterocyclic core and studied for their mesomorphic behavior [24–26]. Amino coumarins are important members of the coumarin, which can easily be synthesized for various applications [27–29]. Coumarin with imine (-CH=N-) linkage has played role in molecular conjugation as well as more suited to the fluorescence and mesogenic properties [30–32]. The properties related to mesomorphism in 7-alkoxy 3-amino coumarin were notably influenced by alterations in the linking groups and length of the terminal alkoxy chain [28,33,34]. This influence stemmed from an overall modification in the polarity and alignment of dipole moments. The mesomorphic properties of the coumarin Schiff base also underwent significant changes due to variations in the terminal polar group, as investigated within our group [35,36]. Earlier, Schiff base derivatives 1

---

and Schiff base derivatives 2 with ester linkages of 7-alkoxy 3-amino coumarin with symmetrical alkoxy chain lengths at both ends of the molecules reported by our group. In this study, for compound 1 (Fig. 1) it was observed that shorter chain members displayed a nematic phase, whereas longer alkyl chain members exhibited a SmA mesophase [37] and in compounds 2 with ester linkage lower members showed nematic mesophase while higher alkoxy group showed Smectic C mesophases [38]. The structural stability, distinctive photosensitivity and non-covalent intermolecular interactions of coumarin derivatives are well known. Very recently, Rina et al. have reported and studied the mesomorphic and photophysical properties of derivative 3. In this series, Schiff base derivatives with intramolecular hydrogen bonding have also exhibited fluorescence due to excited state proton transfer properties [39].

6-amino coumarin is also one of the important members of the coumarin family which is a naturally occurring compound found in plants and also synthesized for various applications [27–28,40]. 6-amino coumarin has interesting properties, such as fluorescence, which makes it useful as a fluorescent probe in bio imaging and sensing applications [41]. Its properties can be modified by careful chemical modification of the amino and coumarin groups, leading to the development of new compounds with novel properties and potential applications.

Paul et al., reported a homologous series of emissive novel coumarins that comprise rod-shaped Schiff bases and their Zn(II) complexes 4. These compounds were shown to have intriguing photophysical characteristics, mesomorphic behavior and gelation behavior [42]. A novel coumarin Schiff base compound with a significant Stokes shift was synthesized by Pegu et al. The structural and spectroscopic properties of the substance 6-(4-n-heptyloxybenzyoloxy)−2-hydroxybenzylidene)

amino)−2H chromen-2-one 5 were investigated both experimentally and theoretically. The first hyper polarizability value in particular, with its huge magnitude, showed its potential application in nonlinear optical devices [43].

As a part of our research work on development of coumarin containing liquid crystalline compounds [28,37,44] we have selected 6-aminocoumarin and designed compounds 10a-g and 12a-h with a void of an ortho hydroxyl group on aldehyde part. Removal of the hydroxyl group will result in loss of intramolecular hydrogen bonding, which will further affect intermolecular interaction and hence mesomorphic properties as well as electronic properties of these compounds. DFT calculations are used to optimize the structures of both the series and literature-reported compound 4 and important electronic properties such as dipole moment and polarizability are compared with mesomorphic trends for studied compounds.

2. Result and discussion

2.1. Chemistry

$2H$-chromen-2-one 6 was nitrated with $HNO_3:H_2SO_4$ at cooling condition. After the addition of the nitrating mixture, the reaction mixture was allowed to stir at room temperature for 2 h. which resulted in the formation of 6-nitro-$2H$-chromen-2-one 7. 6-amino-$2H$-chromen-2-one 8 was obtained by reduction of 7 using iron powder and NH_4Cl in water. Simultaneously, n-alkoxy benzaldehyde 9 was prepared by o-alkylation of 4-hydroxybenzaldehyde using n-alkyl bromide in the presence of anhydrous K_2CO_3 and catalytic amount KI in DMF. Finally, the desired Schiff bases i.e. 10a-g were obtained by reacting n-alkoxy benzaldehyde 9 with 6-aminocoumarin 8 in the presence of 3–4 drops of
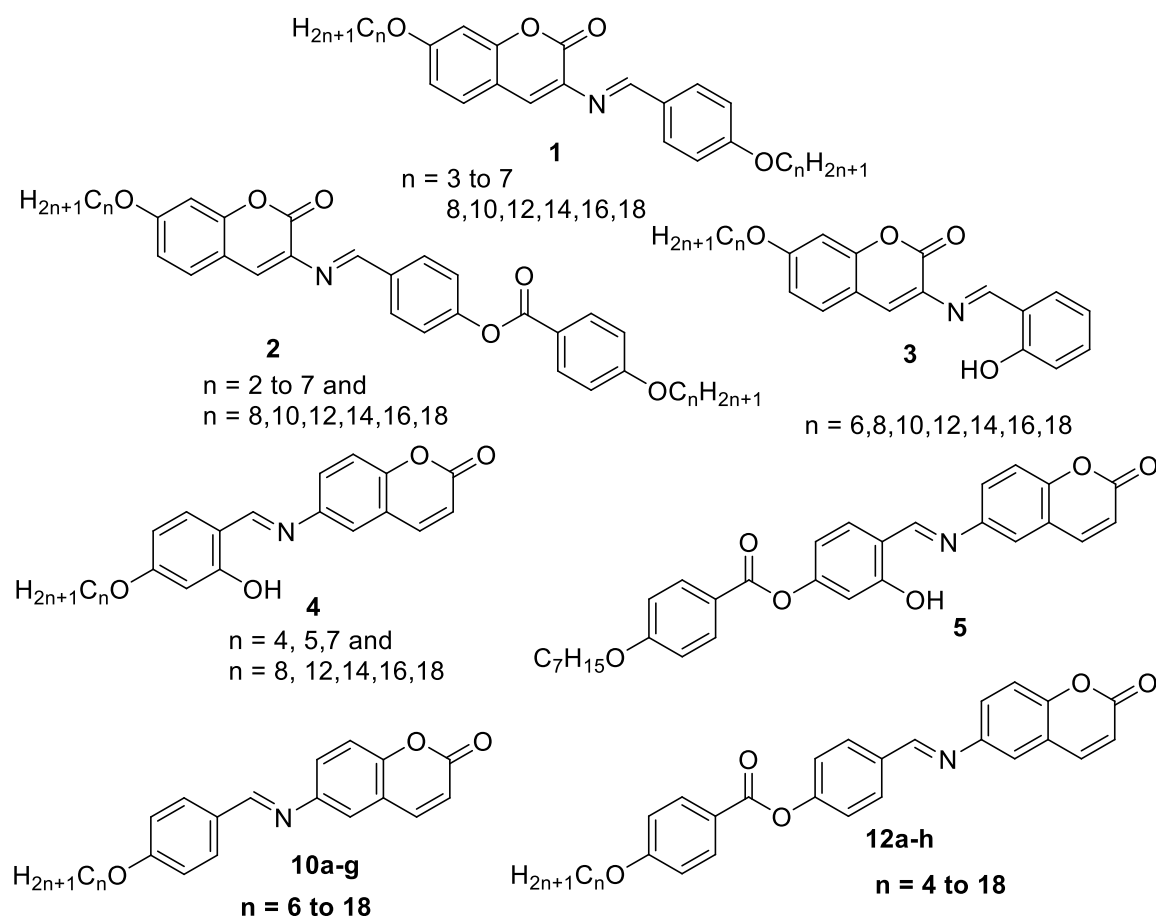

Fig. 1. Coumarin Schiff Base derivatives as thermotropic liquid crystalline material.

glacial acetic acid in absolute ethanol under reflux condition.

In another variations 4-hydroxybenzoic acid was mono alkylated with n-alkyl bromide in KOH, methanol and acidified with HCl, gave 4-(alkyloxy) benzoic acid which was further esterified with 4-hydroxybenzaldehyde using EDC, HOBt and TEA in DCM which gave 4-formylphenyl 4-(alkyloxy) benzoate 11 Finally, the desired Schiff bases i.e. 12a-h were obtained by reacting 8 and 11 in presence of catalytic amount of glacial acetic acid (3–4 drops) in absolute ethanol under reflux condition. All the new Schiff base derivatives 10a-g and 12a-h were characterized by different analytical techniques such as ^{1}H NMR, ^{13}C NMR, ESI-MS, IR and CHN analysis.

In IR spectrum of compounds 10a-g showed an absorption band for –CH stretching in the region of 2922–2834 cm^{-1} and one strong band for the carbonyl group of coumarin ring in the range of 1728–1711 cm^{-1}, while the imine C = N stretching of Schiff Base in the range of 1624 to 1626 cm^{-1}. In ^{1}H NMR, compound 10a-g showed alkyl chain methyl protons as triplet in the range of δ 0.90–0.94 ppm, methylene linkage protons as multiplet from δ 1.26–1.87 and methyleneoxy (–OCH$_2$-) protons were observed as triplet at δ 4.01–4.04 with coupling constant value of 6.4 Hz. For all the compounds, aromatic protons were appeared from δ 6.45 to 6.47 and imine protons in the range of δ 8.41 to 8.42 ppm. In ^{13}C NMR of compounds 10a-g, methyl carbons were observed in the range of δ 14.03 to 14.13 ppm, methylene carbons from δ 22.59–31.93 ppm and methyleneoxy carbon was observed at δ 68.28 ppm. While for all the compounds aromatic carbons were observed from 114.81 to 160.77 ppm. In ^{13}C NMR along with imine carbon and lactone carbonyl carbon at δ 160.77 and 162.26 ppm respectively.

For all the compounds 12a-h, IR spectra showed the alkyl stretching in the region of 2925–2835 cm^{-1}, coumarin carbonyl group and ester carbonyl group as strong band in the range of 1728–1711 cm^{-1}, and the imine C = N stretching of Schiff Base at 1624 cm^{-1}. The methyl and methylene group peaks for compounds 12a-h were in the range of
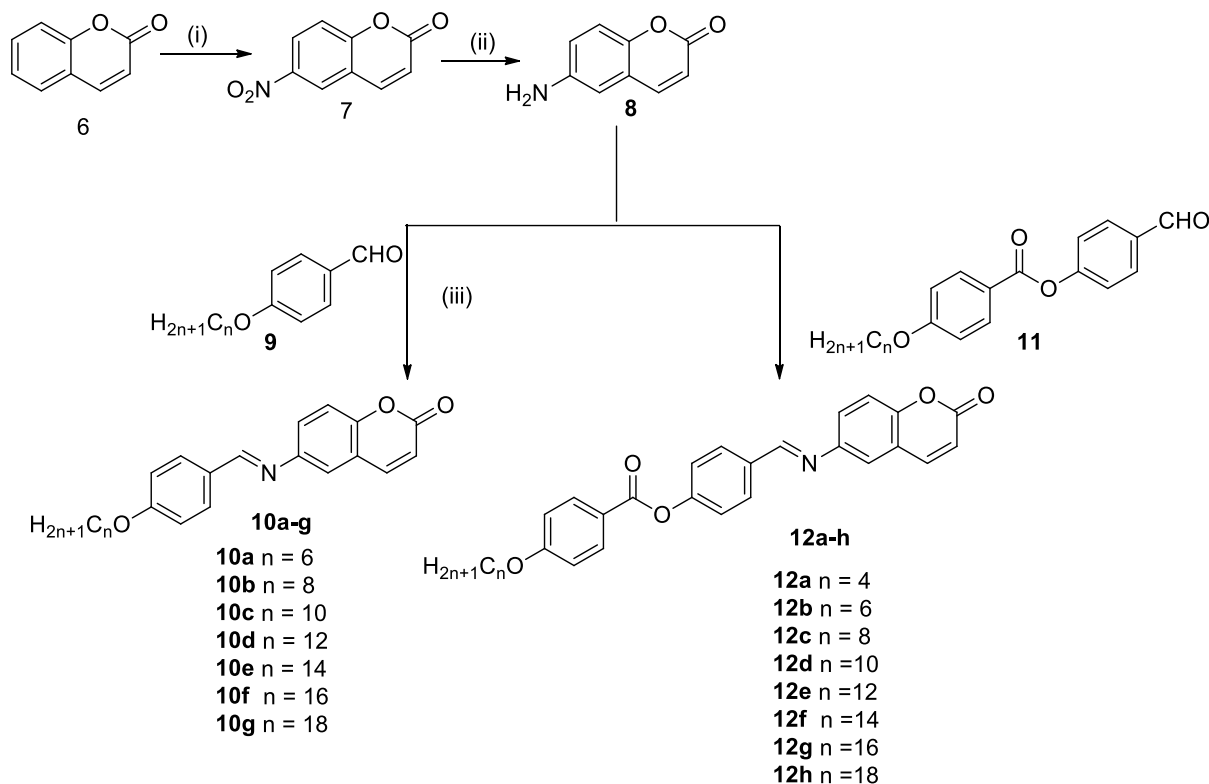
0.91–1.88 ppm, and a methylene group containing oxygen was seen at 4.07 ppm, in ^{1}H NMR. aromatic protons for all the compounds were appeared in the range of 6.49–8.17 ppm and imine proton as singlet at 8.52 ppm. In ^{13}C NMR analysis of compound 12a-h, the methyl and methylene carbons were appeared between 14.13–31.90 ppm, methyleneoxy carbon at 68.41 ppm, aromatic carbons, lactone carbonyl carbon and ester carbonyl carbon appeared from 114.42 to 163.79 ppm and imine carbon was observed at 164.54 ppm.

2.2. Mesomorphic properties

The newly synthesized imine derivatives 10a-g and 12a-h were examined using a polarizing optical microscope. To identify mesophase texture, POM analysis of the compounds were performed as a thin film sandwich between the glass slide and cover at a rate of 10 °C/min during the first cooling cycle and the second heating cycle. Additionally, all the compounds were analyzed using differential scanning calorimetry (DSC) during heating and cooling scans at a rate of 10 °C/min. The thermograms generated were used to measure temperatures associated with phase transition and change in enthalpy (ΔH kJmol^{-1}). POM analysis produced good mesophase textures and transition temperature along with enthalpy changes were calculated using DSC thermograms for all the examined substances after numerous heating and cooling cycles, which are summarized in (Table 1).

2.3. Polarizing optical microscopy (POM) study

Schiff base derivatives 10a-g in which imine derivative with lower alkyloxy chain length did not show any mesogenic behavior during heating and cooling cycle. The compound 10b with octyloxy chain length showed monotropic mesophase of nematic type with the characteristic Schlieren texture (Fig. 2) and changed to crystalline solid on

Reagents and Conditions:(i) HNO$_3$:H$_2$SO$_4$ (1:3)Conc. H$_2$SO$_4$, RT, 2hr (ii) Fe (powder), NH$_4$Cl, H$_2$O Reflux,80°C (iii)EtOH, Cat. AcOH,Reflux 16 hr

Scheme 1. Synthesis of Schiff base derivatives 10a-g and 12a-h.

10a n = 6
10b n = 8
10c n = 10
10d n = 12
10e n = 14
10f n = 16
10g n = 18

12a n = 4
12b n = 6
12c n = 8
12d n = 10
12e n = 12
12f n = 14
12g n = 16
12h n = 18

Table 1
Phase assignments, transition temperature °C of compounds 10a-g and 12a-h as determined by POM and DSC.

Compd	n	2nd heating process[a] Temp °C (ΔH kJmol^{-1})	1st cooling process[a] Temp °C (ΔH kJmol^{-1})
10a	6	Cr148.0(−21.64) Iso	I 92.2(23.15) Cr
10b	8	Cr 124.0(−51.12) I	I 108.0(0.55) N 95.3 (46.25) Cr
10c	10	Cr^{1}97.70(−8.51)Cr^{2}113.1(−20.63) SmA 122.78(−1.19) I	I 116.08(1.72) SmA 94.1 (21.35) Cr
10d	12	Cr 117.8(−17.90) SmA 132.2 (−2.63) I	I 129.6(1.53) SmA 109.0 (18.01) Cr
10e	14	Cr 113.3(−15.34) SmA 137.8 (−3.45) I	I 132.8(3.17)SmA 101.7 (24.06)Cr
10f	16	Cr 108.0(−44.98.01) SmA 134.2 (−3.31)I	I 127.0(3.11) SmA 94.8 (24.47) Cr
10 g	18	Cr 114.7(−39.27) SmA 139.9(−1.3) I	I 116.1(1.8) SmA 93.21 (19.16) Cr
12a	4	Cr 179.1(−31.69) N 315.0(−0.42) I	I 289.4(0.57) N 115.0(9.5) Cr
12b	6	Cr 156.8(−33.01)N 292.2(−0.65) I	I 279.8(0.60)N 127.7 (20.18) Cr
12c	8	Cr 155.9(−24.05)N 274.0(−0.30) I	I 262.1(0.51) N 125.0 (20.01) Cr
12d	10	Cr 133.7(−44.10) SmA 248.0N* 256.1(−4.42) I	I 253.0N* 239.9(4.44) SmA 92.13 (31.00) Cr
12e	12	Cr 135.2(−33.19)SmA 255.7 (−3.55) I	I 243.5(3.05)SmA 104.4 (14.56)Cr
12f	14	Cr 131.7(−34.72)SmA 253.8 (−4.31) I	I 243.4(1.72)SmA 109.8 (22.17) Cr
12 g	16	Cr 137.4(−28.65)SmA 253.6 (−3.73) I	I 246.3(2.64) SmA 122.9 (23.58) Cr
12h	18	Cr 113.1(−35.24) SmA 249.3 (−2.05) I	I 232.7(2.68) SmA 105.3 (26.19) Cr

[a] Cr = Crystal, Iso = isotropic liquid state, *N* = nematic phase, SmA= smectic A phase, *I* = isotropic state, *The phase transitions of the compounds were studied under POM only. The enthalpy values are enclosed in brackets.

further cooling. When octyloxy chain was replaced by decyloxy chain compound 10c exhibited enantiotropic mesophase, on heating compound 10c crystalline solid changed to smectic A mesophase further on heating it converted to isotropic liquid while on cooling cycle isotropic liquid transformed to smectic A mesophase and again further cooling transform to crystalline solid. Compounds 10d-g with higher alkyloxy

chain length (*n* = 12–18) exhibited enantiotropic stable smectic A conic mesophase during the both heating and cooling cycle.

Schiff bases with n alkoxy ester compounds 12a-h have been analyzed for their mesomorphic properties. When the lower alkyloxy chain changed to higher chain length compound 12d with decyloxy chain length on heating cycle exhibited smectic A mesophase further on heating smectic A changed to nematic droplet texture which converted to isotropic liquid on further heating (Fig. 2), while it exhibited nematic first and then smectic A mesophase on cooling. By varied higher alkyloxy chain length *n* = 12 to 18 in compounds 12e-h exhibited enantiotropic smectic A mesophase with very good thermal stability as well as broad temperature range.

2.4. Differential scanning calorimetry study (DSC)

To measure the exact transition temperature and associated energy, differential scanning calorimetry analysis is very important. All the compounds 10a-g and 12a-h were studied for DSC thermograms at a rate of $10\,^\circ$C min^{-1} for both heating–cooling cycle from ambient temperature to isotopic temperature and back. In DSC studies, all the compounds exhibited clear-cut transition temperatures as well as associated enthalpy values in the DSC thermograms, which were further compiled and shown in Table 1.

In DSC analysis, compound 10b showed monotropic phase transition with two exothermic transitions corresponding to I-N and N—Cr at 108.4 °C and 95.3 °C respectively, while only one endotherm for I-Cr transition at 124.0 °C. Compounds 10c and 10d showed three endotherms for Cr1-Cr transition, Cr-N and N-Iso during the heating scan, while on cooling two exotherms (Fig. 3a). From 10e-10 g all the compounds showed two endotherms for Cr-SmA and SmA-I and two exotherms from I-SmA and SmA-Cr during the heating and cooling cycle respectively.

In second series, compound in which lower alkoxy ester attached Schiff base 12a exhibited two endothermic curves for Cr-N and N-Iso at temperature 179.1 °C and 315.0 °C and two exotherms for Iso-N and N—Cr at temperature 289.4 °C and 115.0 °C respectively during cooling cycle. Similar set of transition peaks were observed for compound 12b (Fig. 3c) and 12c with two endothermic curves for Cr-N and N-Iso and two exothermic curves for Iso-N and N—Cr. Replacement of octyloxy group by decyloxy group, compound 12d showed two endotherms for

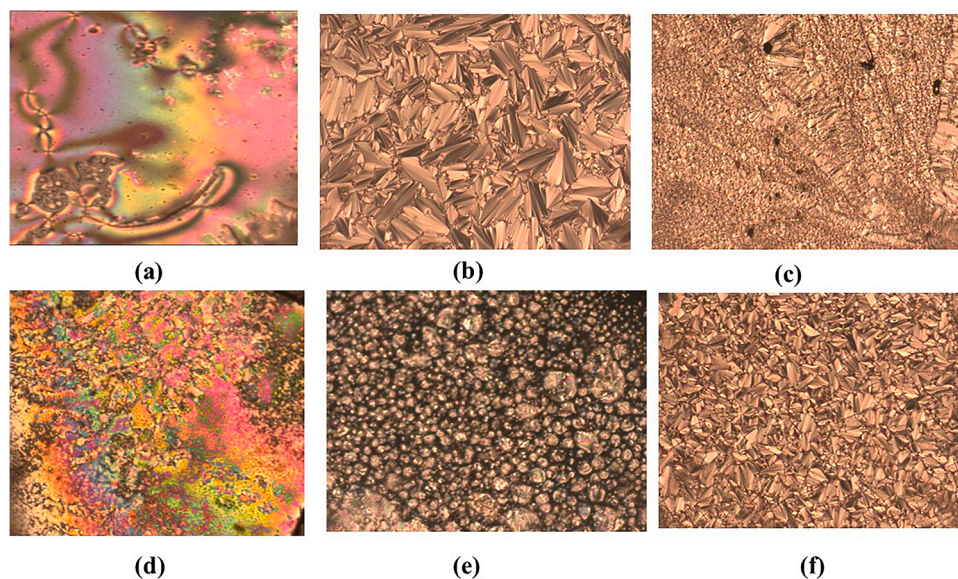**Fig. 2.** POM textures of coumarin Schiff base mesogens (a) Nematic schlieren texture of 10b upon cooling at 108.41 °C; (b) SmA focal conic fan texture of 10d upon heating at 132 °C; (c) SmA transition of 10e on cooling 132.8 (d) Nematic marble texture of 12d on heating at 256.1 °C; (e) Nematic droplet texture of 12d on cooling at 175.4 °C; (f) SmA transition of 12e on further cooling at 243.5 °C.
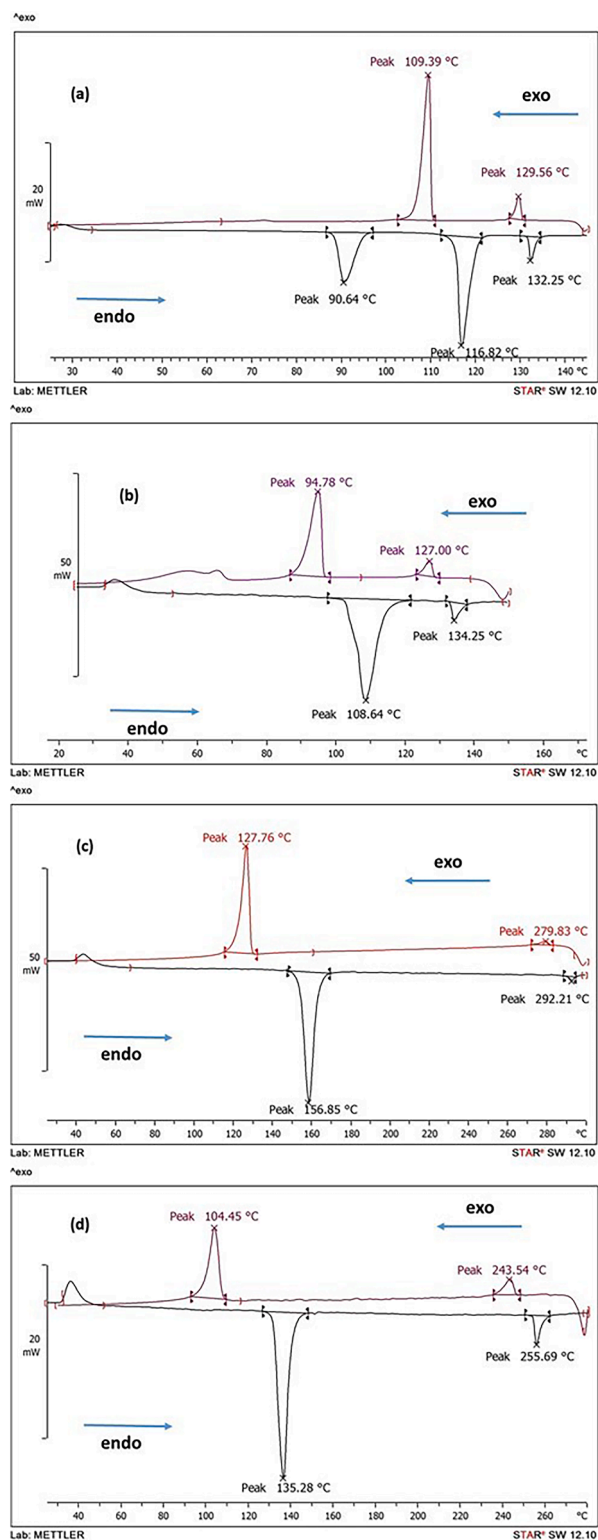
Fig. 3. DSC thermograms of compounds 10d, 10f, 12b and 12e.

Cr-SmA and SmA-I at temperature 133.7 °C and 256.1 °C on heating scan and two exotherms from I-SmA and SmA –Cr at temperature 239.9 °C and 92.1 °C during the cooling cycle, due to very low energy nematic transition was not observed in DSC thermograms, however, it is well observed and captured from POM analysis hence temperature observed in POM analysis were reported in the table. Increasing chain length to dodecyloxy in compound 12e, resulted in enantiotropic smectic

mesophase and showed two endotherms corresponding to Cr-SmA at temperature 135.2 °C and SmA to I at temperature 255.7 °C whereas two exotherms on cooling correspond to I-SmA at temperature 243.5 °C and SmA to Cr at temperature 104.4 °C shown in (Fig. 3d). Higher analogues of this series of compounds 12e-h (with $n = 12$–18) showed two endotherms corresponds to Cr-SmA and SmA-I and two exotherms on cooling corresponds to I-SmA and SmA-Cr.

2.5. X-ray diffraction studies

Compounds of both the homologous series 10a-g and 12a-h were studied for their mesomorphic properties using POM and DSC analysis and showed very good mesophase textures and transition temperatures. Based on this, compounds 10d and 12d were selected and analyzed for powder X-ray diffraction analysis (Fig. 4) and interlayer spacing for peaks observed were calculated using Bragg's diffraction equation from the 2θ values.

In powder XRD analysis of compound 10d at 125 ºC, two peaks were appeared one sharp peak with layer spacing 40.2 Å in the small angle regime while second peak as a broad hump with layer spacing 4.8 Å (Fig. 4a). The sharp peak at the small angle regime has confirmed the correct identification of mesophase which is smectic A. Similarly, compound 12d showed first sharp peak in small angle regime ($d = 40.2$ Å) and second broad hump in wide angle regime ($d = 4.8$ Å) (Fig. 4b) in powder XRD analysis at 240 °C. The same compound when analyzed at 252 °C, the intensity of first sharp peak was decreased as compared to that appeared earlier for smectic A mesophase at lower temperature 240 °C, which further confirms nematic mesophase in compounds 12d However, the diffused broad halo around 4.8 Å has remained unaffected as corresponding to liquid like nature of alkoxy terminal. The orthogonal smectic A mesophase was further confirmed by tilt angle, which was found to be near to zero.

2.6. DFT calculation

2.6.1. The geometrical structures

Gaussian 9 was utilized for performing theoretical DFT calculations employing both DFT and B_3LYP-6–311 G basis set. The optimized geometries of all structures were confirmed as stable, as no imaginary frequencies were observed [45]. A comparative analysis was conducted between the synthesized compound and a previously reported compound 4 which contains a group. The molecular structures of these compounds are depicted in (Fig. 5). All the optimized structures displayed excellent stability, and the frequencies of all compounds were determined using the same basis set for computing various parameters (SI, Figure S1). Using the same method, basis set and optimized molecular structures, calculations of frequency were conducted which were further used for computing different thermodynamic parameters.

2.6.2. Frontier molecular orbitals (FMO's) and molecular electrostatic potential (MEP)-

The highest occupied molecular orbital (HOMO) and lowest unoccupied molecular orbital play distinct roles in the molecule, HOMO represents the highest energy level occupied by electrons functioning as electron donors. Conversely, the LUMO, is characterized as an orbital with the lowest energy that can accept electrons and act as an electron acceptor [46]. As a combined also called Frontier Molecular orbitals (FMO's) provides a reasonable qualitative prediction of both excitation properties and electron transport capability. Additionally, these quantum chemical parameters can be used to determine the reactivity of the molecules. HOMO and LUMO images of all the optimized structures are shown in (SI Figure S2) and (Fig. 6) shows the HOMO and LUMO, their energies and the energy gap of some representative compounds. 10b and Schiff base derivative with ester linkage 12c were compared with the reported compound 4, it is observed that HOMO is mainly appeared on coumarin and attached aromatic ring in compounds 4 and 10b. While

Fig. 4. Powder X-ray diffraction analysis graph as the scattering intensity (in counts) vs the scattering angle, 2θ (a) compound 10d at 125 °C (b) compound 12d at 240 °C (c) compound 12d at 252 °C.

Fig. 5. The estimated molecular geometry of the investigated compounds 4, 10b and 12c.

LUMO is mainly found on coumarin ring however in compound 10b distribution of LUMO is on coumarin ring as well as the aromatic ring partially. In Schiff base derivative 12c with ester linkages, HOMO is located on coumarin and imine part, however, LUMO is located on the coumarin, imine aromatic ring as well as on ester linkage. Molecular electrostatic potentials (MEP) for all synthesized compounds are shown in (SI Fig. S3). Various parameters such as chemical hardness (η) and global softness (S) can be calculated from these HOMO and LUMO

energies [47]. These parameters provide information of charge transfer resistance and photoelectric behavior of the compounds whose results are shown in (Table 2). The global softness $(S) = 1/(E_{LUMO} - E_{HOMO})$, while the chemical hardness $(\eta) = (E_{LUMO} - E_{HOMO})/2$. The degree of global softness (S) may indicate how susceptible the π electron cloud of a more polarizable substance is to disruptions caused by chemical reactions. Chemical hardness (η) shows the charge transfer resistance. The electronegativity (χ) is a measure of the Lewis acidity ability of the

Fig. 6. Frontier Molecular orbitals (FMOs) and Molecular electrostatic potentials (MEP) for the prepared compounds 4, 10b and 12c.

Table 2
Frontier molecular orbitals energies (eV), chemical hardness η(eV), and global softness S, electrophilicity index (ω) of the investigated compounds 4, 10b, 12c.

Comp.	LUMO (eV)	HOMO (eV)	ΔE (eV)	χ	η	s	ω
4	−1.89227	−5.75194	3.85967	−3.8221	1.9298	0.2590	3.78496
10b	−1.81582	−5.66922	3.85339	−3.7416	1.92656	0.2595	3.63489
12c	−1.83241	−5.89752	4.06511	−3.8640	2.03269	0.2460	3.67463

compounds The electrophilicity index (ω), which represents the amount of energy involved in electronic transitions, could also be estim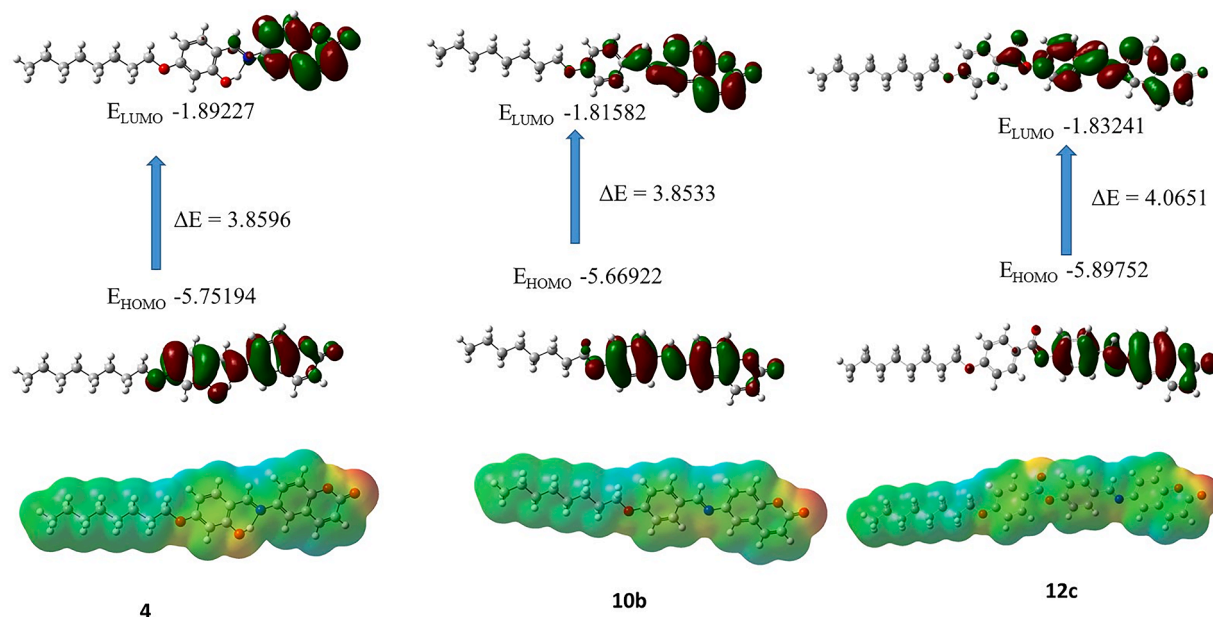ated from the values of the electronegativity and chemical hardness. These descriptors provide valuable insights into the electronic properties of the synthesized compounds. These parameters serve as determinants for assessing the suitability of employing LCs in specific applications. For all the studied compounds, the energy values of the HOMO and LUMO were calculated and used for calculating other parameters such as the global softness and chemical hardness (SI Table S1). An observation can be made that the energy gap between 4 and 10b of these FMOs is not much affected by the additionally –OH group on compound 4, while in 12c with ester linkage effect on energy gap, its ΔE value is greater than the

Schiff base derivatives 4 and 10b, therefore, does not exert an influence on the global softness and so that on chemical hardness as well.

2.6.3. Polarizability, aspect ratio and dipole moment

The impact of polarizability is influenced by various factors, including the size of studied compounds, the type of mesogenic core as well as on the polarity of terminal moiety. Polarizability refers to the sensitivity of a molecular system's electron cloud to the presence of a charge [48]. Consequently, larger molecules exhibit higher polarizability compared to smaller ones. Moreover, the mesophase stability of the liquid crystalline compounds can be affected by changes in the polarizability of the mesogenic core compounds [36]. As a result, our

Table 3
Mesomorphic parameters for heating cycle (°C), polarizability (Bohr^3), dipole moment (Debye), the estimated dimensions (Å), and the aspect ratio of the studied compounds.10a-g and 12a-h.

Comp	n	ΔT$_{Cr}$	ΔT$_{SmA}$	ΔT$_N$	Dipole Moment	Polarizability	Dimensions (Å)		Aspect Ratio L/D
							Length (L)	Width (D)	
10a	6	–	–	–	7.769	307.16	22.31	5.50	4.05
10b	8	12.7		12.7	7.818	330.70	24.88	5.50	4.53
10c	10	22.0	22.0		7.844	353.93	26.66	5.49	4.86
10d	12	20.6	20.0		7.858	376.99	30.00	5.48	5.47
10e	14	31.1	31.1		7.872	399.97	32.56	5.48	5.94
10f	16	32.2	32.2		7.879	422.88	35.13	5.48	6.41
10 g	18	23.7	23.7		7.882	445.73	37.69	5.47	6.88
12a	4	174.4		174.4	9.609	374.11	26.07	5.41	4.82
12b	6	152.1		152.1	9.716	398.06	28.64	5.60	5.12
12c	8	137.1		137.1	9.767	421.489	31.20	5.68	5.49
12d	10	160.9	146.9	14.0	9.796	444.67	33.77	5.73	5.89
12e	12	139.3	139.3		9.810	467.66	36.33	5.76	6.31
12f	14	133.6	133.6		9.819	490.580	38.899	5.77	6.74
12 g	16	123.4	123.4		9.826	513.463	41.464	5.77	7.18
12h	18	127.4	127.4		9.768	536.478	44.017	5.47	8.04

theoretical methodology encompasses the computation of polarizability for the compounds under investigation, with the numerical outcomes presented in (Table 3). Upon comparing the calculated values for 10a-g and 12a-h it is evident that greater terminal alkoxy chain lengths lead to heightened polarizability for the entire compound. It also observed that Schiff base derivatives with ester linkages 12a-h variant display greater polarizability than 10a-g. Additionally, the compounds 12a-h exhibit a broader nematic and smectic mesophase range as compared to the compounds 10a-g. Conversely, the absence of a mesophase in the 10a compound could be attributed to its low polarizability value, leading to reduced end-to-end interactions and subsequently lowering molecular packing density.

The term aspect ratio pertains to the proportion between the length and width of an elongated molecule. This concept holds particular significance in the study of liquid crystals, especially those with rod like structures [49]. The aspect ratio serves as a vital structural characteristic that can elucidate the behavior of liquid crystals and impact their various mesophases. By determining the ratio of molecular length to width, the aspect ratio offers insight into the collision diameter of these molecules. Consequently, this ratio can influence both lateral and terminal interactions between molecules, a correlation that varies based on these values [37,50]. Molecules characterized by higher aspect ratios, indicative of elongation and anisotropy, tend to exhibit a greater propensity for organizing into ordered mesophases, particularly within the smectic and nematic phases, L/D values effectively encapsulate the length-to-diameter ratio of the molecules and their respective aspect ratios, indicating their shape and propensity for certain liquid crystal phases [39,51]. These values describe the dimensions of the molecules and their aspect ratios, which are crucial for determining the types of liquid crystal phases that can form. These findings have been compiled in a tabulated form shown in Table 3, in which the Schiff base derivatives 10a-g, it was noted that there is an overall increase in the range of mesophase as the aspect ratio increases. For instance, compound 10b, featuring an octyloxy chain length, a nematic mesophase range was evident due to its lower aspect ratio compared to 10c-g. However, the prevalence of nematic stability diminishes with longer terminal alkoxy groups, with predominance shifting toward shorter chain lengths due to increasing terminal intermolecular interactions. For compounds 10c-g it is observed that the stability range of smectic mesophase was increased with the increment of aspect ratio. In another series involving homologous Schiff bases 12a-h with ester linkages, a different trend emerged. For compounds 12a-d, with $n = 4$ to10, there was a decrease in the range of nematic mesophase up to $n = 8$ as the aspect ratio increased. Conversely, compound 12d exhibited a notably limited nematic mesomorphic range compared to 12a-c with further increase in aspect ratio. Subsequent compounds 12e-h ($n = 10$ up to 18) experienced an increment of the smectic A mesophase range. An increase in the aspect ratios correlates with increased intermolecular interaction. These interactions as area expands, alongside give rise to the degree of π-π interaction. Consequently, greater molecular packing density enhances the appearance of the more ordered smectic mesophase in higher analogues prevailing over nematic mesophase [37,44,52].

Out of all the electronic parameters, dipole moment is one of them which affects the mesomorphic stability of thermotropic liquid crystalline compounds [53]. Dipole moment value is low for compound 10a has resulted in the absence of any mesophase, while on increasing chain length has increased the dipole moment as a result of the weak intermolecular interactions leading to nematic mesophase in compound 10b (Table 3). Further, on increasing chain length from $n = 10$ to18, the relative increase in dipole moment value allowed side–side interactions which overall resulted in the orthogonal smectic A mesophase. When ester linkage is introduced in between of terminal alkoxy group in compounds 12a-h dipole moment values were relatively high as compared to that of compounds10a-g and hence showed very good total mesophase range stability (Fig. 7). In this particular series with ester linkage, compounds 12a-c with lower dipole moment resulted in

terminal interaction to produce stable nematic mesophase. As terminal alkoxy chain length increased in compounds 12d-h resulted in rise of dipole moment as well as parallel interaction to give rise stable smectic A mesophase

Electronic parameters such as polarizability and dipole moment of compounds 10b and 12c were compared with reference compound 4 (Table 4). Compound 4 with intramolecular hydrogen bonding, has shown very good polarizability leading to stable smectic A mesophase. However, the removal of the hydroxyl group in compound 10b, resulted in a drop in polarizability and the overall formation of comparatively less stable nematic meosphase (Fig. 8). On introduction of ester linkage in compound 12c lead to increase in total polarizability to easily form terminal aggregation and resulted in stable nematic mesophase formation.

3. Conclusion

In the first series of Schiff base derivatives of 6-aminocoumarin, compounds 10a-g were designed with void of hydroxyl group. All the compounds were synthesized, characterized and their mesomorphic properties were studied using POM and DSC analysis. Removal of the hydroxyl group on aldehyde part in compounds 10a-g has resulted in decrease in parallel interaction in lower analogue 10b with $n = 8$ leading to showing monotropic nematic mesophase. Higher analogues of this series, compounds 10c-g ($n = 10$–18) have shown enantiotropic smectic A mesophase, however, their stability were lower as compared to that reported for compounds with ortho hydroxyl group on aldehyde part. In second series, ester linkage has been introduced along with Schiff base in compounds 12a-h. In which, compounds 12a-c ($n = 4$–8) have shown very stable enantiotropic nematic mesophase, while higher analogues 12d-h ($n = 10$–18) have shown enantiotropic smectic A mesophase. Transition of nematic to smectic A mesophase has been observed in compound 12d ($n = 10$) however, the stability of nematic mesophase was very low energy and could not detected in DSC thermograms. Hence, compounds 10d from the first series and 12d from the second series were studied for powder XRD analysis to identify the type of mesophase, which further confirmed orthogonal smectic A mesophase for compound 10d at 125 °C and 12d at 240 °C. Further compound 12d showed nematic behavior at 252 °C in powder XRD analysis. Compounds of both the series as well as reference compound 4 were optimized using DFT calculations. Based on optimized geometries, various structural and electronic parameters were calculated and compared. Overall dipole moment values for compounds 12a-h with ester linkage were found to be much higher as compared to that of compounds 10a-g leading to more intermolecular interactions as well as higher mesophase stability. At the same time removal of the hydroxyl group from reference compound 4 in compound 10b, has resulted in a decrease in polarizability and hence lower intermolecular interaction with less stable nematic mesophase. However, the introduction of ester linkage in compound 12c has enhanced the polarizability which has affected the parallel interactions within the molecules and led to formation of highly stable smectic A mesophase.

3.1. Experimental

Reagent grade chemicals and solvents were purchased from local suppliers and used further after purification. Thin-layer chromatography (TLC) was performed on silica gel F 254 plates. FT- IR spectra were recorded on Bruker spectrometer as KBr pellets. ^{1}H NMR and ^{13}C NMR spectral data were recorded on Advance Bruker 400 spectrometer (400 MHz) with Deuterated chloroform (CDCl$_3$) as solvent and TMS as internal standard. *J* values are in Hz. Thermosinnigan Flash 11–12 series EA was used to carry out for elemental analyses. TG-DTA analyses were carried out using SII EXSTAR60 0 0TG-DTA instrument. Aluminium pans and 2–3 mg sample amounts were used for DSC measurements investigation. 30 ml/min nitrogen gas inert atmosphere and 10 °C/min
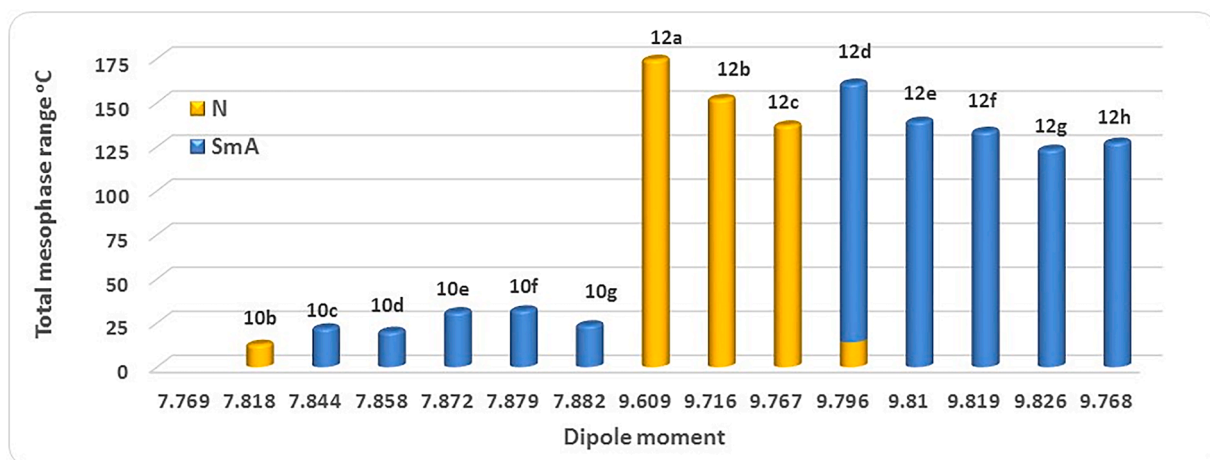
Fig. 7. Graph of the dipole moment versus the total mesophase range of compounds 10a-g and 12a-h.

Table 4
Mesomorphic data for heating cycle (°C), polarizability (Bohr^3), and dipole moment (Debye) of the studied compounds.4, 10b and 12c.

Comp	ΔT_{Cr}	ΔT_{SmA}	ΔT_N	Dipole Moment	Polarizability	Aspect Ratio L/D
4	43.4	43.4		6.674	335.42	4.79
10b	12.74	-	12.74	7.818	330.70	4.53
12c	137.1	-	137.1	9.767	421.489	5.49

heating rate were selected for all measurements and all transitions were recorded from the first cycle of heating and cooling. Utilizing a Polarizing Optical Microscope (POM) LEICA DM 2500P (Wien, Austria) coupled with a CAMERA-LEICA-DFC 295, liquid crystalline properties were investigated. With the sample in a thin film sandwiched between a glass slide and cover, polarized light with a crossed polarizer at an angle of 45° and 10x magnification were used to observe the textures of the compounds. 6-aminocoumarin, 4-alkoxy benzaldehyde, 4-alkoxy benzoic acid, and Schiff base derivatives were synthesized according to literature reported methods with minor modifications [28,31,34,35].

3.2. Synthesis of 6-nitrocoumarin (7)

To a cold solution of coumarin (10.0 g, 68.5 mmol) in concentrated H_2SO_4 (50 mL), was added 20 ml of mixed acid (HNO_3: H_2SO_4 = 1:3, v/v). The resulting mixture was stirred at 0 °C for 15 min and then at room temperature for 2 h. The reaction mixture was poured into ice-cold water to give a white solid. The solid was filtered washed with cold water and recrystallized using acetic acid.

3.3. Synthesis of 6-amino coumarin (8)

To a suspension of 6-nitrocoumarin (10.0 g, 52.38 mmol) and Fe powder (20 g) in water (170 mL) was added ammonium chloride (3.25 g, 60.75 mmol) in several portions over a period of 10 mins. The resulting mixture was heated at 80 °C for 6 h. The completion of the reaction was checked by TLC. After completion of the reaction, the reaction mixture was filtered and brown solid was dissolved in ethyl acetate. The organic layer was filtered to remove insoluble solids and filtrate was concentrated on a rotavapor to give the compound as silky golden crystals (M. P. 158 °C)

3.4. 4-Alkyloxy benzaldehyde (9)

To a solution of 4-hydroxy benzaldehyde (1.0 eq) in DMF (20 mL) was added anhydrous K_2CO_3 (2.5 eq) and stirred at room temperature for 10–15 min. To this mixture, alkyl bromide (1.0 mmol) was added and resulting solution was stirred at room temperature for 16–18 h. The completion of reaction was checked by TLC. After completion of reaction, the reaction mixture was poured into ice-cold water. The crude compounds were obtained was directly used for next step. Yield: 70–85 %.

3.5. Synthesis of 4-(n-alkyloxy) benzoic acid

To a solution of 4-hydroxy benzoic acid (3.5 g, 0.03 mmol, 1 eq) in methanol (25 ml) was added potassium hydroxide followed by N-alkyl bromide (1.2 eq) and refluxed for 7–8 h. Afterward, potassium hydroxide (20 % solution, 5 ml) was added and again refluxed for an
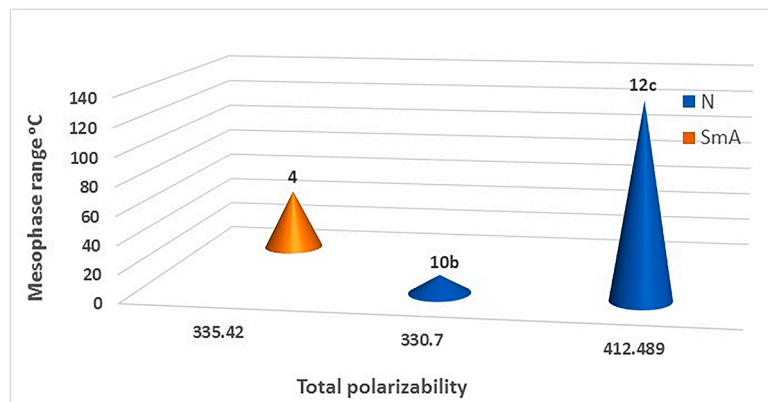

Fig. 8. Graphical relation between the polarizability and the thermal stability of nematic smectic C mesophase for compounds 4, 10b and 12c.

additional two hours. To precipitate 4-(n-alkyloxy) benzoic acid, the reaction mixture was poured into ice-cold water and acidified with dil. HCl. The solid separated was filtered, dried, and recrystallized from ethanol.

3.6. Synthesis of ester of (n-alkyl benzoic acid) (11)

EDC (1.5 eq) and HOBt (1.0 eq.) were added to a solution of 4-(n-alkyloxy) benzoic acid (0.5 g, 1.0 eq) in DCM (25 ml) (2.5 eq.) followed by TEA (2.5 eq) and cooled to 0–5 °C. To this, 4-hydroxy benzaldehyde (0.20 g, 1.0 eq.) was added and stirred at 0–5 °C for additional 30 min and subsequently at room temperature for 20 h. After the reaction was completed on TLC, the mixture was diluted with water (30 mL) and extracted with DCM (3 x 20 mL). The organic layer was separated, washed with water (20 mL), brine solution (20 mL), dried over anhydrous Na_2SO_4, filtered, and concentrated on a rotavapor. The residue was scratched in methanol, filtered and dried to give compound 11 as white solid.

3.7. General procedure for Schiff base (10a-g) and (12a-h)

To a suspension of 6-amino-chromen-2-one (1.0 eq) and 4-alkoxy benzaldehyde/4-formylphenyl 4-(n-alkyloxy) benzoate (1.0 eq) in ethanol (10 mL) was added 3–4 drops of acetic acid and then refluxed for 18–20 h. During the heating, the solid separated. The mixture was cooled, filtered and washed with cold ethanol to give desired compound.

3.8. (E)−6-((4-(Hexyloxy)benzylidene)amino)−2H-chromen-2-one (10a)

Yield: 87 % (0.20 g); Melting Point :143–145 °C; IR (KBr) : 3429, 3086, 2935, 2868 (-C-H), 1725 (C=O, ester), 1625 (-CH=N-), 1605, 1564, 1511, 1483, 1421, 1392, 1308, 1252 (-C-O, alkoxy chain), 1189, 1170, 1138, 1105, 1024, 970, 908, 835, 808, 773, 710, 639, 601 cm^{-1}; ^{1}H NMR (400 MHz CDCl$_3$) : δ ppm 0.94 (t, J = 6.8 Hz, 3H, -C$\underline{H}_3$), 1.35–1.39 (m, 4H, -(H$_2$C)$_2$—C-C—C-O-), 1.48–1.51 (m 2H, -$\underline{H}_2$C-C-C-O-), 1.74–1.87 (m, 2H, -$\underline{H}_2$C—C-O), 4.04 (t, J = 6.8 Hz, 2H, -O-C$\underline{H}_2$-), 6.47 (d, J = 9.6 Hz, 1H, Ar-$\underline{H}$), 7.00 (d, J = 8.8 Hz, 2H, Ar-$\underline{H}$), 7.30 (d, J = 2.0 Hz, 1H, Ar-$\underline{H}$),7.36 (d, J = 8.8 Hz, 1H, Ar-$\underline{H}$), 7.42 (dd, J = 2.4 Hz, and 8.8 Hz, 1H, Ar-$\underline{H}$), 7.74 (d, J = 9.6 Hz, 1H, Ar-$\underline{H}$), 7.85 (d, J = 8.8 Hz, 2H, Ar-$\underline{H}$), 8.42 (s, 1H, -C$\underline{H}$=N); ^{13}C NMR (100 MHz CDCl$_3$) : δ ppm 14.03 (-C$\underline{H}_3$), 22.59 (-C-C$\underline{H}_3$), 25.68 (-C-C-C-C-O), 29.13 (-C-C—C-O), 31.56 (-C-C—C-O), 68.28 (-O-C) 114.81, 117.04, 117.54, 119.18, 119.20, 124.93, 128.60, 130.68, 143.36, 148.83, 151.98, 160.47, 160.77 (C=N), 162.26 (C=O); ESI-MS: 350.17 [M+H]$^+$; Anal. Calc. for C$_{22}$H$_{23}$NO$_3$; C, 75.62; H, 6.63; N, 4.01 % found: C, 75.64; H, 6.60, N, 4.03 % Characterization data for compounds 10b-10 g are provided in supporting information.

3.9. (E)−4-(((2-Oxo-2H-chromen-6-yl)imino)methyl)phenyl 4-(butoxy) benzoate (12a)

White solid; Yield: 84 % (0.22 g); M.P: 312–313℃; IR (KBr): 3038, 2962, 2875 (-C-H), 1731 (C=O, ester), 1628 (-CH=N-), 1601, 1559, 1508, 1475, 1398, 1374, 1323, 1302, 1256 (-C-O, alkoxy chain), 1200, 1159, 1100, 1033, 907, 830, 761, 653cm^{-1}; ^{1}H- NMR (400 MHz, CDCl$_3$): δ ppm 1.02 (t, J = 7.4 Hz, 3H, -$\underline{H}_3$), 1.49–1.59 (m, 2H, -$\underline{H}_2$C-C-O)), 1.80–1.87 (m, 2H, -$\underline{H}_2$C-C-O), 4.07 (t, J = 6.6 Hz, 2H, -O-C$\underline{H}_2$-), 6.48 (d, J = 9.6 Hz, 1H, Ar-$\underline{H}$), 7.0 (d, J = 9.2 Hz, 2H, Ar-$\underline{H}$), 7.34–7.39 (m, 4H, Ar-$\underline{H}$), 7.45 (dd, J = 8.8, 2.4 Hz, 1H, Ar-$\underline{H}$), 7.75 (d, J = 9.6 Hz, 1H, Ar-$\underline{H}$), 7.99 (d, J = 8.4 Hz, 2H, Ar-$\underline{H}$), 8.16 (d, J = 8.8 Hz, 2H, Ar-$\underline{H}$), 8.51 (s, 1H, -C$\underline{H}$=N); ESI-MS: 442.16[M+H]$^+$; Anal. Calc. for C$_{27}$H$_{23}$NO$_5$; C, 73.46; H, 5.25; N, 3.17 % found: C, 73.44; H, 5.23, N, 3.20 % Characterization data for compounds 12b-12 h are provided in supporting information.

References

[1] D. Andrienko, Introduction to liquid crystals, J. Mol. Liq. 267 (2018) 520–541, https://doi.org/10.1016/j.molliq.2018.01.175.
[2] G. Vertogen, W.H. de Jeu, Thermotropic Liquid Crystals, Fundamentals, Springer, Berlin Heidelberg, Germany, 2012.
[3] J.W. Goodby, R.J. Mandle, E.J. Davis, T. Zhong, S.J. Cowling, What makes a liquid crystal? The effect of free volume on soft matter, Liq. Cryst. 42 (2015) 593–622, https://doi.org/10.1080/02678292.2015.1030348.
[4] Y. Matsunaga, S. Miyamoto, Mesomorphic Behavior of 2,4-Bis-(4-alkoxybenzylidene)cyclopentanones and related compounds, Mol. Cryst. Liq. Cryst. Sci. Technol. Sect. A. Mol. Cryst. Liq. Cryst. 237 (1993) 311–317, https://doi.org/10.1080/10587259308030145.
[5] V.S. Bezborodov, S.G. Mikhalyonok, N.M. Kuz'menok, V.I. Lapanik, G. M. Sasnouski, Polyfunctional intermediates for the preparation of liquid-crystalline and anisotropic materials, Liq. Cryst. 42 (2015) 1124–1138, https://doi.org/10.1080/02678292.2015.1025870.
[6] V.K. Narayanaswamy, R.M. Gleiser, K. Kasumbwe, B.E. Aldhubiab, M.V. Attimarad, B. Odhav, Evaluation of halogenated coumarins for antimosquito properties, Sci. World J. (2014) 2014, https://doi.org/10.1155/2014/189824.
[7] G. Jones, W.R. Jackson, C.Y. Choi, W.R. Bergmark, Solvent effects on emission yield and lifetime for coumarin laser dyes. Requirements for a rotatory decay mechanism, J. Phys. Chem. 89 (1985) 294–300, https://doi.org/10.1021/j100248a024.
[8] G.H. Brown, J.W. Doane, V.D. Neff, Struct. Phys. Prop. Liq. Cryst. (1970), https://doi.org/10.1080/10408437008243422.
[9] T. Hatakeyama, L.J. Zhenhai, Hand Book of Thermal Analysis Chichester, Wiley and Sons Ltd., West Sussex, England, 1998.
[10] U. Matern, P. Lüer, D. Kreusch, Biosynthesis of coumarins, Compr. Nat. Prod. Chem. (1999) 623–637, https://doi.org/10.1016/b978-0-08-091283-7.00026-6.
[11] J.W. Goodby, Nano-objects - sculpting and shape in molecular material design (The Pierre Gilles de Gennes ILCS prize lecture), Liq. Cryst. 46 (2019) 1901–1924, https://doi.org/10.1080/02678292.2019.1643508.
[12] Q. Zhang, D.H. Qu, X. Ma, H. Tian, Sol—Gel conversion based on photoswitching between noncovalently and covalently linked netlike supramolecular polymers, Chem. Commun. 49 (2013) 9800–9802, https://doi.org/10.1039/c3cc46297h.
[13] G.Y. Yeap, F. Osman, C.T. Imrie, Non-symmetric dimers: effects of varying the mesogenic linking unit and terminal substituent, Liq. Cryst. 42 (2015) 543–554, https://doi.org/10.1080/02678292.2015.1004843.
[14] S.M. Gomha, H.M. Abdel-aziz, M.G. Badrey, M.M. Abdulla, Efficient synthesis of some new 1,3,4-thiadiazoles and 1,2,4-triazoles linked to pyrazolylcoumarin ring

system as potent 5α-reductase inhibitors, J. Heterocycl. Chem. 56 (2019) 1275–1282, https://doi.org/10.1002/jhet.3487.

[15] S.M. Gomha, H.M. Abdel-aziz, T.Z. Abolibda, S.A. Hassan, M.M. Abdalla, Green synthesis, molecular docking and pharmacological evaluation of new triazolo-thiadiazepinylcoumarine derivatives as sedative-hypnotic scaffold, J. Heterocycl. Chem. 57 (2020) 1034–1043, https://doi.org/10.1002/jhet.3827.

[16] L.A. Alshabanah, L.A. Al-Mutabagani, S.M. Gomha, H.A. Ahmed, Three-component synthesis of some new coumarin derivatives as anticancer agents, Front. Chem. 9 (2022) 1–11, https://doi.org/10.3389/fchem.2021.762248.

[17] S.M. Gomha, H.M. Abdel-aziz, A.A.M. El-Reedy, Facile synthesis of pyrazolo[3,4-c] pyrazoles bearing coumarine ring as anticancer agents, J. Heterocycl. Chem. 55 (2018) 1960–1965, https://doi.org/10.1002/jhet.3235.

[18] T.Z. Abolibda, M. Fathalla, B. Farag, M.E.A. Zaki, S.M. Gomha, Synthesis and molecular docking of some novel 3-thiazolyl-coumarins as inhibitors of VEGFR-2 kinase, Molecules. (2023) 28, https://doi.org/10.3390/molecules28020689.

[19] S.M. Gomha, H.M. Abdel-aziz, Synthesis and antitumor activity of 1,3,4-thiadiazole derivatives bearing coumarine ring, Heterocycles 91 (2015) 583–592, https://doi.org/10.3987/COM-14-13146.

[20] J.Y. Al-Humaidi, A.A. Nayl, M.M. Abdalla, S.M. Gomha, Synthesis and biological activity evaluation of some new coumarin derivatives as potent anticonvulsant and CNS-depressant agents, Polycycl. Aromat. Compd. 43 (2023) 2680–2689, https://doi.org/10.1080/10406638.2022.2050268.

[21] N. Ahmed, W. Zareen, Z. Shafiq, S.F.A. Morais, M. Khalid, A.A. Braga, K. S. Munawar, Y. Yong, A coumarin based Schiff Base: an effective colorimetric sensor for selective detection of F– ion in real samples and DFT studies, Spectrochemica Acta Part A Mol.and Biomol. Spectro. 286 (2023) 121964, https://doi.org/10.1016/j.saa.2022.121964.

[22] J.V. Patil, S. Umar, R. Soni, S.S. Soman, S. Balakrishnan, Design, synthesis and anticancer activity of amide derivatives of substituted 3-methyl-benzofuran-2-carboxylic acid, Synth. Commun. 53 (2023) 217–233, https://doi.org/10.1080/00397911.2022.2160648.

[23] E. Calcio Gaudino, S. Tagliapietra, K. Martina, G. Palmisano, G. Cravotto, Recent advances and perspectives in the synthesis of bioactive coumarins, RSC Adv. 6 (2016) 46394–46405, https://doi.org/10.1039/c6ra07071j.

[24] C.V. Yelamaggad, N.L. Bonde, A.S. Achalkumar, D.S. Shankar Rao, S.K. Prasad, A. K. Prajapati, Frustrated liquid crystals: synthesis and mesomorphic behavior of unsymmetrical dimers possessing chiral and fluorescent entities, Chem. Mater. 19 (2007) 2463–2472, https://doi.org/10.1021/cm0625880.

[25] Y. Morita, H. Ushijima, K. Era, K. Kasatani, H. Okamoto, Synthesis and physico-chemical properties of polar liquid crystal materials incorporating a coumarin skeleton at the terminal position, Mol. Cryst. Liq. Cryst. 494 (2008) 282–292, https://doi.org/10.1080/15421400802430000.

[26] H.T. Srinivasa, B.S. Palakshamurthy, A.K.T. Mohammad, Ethyl 7-hydroxycou-marin-3-carboxylate derivatives: synthesis, characterization and effect of liquid crystal properties, J. Mol. Struct. 1155 (2018) 513–519, https://doi.org/10.1016/j.molstruc.2017.11.055.

[27] C.T. Imrie, L. Taylor, The preparation and properties of low molar mass liquid crystals possessing lateral alkyl chains, Liq. Cryst. 6 (1989) 1–10, https://doi.org/10.1080/02678298908027317.

[28] W.R. Mahmoud, Y.M. Nissan, M.M. Elsawah, R.H. Refaey, M.F. Ragab, K.M. Amin, Neurobehavioral investigation and acetylcholinesterase inhibitory activity study for some new coumarin derivatives, Eur. J. Med. Chem. 182 (2019) 111651, https://doi.org/10.1016/j.ejmech.2019.111651.

[29] S. Guha, S. Lohar, M. Bolte, D.A. Safin, D. Das, Crystal structure and interaction of 6-amino coumarin with nitrite ion for its selective fluorescence detection, Spectrosc. Lett. 45 (2012) 225–235, https://doi.org/10.1080/00387010.2011.605416.

[30] F.N. da Silva, A.S. da Silva, I.H. Bechtold, E. Zapp, A.A. Vieira, Luminescent liquid crystals based on 2,1,3-benzoxadiazole: conducive heterocycle or poor cousin of benzothiadiazole? Liq. Cryst. 46 (2019) 1707–1717, https://doi.org/10.1080/02678292.2019.1595754.

[31] Y. Arakawa, Y. Ishida, K. Komatsu, Y. Arai, H. Tsuji, Thioether-linked benzylideneaniline-based twist-bend nematic liquid crystal dimers: insights into spacer lengths, mesogenic arm structures, and linkage types, Tetrahedron 95 (2021) 132351, https://doi.org/10.1016/j.tet.2021.132351.

[32] H.T. Srinivasa, A.K.T. Mohammad, Influence of terminally attached branched alkyloxy chains on the mesophase behaviour of calamitic liquid crystals, Phase Trans. 94 (2021) 256–269, https://doi.org/10.1080/01411594.2021.1931202.

[33] P. Shah, R. Soni, S.S. Soman, Synthesis and mesomorphic properties of bis ester derivatives of coumarin containing chalcone linkage, J. Mol. Liq. 335 (2021) 116178, https://doi.org/10.1016/j.molliq.2021.116178.

[34] T. Wohrle, I. Wurzbach, J. Kirres, A. Kostidou, N. Kapernaum, J. Litterscheidt, J. C. Haenle, P. Staffeld, A. Baro, F. Giesselmann, S. Laschat, Discotic Liquid Crystals, Chem. Rev. 116 (2016) 1139–1241, https://doi.org/10.1021/acs.chemrev.5b00190.

[35] K.D. Katariya, R. Soni, K.J. Nakum, S.S. Soman, M. Hagaar, Coumarin derivatives containing schiff base and ester mesogenic core: synthesis, mesomorphic behaviour and DFT calculations, J. Mol. Struct. 1262 (2022) 133043, https://doi.org/10.1016/j.molstruc.2022.133043.

[36] R. Soni, K.J. Nakum, K.D. Katariya, S.S. Soman, S. Nada, M. Hagar, Synthesis, mesomorphic properties and DFT calculations of new coumarin Schiff base-ester liquid crystals, Liq. Cryst. 50 (2023) 636–651, https://doi.org/10.1080/02678292.2022.2145378.

[37] S.D. Durgapal, R. Soni, S.S. Soman, A.K. Prajapati, Synthesis and mesomorphic properties of coumarin derivatives with chalcone and imine linkages, J. Mol. Liq. 297 (2020) 111920, https://doi.org/10.1016/j.molliq.2019.111920.

[38] K.D. Katariya, K.J. Nakum, R. Soni, S.S. Soman, M.A. Hagar, Coumarin Schiff base-esters liquid crystals with symmetrical and unsymmetrical alkoxy chains: synthesis, mesomorphic properties and DFT approach, J. Mol. Liq. 357 (2022) 119073, https://doi.org/10.1016/j.molliq.2022.119073.

[39] K.D. Katariya, K.J. Nakum, R. Soni, S.S. Soman, S. Nada, M. Hagar, Coumarin Schiff base derivatives: synthesis, mesomorphic properties, photophysical properties and DFT studies, J. Mol. Struct. 1278 (2023) 134934, https://doi.org/10.1016/j.molstruc.2023.134934.

[40] Y. Jin, Y. hao Ding, Y. jing Dong, Y. Wei, S. hong Hao, B. cheng Feng, Design, synthesis and agricultural evaluation of derivatives of N-Acyl-N-(m-fluoro-benzyl)-6-amino coumarin, Nat. Prod. Res. 36 (2022) 798–804, https://doi.org/10.1080/14786419.2020.1806268.

[41] R. Wang, Q. Wan, F. Feng, Y. Bai, A novel coumarin-based fluorescence chemosensor for Fe3+, Chem. Res. Chinese Univ. 30 (2014) 560–565, https://doi.org/10.1007/s40242-014-3192-1.

[42] M.K. Paul, Y.D. Singh, A. Dey, S.K. Saha, S. Anwar, A.P. Chattopadhyay, Coumarin based emissive rod shaped new schiff base mesogens and their zinc(II) complexes: synthesis, photophysical, mesomorphism, gelation and DFT studies, Liq. Cryst. 43 (2016) 343–360, https://doi.org/10.1080/02678292.2015.1108467.

[43] D. Pegu, J. Deb, S.K. Saha, M.K. Paul, U. Sarkar, Molecular structure, chemical reactivity, nonlinear optical activity and vibrational spectroscopic studies on 6-(4-n-heptyloxybenzoyloxy)-2-hydroxybenzylidene)amino)-2H-chromen-2-one: a combined density functional theory and experimental approach, J. Mol. Struct. 1160 (2018) 167–176, https://doi.org/10.1016/j.molstruc.2018.01.090.

[44] J.V. Patil, R. Soni, A. Nandawana, S.S. Soman, Design of unsymmetric coumarin chalcone derivatives with tunable self-assembling behavior, J. Mol. Struct. 1287 (2023) 135739, https://doi.org/10.1016/j.molstruc.2023.135739.

[45] L.R. Almeida, M.M. Anjos, G.C. Ribeiro, C. Valverde, D.F.S. Machado, G. R. Oliveira, I.H.B. Napolitano, H.C.B. De Oliveira, Synthesis, structural characterization and computational study of a novel amino chalcone: a potential nonlinear optical material, New J. Chem. 41 (2017) 1744–1754, https://doi.org/10.1039/c5nj03214h.

[46] Z.Y. Zhang, J.T. Sun, Y.M. Wang, Z.X. Ge, Y.G. Jia, M. Tian, D.S. Yao, Synthesis and phase behavior of Y-shaped Schiff base liquid crystal oligomers, Liq. Cryst. 50 (2022) 596–611, https://doi.org/10.1080/02678292.2022.2143588.

[47] H.A. Ahmed, E. Mansour, M. Hagar, Mesomorphic study and DFT simulation of calamitic Schiff base liquid crystals with electronically different terminal groups and their binary mixtures, Liq. Cryst. 47 (2020) 1–13, https://doi.org/10.1080/02678292.2020.1794067.

[48] K.D. Katariya, K.J. Nakum, H. Soni, S. Nada, M. Hagar, Imine based Four-Ring Chalcone-Ester Liquid Crystals: synthesis, Characterization, mesomorphic behaviour and DFT approach, J. Mol. Liq. 380 (2023) 121719, https://doi.org/10.1016/j.molliq.2023.121719.

[49] S.Z. Mohammady, D.M. Aldhayan, M.M.T. El-Tahawy, M.T. Alazmid, Y. El Kilany, M.A. Zakaria, K.A. Abu Al-Ola, M. Hagar, Synthesis and DFT investigation of new low-melting supramolecular schiff base ionic liquid crystals, Crystals 12 (2022) 136, https://doi.org/10.3390/cryst12020136 (Basel).

[50] V. Jevtovic, H.A. Ahmed, M.T. Khan, S.A. Al-Zahrani, N. Masood, Y.A. Jeilani, Preparation of laterally chloro-substituted schiff base ester liquid crystals: mesomorphic and optical properties, Crystals 13 (2023) 835, https://doi.org/10.3390/cryst13050835 (Basel).

[51] E.S. Sales, G.M. dos Santos, R.J. Mandle, W.C. Costa, I.H. Bechtold, I.L. Gonçalves, V.L. Eifler-Lima, A.A. Merlo, Insight into out-of-layer fluctuations in the smectic a stability of 3,5-diarylisoxazole liquid crystals, Chemphyschem 21 (2020) 1408–1419, https://doi.org/10.1002/cphc.202000276.

[52] H.E. Gulbas, D.G. Coskun, Y.H. Gursel, B. Bilgin-Eran, Synthesis, characterization and mesomorphic properties of side Chain liquid crystalline oligomer having schiff base type mesogenic group, Adv. Mater. Lett. 5 (2014) 333–338, https://doi.org/10.5185/amlett.2014.amwc.1022.

[53] N.H.S. Ahmed, G.R. Saad, H.A. Ahmed, M. Hagar, New wide-stability four-ring azo/ester/Schiff base liquid crystals: synthesis, mesomorphic, photophysical, and DFT approaches, RSC Adv. 10 (2020) 9643–9656, https://doi.org/10.1039/c9ra10499b.

ChemistrySelect

Research Article
doi.org/10.1002/slct.202303391

Chemistry Europe
European Chemical Societies Publishing

www.chemistryselect.org

Synthesis of pyrazolone derivatives of coumarin as anticancer agents

Jayashree V. Patil,[a] Shubhangi S. Soman,*[a] Shweta Umar,[b] Pankaj Girase,[c] and Suresh Balakrishnan.[b]

Pursuing on our efforts towards searching for efficient anti-cancer agents herein we have designed and synthesized pyrazolone derivatives of 7-amino 4-methyl coumarin and 6-amino coumarin. Anticancer activity of all the compounds were performed against lungs cancer cell line (A549) and breast cancer cell line (MCF-7) using MTT assay. Out of all the compounds, compounds **17c** and **19b** exhibited remarkable activity with IC_{50} value of 1.22 μM and 1.66 μM against lungs cancer cell line (A549) breast cancer cell line (MCF-7) respectively. Consequently, both compounds **17c** and compound **19b** were selected to study their cytotoxicity mechanism using different assays which includes EtBr/AO assay in respective cell, quantification of ROS using DCFH-DA dye. To explore the

behavioral and selective properties of the synthesized molecules, experimental analysis was complemented with computational methods. The electronic and structural parameters for both compound **17c** and **19b** were calculated using density functional theory (DFT) calculations and correlated with the observed biological activity. Molecular docking was conducted to explore the interaction of compounds **17c** and **19b** with pivotal apoptotic genes, namely p53 and caspase 3. Compound **17c** exhibited docking scores of −8.6 and −8.4 kcal/mol for p53 and caspase 3, while compound **19b** showed scores of −9.3 kcal/mol for both genes, significantly surpassing fluorouracil. Hence, compound **17c** and **19b** can be pursued for further studies, including molecular and *In Vivo* investigations.

Introduction

Cancer has become second leading threat to human beings with highest fatality human diseases. DNA mutation, brought on by flaws in the biological repair mechanism leads to unfavorable conditions, are major causes of cancer. Breast cancer and lungs cancer are well-known and very common of all cancers, which are found to be the supreme reason of death.[1] The prevalence of cancer as a worldwide health issue is emphasized by the recent research on the disease's incidence in industrialized and developing nations. Even though there are numerous treatments available to treat this condition, millions

of individuals lose their lives to cancer each year.[2] Therefore, one of the main goals should be to study and explore new anticancer medicines that are dependable, selective, and less cytotoxic. Heterocycles are class of compounds which have found to play important role in many active anti-cancer drugs.[3,4]
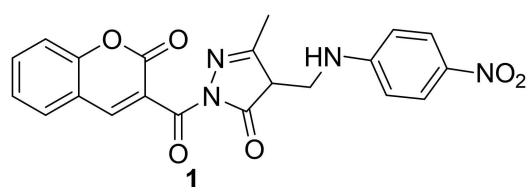
Pyrazolone is one of the important class of heterocyclic compounds and the primary structural component of numerous molecules with biological and pharmacological effects. A wide range of biological effects, including anti-inflammatory,[5] antibacterial,[6] antidepressant, antitubercular[7] and anticancer[8] are displayed by them. The insertion of heterocyclic rings into prospective candidates is a crucial technique utilized to create more effective and selective pharmaceutical prospects. Coumarin scaffold is pervasive in nature and is a highly privileged motif for the development of novel drugs due to its biodiversity and versatility. Many substituted coumarins and their derivatives have been developed synthetically with wide range of biological activities.[9–11] In the recent years, coumarin-pyrazolone derivatives have been reported which contain potent biological activity with less side effects for medicinal applications leading to design and development of derivatives based on this class.[12,13] Sivakumar *et al.* synthesized different pyrazolone derivatives of coumarin and out of all the screened compounds, compound **1** showed nearly equipotent anti-inflammatory and analgesic activity than the standard drug (Figure 1).[14] Moreover, the synthetic and natural drugs containing coumarin scaffolds are well-known as anti-bacterial and antifungal agents. Parekh *et al.* synthesized coumarin pyrazolone derivatives **2** with very good antibacterial activity.[15] Hybrid compound is a combination of two or more heterocyclic pharmacophores into a single molecule to increase its therapeutic activity and affinity

[a] *J. V. Patil, S. S. Soman*
Department of Chemistry
Faculty of Science
The M.S. University of Baroda
Vadodara – 390002, India
E-mail: shubhangiss@rediffmail.com

[b] *S. Umar, S. Balakrishnan.*
Department of Zoology
Faculty of Science
The M.S. University of Baroda
Vadodara – 390002, India

[c] *P. Girase*
Department of Pharmaceutical Chemistry
Discipline of Pharmaceutical Sciences
College of Health Sciences
University of KwaZulu-Natal (Westville)
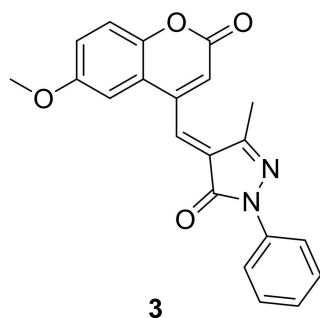*Durban, 4000, South Africa*

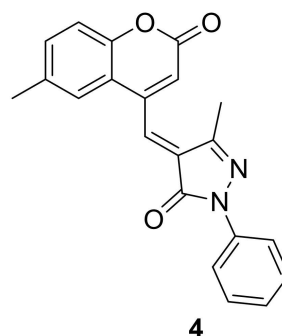💻 *Supporting information for this article is available on the WWW under https://doi.org/10.1002/slct.202303391*

ChemistrySelect

Research Article
doi.org/10.1002/slct.202303391

Chemistry
Europe
European Chemical
Societies Publishing

1
Anti-inflammatory activity
% Inhibition after 4h =61.90%
% Inhibition after 6h =71.96%

2
Antibacterial activity
Gram-positive *E. coli*-11μgmL^{-1}
Gram-Negative *S. aureus*-11μgmL^{-1}

3
Anticancer Activity
Non-small lung cancer NCI-H23 (GI -69.69)
Breast cancer T-47D (GI-44.14)

4
Anticancer Activity
Non-small lung cancer NCI-H23 (GI -48.49)
Breast cancer T-47D (GI-34.19)

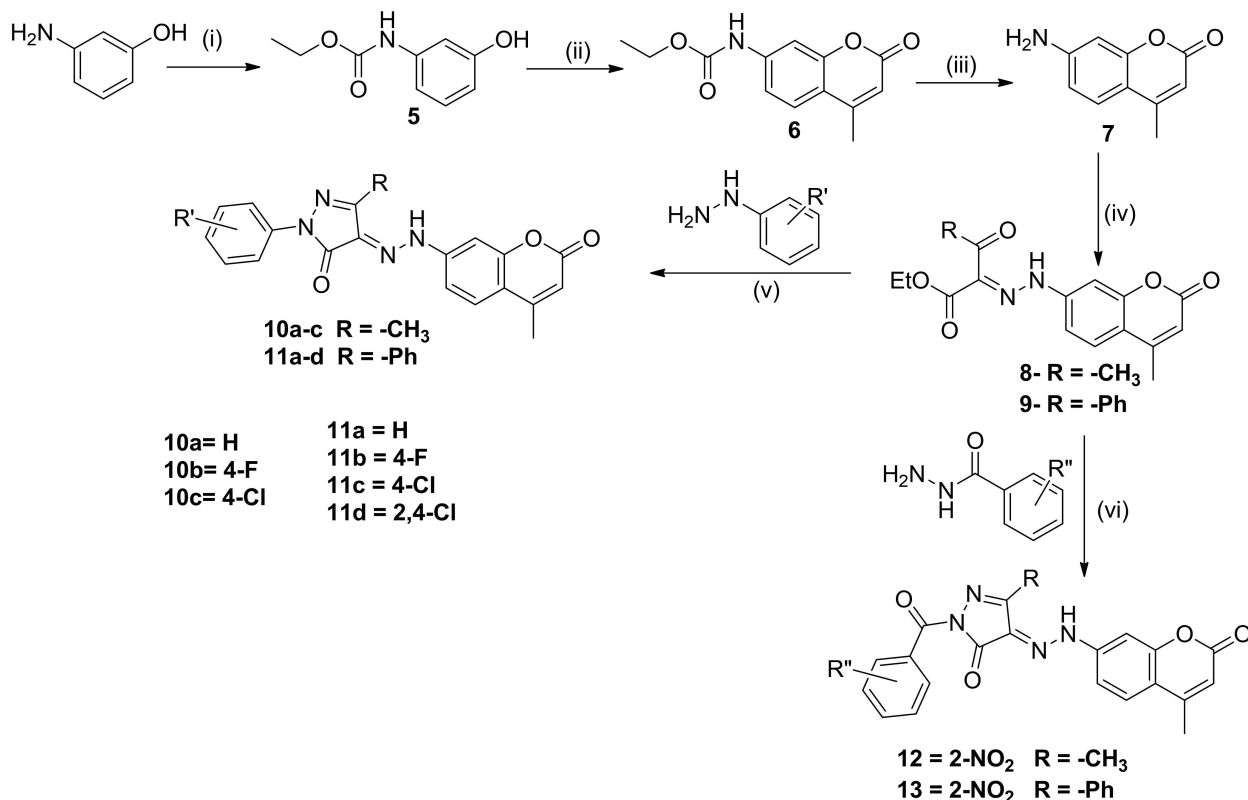**Figure 1.** Coumarin-pyrazolone derivatives with different biological applications.

while lowering adverse effects and combating drug resistance. Thus, coumarin-containing hybrids occupy an important position in the recent research in anticancer agents. Kulkarni *et al.* synthesized series of novel coumarin-pyrazolones with excellent yield for their anticancer activities with different substituent like methoxy, methyl group on coumarin nucleus. Compounds **3** showed marked anticancer activity against non-small lung cancer cell line (NCI–H23) and breast cancer (T-47D) and compound **4** is moderately active against both (NCI–H23) and (T-47D).[16] Therefore, coumarin moiety hybridized with additional anticancer pharmacophores may result in novel anticancer candidates with low toxicity, high specificity, and great efficacy against both drug-susceptible and drug-resistant cancers.

On the basis of the above facts and our ongoing focus on developing novel candidates featuring potential anticancer activity of coumarin hybrids[17–19] we synthesized a new series of pyrazolone derivatives of 7-amino 4-methylcoumarin and 6-aminocoumarin. These molecules were studied against Lungs cancer cell lines (A549) and Breast cancer cell lines (MCF-7) for their anticancer activities using MTT assay. Furthermore, the experimental findings were fine-tuned through the utilization of density functional theory (DFT) investigations.

Results and discussion

Chemistry

Compounds **10a–c**, **11a–d**, **12**, **13** were synthesized from 7-amino-4-methylcoumarin **7** (Scheme 1). In the first step carbamate protection of 3-aminophenol was carried out followed by Pechmann reaction to give 7-carboethoxy amino coumarin **6** with moderate yield (70%). Further, carbamate deprotection of carbamate group in compound **6** was carried out under acidic conditions (sulfuric acid: acetic acid (1:1)) to give desired 7-amino-4-methylcoumarin **7** with yield 62%. Further diazotization of compound **7** was carried out by dissolving compound **7** in concentrated HCl and Acetic Acid (1:1) and stirred until amine completely dissolved then the mixture cooled to temperature (0–5 °C). Sodium nitrite solution in water was then added dropwise with vigorous stirring during 30 minutes then this solution was poured into the cold solution of sodium acetate, ethyl acetoacetate (Scheme 1) or ethyl benzoyl acetate in absolute ethanol, then stirred for completion of reaction at room temperature for 2 hours to give compound **8** (with Ethyl acetoacetate) with good yield (76%) and compound **9** (with Ethyl benzoyl acetate) with good yield (85%). Lastly, pyrazolone synthesis was carried out, for that compound **8** and **9** were refluxed with different substituted phenyl hydrazines in absolute ethanol to gives pyrazolone derivatives **10a–c** and **11a–d** with moderate to good yield in

ChemistrySelect

| Research Article
doi.org/10.1002/slct.202303391

**Chemistry
Europe**

European Chemical
Societies Publishing

Reaction Conditions: (i) CH_3CH_2OCOCl, ethyl acetate, rt;(ii) CH_3COCH_2COOEt, H_2SO_4:C_2H_5OH(3:7),rt; (iii) H_2SO_4:CH_3COOH(1:1),reflux; (iv) $NaNO_2$; HCl:AcOH(1:2),Sodium acetate,EAA/Ethyl benzoyl acetate Ethanol,0°Cto 5°C; (v)/(vi) absolute Ethanol,1-2 drops AcOH, reflux

Scheme 1. Pyrazolone derivatives **10a–c**, **11a–d**, **12** and **13**.
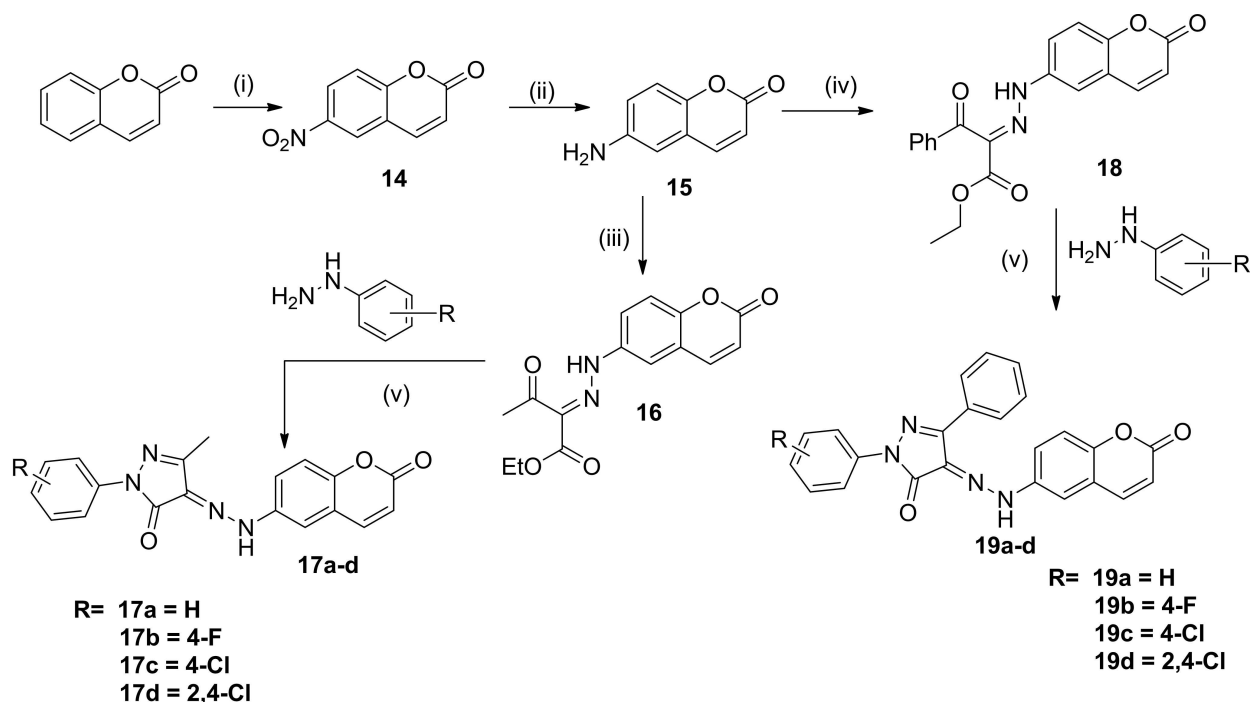
the range of 72–89% and substituted phenyl hydrazides gave pyrazolone derivatives **12** and **13** with good yield (70–85%). All the final compounds were characterized by using different analytical techniques such as ^{1}H-NMR, ^{13}C-NMR, IR, ESI-MS and CHN analysis.

When methyl group is attached to pyrazolone ring in compound **10a–c**, the IR spectra of compounds **10a–c** showed one band for N–H stretching in the range of 3075–3450 cm^{-1}, while carbonyl stretching for lactone at 1729–1740 cm^{-1} and for amide carbonyl frequency at 1611–1672 cm^{-1}. The —C═N stretching frequency of pyrazolone ring observed from 1530–1560 cm^{-1}. In ^{1}H-NMR analysis, compound **10a** exhibited two singlets one for methyl group of coumarin ring at δ 2.41 and other for methyl group of pyrazolone ring at δ 2.46. Compound **10a** showed all aromatic protons in region of δ 6.27–7.97 and N–H proton at δ 13.58. ^{13}C-NMR of compound **10a** showed two —CH$_3$ carbons at δ 11.85 and 18.72 ppm, aromatic carbons in the range of δ 103.15–157.44 ppm along with amide carbonyl carbon observed at δ 155.00, while lactone carbonyl carbon was observed at 157.44 ppm. In ESI-MS analysis of compound **10a**, it showed [M$^+$H]$^+$peak at 361.13.

In compounds **11a–d** when phenyl ring is attached to the pyrazolone ring in place of methyl group, the IR spectra of compound **11a–d**, N–H stretching band was observed in the

range of 3075–3450 cm^{-1}, stretching frequency for carbonyl of lactone was observed at 1720–1730 cm^{-1} and for amide carbonyl frequency at 1614–1652 cm^{-1}. —C═N stretching frequency of pyrazolone ring observed from 1526–1558 cm^{-1}. In ^{1}H-NMR spectrum of compound **11c**, —CH$_3$ protons for only one methyl was observed as singlet at δ 2.44 which is attached to 4th carbon of coumarin ring. Aromatic protons of compound **11c** observed in the range of δ 6.25–8.16. One N–H proton appears at δ 13.89 as a singlet. In ^{13}C-NMR of compound **11c**, one —CH$_3$ carbons was observed at δ 18.73, aromatic carbons in the range of δ 103.34–160.57 ppm along with amide carbonyl carbon and lactone carbonyl carbon. ESI-MS analysis of compound **11c** exhibited [M$^+$H]$^+$peak at 457.11.

We have also synthesized pyrazolone derivatives of 6-amino coumarin. First we have synthesized 6-aminocoumarin from simple coumarin. Nitration reaction of coumarin carried out by using nitrating mixture of H_2SO_4 and HNO_3 which gave 6-nitrocoumarin **14** with very good yield 92% which on reduction by using Fe powder ammonium chloride in water gave 6-aminocoumarin **15** (yield:52%) (Scheme 2). Diazotisation of 6-aminocoumarin was carried out by using ethyl acetoacetate and ethyl benzoyl acetate (Scheme 2) to give compounds **16** with good yield upto 83% and **18** (yield:86%). Compounds **16** and **18** were refluxed with different substituted phenyl

ChemistrySelect

Research Article
doi.org/10.1002/slct.202303391

Chemistry Europe
European Chemical
Societies Publishing

Reaction Conditions: (i)HNO$_3$:H$_2$SO$_4$ (1:3) Conc. H$_2$SO$_4$ RT, 2hr (ii)Fe (powder), NH$_4$Cl,H$_2$O, 80°C
(iii)/(iv) NaNO$_2$; HCl:AcOH(1:2),Sodium acetate,EAA/Ethyl benzoyl acetate Ethanol,0°Cto 5°C;
(v)Ethanol,1-2 drops AcOH, reflux

Scheme 2. Pyrazolone derivatives **17 a–d** and **19 a–d**.

hydrazine in absolute ethanol with addition of catalytic amount of glacial acetic acid to give pyrazolone derivatives **17 a–d** and **19 a–d** with good yields in range of 70–75%. All the final compounds were characterized using ¹H-NMR, ¹³C-NMR, IR, ESI-MS and CHN analysis.

The IR spectra of compounds **17 a–d** showed one band for N–H stretching in the range of 3416–3438 cm^{-1}, lactone carbonyl at 1712–1725 cm^{-1} and amide carbonyl at 1654–1687 cm^{-1}. The —C≡N pyrazolone ring observed at 1530–1565 cm^{-1}. In ¹H-NMR spectrum of compound **17 c**, methyl attached pyrazolone ring appeared at δ 2.41 and all aromatic protons appeared the range of δ 6.54–7.96, while N–H proton at δ 13.65 as a singlet. In ¹³C-NMR of **17 c** one peak at 11.56 ppm was observed for one methyl group attached to pyrazolone ring. All aromatic carbons observed in the range of δ 114.71 to 159.57 including amide carbonyl carbon and lactone carbonyl carbon. In IR spectra of compounds **19 a–d**, phenyl ring attached to pyrazolone in place of methyl, the N–H stretching observed in the range of 3425–3445 cm^{-1}, lactone carbonyl stretching at 1713–1721 cm^{-1}and amide carbonyl observed at 1657–1670 cm^{-1}. In ¹H-NMR similar pattern was observed as previous one, only additional protons were observed in aromatic region due to attachment of phenyl on pyrazolone ring, aromatic protons observed from δ 6.44–8.23,

while N–H proton observed in the range δ12.80–14.00. In ¹³C-NMR of compound **19 a–d**, all the aromatic carbons as well as amide and lactone carbonyl carbon observed between δ 113.91–160.05 ppm.

Biological Evaluation

Anticancer activity by MTT assay:

Pyrazolone derivatives of 7-amino 4-methyl coumarin **10 a–c, 11 a–d** on reaction with substituted hydrazines and hydrazides (for **12** and **13**) with methyl or phenyl group attached to pyrazolone ring at third position were studied for their anticancer activity using MTT assay against A549 (Lung cancer cell line), MCF-7 (Breast cancer cell line) (Table 1). In methyl substituted pyrazolone derivatives (**10 a–c**), compound **10 a** showed poor activity against both the tested cell lines, while substitution of 4-fluoro group on aryl ring of hydrazine part in compound **10 b**, resulted in improvement of activity against A549 cell line with IC$_{50}$ value 2.32 ± 0.006 μM and showed moderate activity against MCF-7 cell line with IC$_{50}$ value 18.6 ± 0.008 μM. On replacing 4-fluoro with 4-chloro in compound **10 c**, resulted in loss of anticancer activity against A549 cell lines

ChemistrySelect

Research Article
doi.org/10.1002/slct.202303391

Chemistry
Europe
European Chemical
Societies Publishing

Table 1. Anticancer activity against A549 (Lungs cancer cell line), MCF-7 (Breast cancer cell line) for compounds **10a–c**, **11a–d**, **12** and **13**.

Compound	IC$_{50}$ μM[a]	
	A549	MCF-7
10a	141.7 ± 2.4	86.9 ± 6.08
10b	2.32 ± 0.06	18.6 ± 0.08
10c	1145 ± 17.9	624 ± 12.2
11a	62.4 ± 3.6	32.6 ± 4.02
11b	1.26 ± 0.005	5.9 ± 0.074
11c	809.3 ± 7.69	301.2 ± 8.5
11d	167.8 ± 3.98	206.5 ± 10.23
12	382 ± 12.1	417.5 ± 13.2
13	2.34 ± 0.063	10.3 ± 0.056
Fluorouracil	11.13 ± 0.083	45.04 ± 1.02

[a]IC$_{50}$ values were determined based on MTT assay using GraphPad Prism software. Each experiment was performed in triplicates.

Table 2. Anticancer activity against A549 (Lung cancer cell line), MCF-7 (Breast cancer cell line) for compounds **17a–d** and **19a–d**.

Compound	IC$_{50}$ μM[a]	
	A549	MCF-7
17a	1.44 ± 0.068	9.14 ± 0.98
17b	12.48 ± 1.06	8.6 ± 0.056
17c	1.22 ± 0.048	65.29 ± 1.81
17d	34.34 ± 1.67	59.6 ± 3.8
19a	4.11 ± 0.048	2.21 ± 0.014
19b	3.32 ± 0.058	1.66 ± 0.015
19c	6.10 ± 0.050	14 ± 0.011
19d	2.20 ± 0.053	19.76 ± 0.089
Fluorouracil	11.13 ± 0.083	45.04 ± 1.02

[a]IC$_{50}$ values were determined based on MTT assay using GraphPad Prism software. Each experiment was performed in triplicates.

and MCF-7 cell lines. Replacing methyl substituent by phenyl in pyrazolone derivatives (**11a–d**) has shown improvement in anticancer activity. Compound **11a** showed poor activity but activity was found to be good as compared to methyl attached to pyrazolone in compound **10a**. Whereas 4-fluoro analogue in compound **11b** showed very good improvement in anticancer activity with IC$_{50}$ values 1.26 ± 0.005 μM and 5.9 ± 0.074 μM against A549 and MCF-7 cell lines respectively. On replacing 4-fluoro with 4-chloro in compound **11c** resulted in drastic drop in activity against both tested cell lines. Addition of one more chloro as 2,4-dichloro in compound **11d** showed slight increase in activity against both tested cell line as compared to compound **11c**.

On reaction with hydrazides from compound **12** (R = —CH$_3$) and **13** (R = —Ph), compound **12** with electron withdrawing group 2-NO$_2$ attached to phenyl ring showed poor anticancer activity. Interestingly, similar variation on phenyl substituted pyrazolone derivative, compound **13** showed very good anticancer activity as compared to standard drug, with IC$_{50}$ value 2.34 ± 0.063 μM against A549 cell line and that of 10.3 ± 0.056 μM against MCF-7 breast cancer cell line (Table 2).

In another variation we have also synthesized pyrazolone derivatives with 6-aminocoumarin by changing the position of amino group change from 7th position to 6th in compound **15** to give pyrazolone derivatives **17a–d** and **19a–d** and all synthesized compounds were also studied by MTT assay for their anticancer activity. In these particular series with methyl pyrazolone derivatives **17a–d** (R = —CH$_3$), compound **17a** showed very good activity with IC$_{50}$ values 1.44 ± 0.068 μM against A549 tested cell lines as compared to that of standard drug, while remained moderately active against MCF-7 cell line with IC$_{50}$ value 9.14 ± 0.098 μM. Compound **17b** with 4-fluoro as a substituent on aryl ring of hydrazine showed poor activity against A549 tested cell line however activity against MCF-7 cell line remained moderate with IC$_{50}$ value 8.6 ± 0.56 μM. Moreover, replacing 4-fluoro with 4-chloro in compound **17c** showed very excellent activity against A549 cell line with IC$_{50}$ value 1.22 ±

0.048 μM and slight drop in activity against MCF-7 cell line as compared to standard drug. Interestingly, 2,4-dichloro substitution in compound **17d** resulted in loss of anticancer activity against both tested cell line.

In this series with phenyl pyrazolone derivatives **19a–d**, compound **19a** exhibited good activity against A549 cell line with IC$_{50}$ values 4.11 ± 0.48 μM and showed very good activity against MCF-7 cell line as compared to that of standard drug with IC$_{50}$ values 2.21 ± 0.014 μM. Interestingly, substitution of 4-fluoro in compound **19b** resulted in improvement of anticancer activity against both cell lines A549 and MCF-7 with IC$_{50}$ value 3.32 ± 0.058 μM and 1.66 ± 0.015 μM respectively.

On replacing 4-fluoro with 4-chloro substituent in compound **19c** and 2,4-dichloro in compound **19d** resulted in loss of activity against MCF-7 cell line, while compound **19d** showed improvement in activity against A549 cell line (IC$_{50}$ 2.20 ± 0.053 μM).

As compared to pyrazolone derivatives of 7-amino 4-methyl coumarin, pyrazolone derivatives of 6-amino coumarin showed better anticancer activity against both tested cell lines. Compound **17c** (IC$_{50}$ 1.22 ± 0.048 μM against A549 cell line) and compound **19b** (IC$_{50}$ 1.66 ± 0.015 μM against MCF-7 cell line) were studied for cytotoxicity pathway using Ethidium bromide/acridine orange staining assay and ROS activity.

Ethidium bromide/acridine orange staining assay:

The Ethidium Bromide (EtBr) and Acridine Orange (AO) staining assay was conducted with compound **17c** and compound **19b** for the A549 cell line and MCF-7 cell line, respectively. This experimental validation is essential to elucidate the impact of compound **17c** and compound **19b** on the respective cancer cell lines. Ethidium bromide selectively stains cells that have lost membrane integrity, while the essential dye acridine orange stains both live and dead cells. In the EtBr/AO dye staining, necrotic cells exhibit red fluorescence, live cells appear green, early apoptotic cells with evident condensation also exhibit

ChemistrySelect

Research Article
doi.org/10.1002/slct.202303391

Chemistry Europe
European Chemical
Societies Publishing

green fluorescence, and late apoptotic cells with condensation and fragmentation display an orange fluorescence. When cells were treated with IC_{50} concentrations of compound **17c** and compound **19b**, it was observed that the A549 cell line predominantly exhibited late apoptotic characteristics (Figure 2a–c), with no cells in necrosis. While in compound **19b** the majority of the MCF-7 cell line's cells displayed early apoptotic features (Figure 2d–f), with only a limited number in necrosis.

DCFH-DA Assay:

Most chemotherapeutics trigger an overproduction of ROS that surpasses the essential threshold required to induce cytotoxic effects in cancer cells.[20] These heightened levels of ROS are crucial for initiating apoptosis through pathways involving p53 and caspase-8, as well as Fas-associated cell death. According to Ramsey and Sharpless,[21] p53, a redox-sensitive transcription factor, detects increased ROS levels and triggers apoptosis in cancer cells. As a result, this investigation focused on evaluating ROS levels in compounds **17c** and **19b** within the A549 and MCF-7 cell lines, respectively (Figure 3). The marked elevation of ROS levels in both cell lines at the IC_{50} concentration was strongly confirmed by the results.
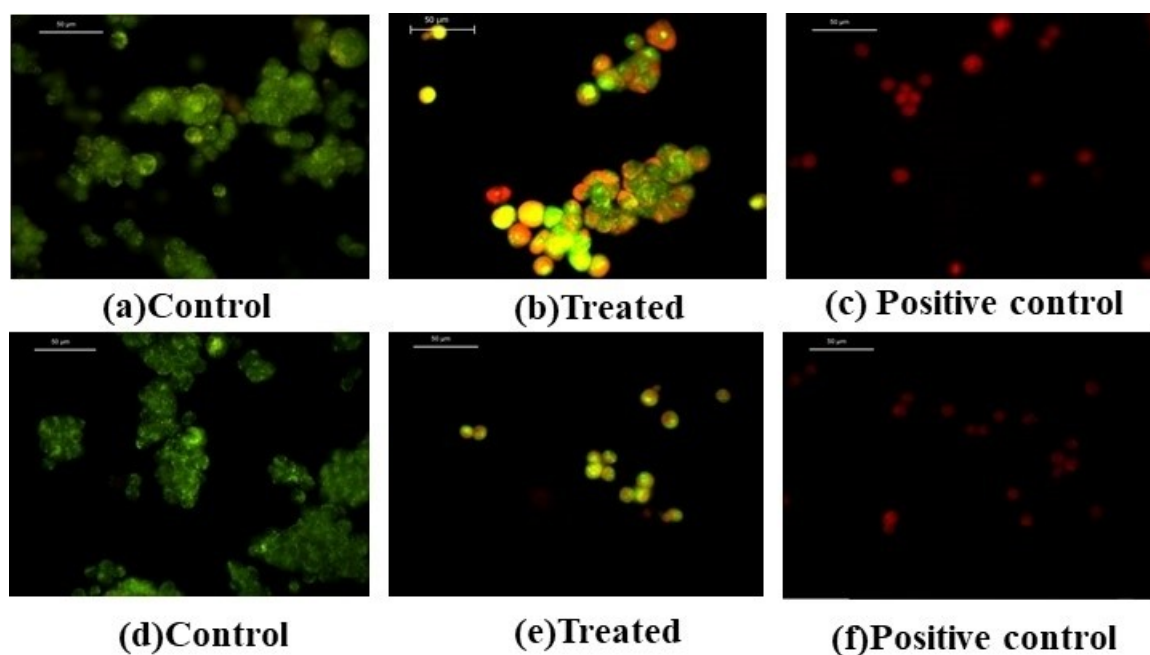

Figure 2. EtBr/AO assay: Performed with (i)A549 Lung cancer cell line for **17c (a,b,c)** images represent control, treated, positive control (ii) MCF-7 breast cancer cell line (d,e,f). For compound **19b, (d, e, f)** Images represent control, IC_{50} conc. of compound **19b** treated and positive control in MCF-7 cell line.
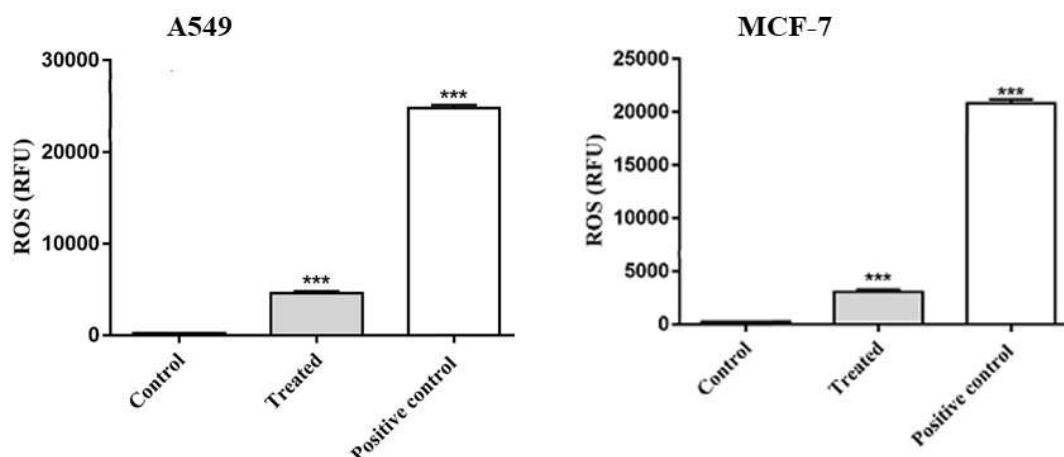

Figure 3. DCFH-DA assay to Estimate the intracellular reactive oxygen species (ROS) level by for compound **17c** in A549 and **19b** in MCF-7 respectively. (***$p \leq .001$).

ChemistrySelect

Research Article
doi.org/10.1002/slct.202303391

Chemistry Europe
European Chemical
Societies Publishing

Table 3. Molecular properties (in eV) compounds **17c** and **19b**.

Parameters	Compound **17c**	Compound **19b**
E_{HOMO} (eV)	−5.9536	−5.7756
E_{LUMO} (eV)	−2.7756	−2.8237
$E_{HOMO}-E_{LUMO}$ gap ΔE (eV)	3.178	2.952
Ionization potential (I) (eV)	5.9536	5.7756
Electron affinity (EA) (eV)	2.7756	2.8237
Global hardness (η)	1.589	1.4760
Global softness (S)	0.3146	0.3387
Electronegativity (χ)	4.3646	4.2996
Electrophilicity index (ω)	5.9942	6.2638
Chemical potential (μ)	−4.3646	−4.2996

DFT Study:

The geometrical structures of both active compounds **17c** and **19b** were optimized using the Gaussian 09 software B3LYP/6–31G level of theory under (d, p) basis set. Further, Figure 4 illustrates the estimated optimized structures of compounds **17c** and **19b** with a true minimum energy.
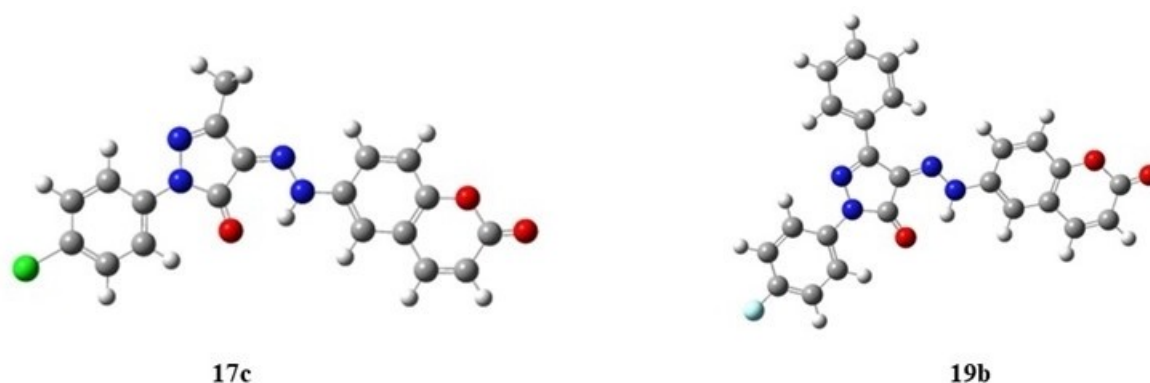
The kinetic as well as chemical stability of the both the compounds **17c** and **19b** were calculated based energy difference between highest occupied molecular orbital (HOMO) and lowest molecular unoccupied molecular orbital (LUMO).[22] For both compounds their frontier molecular orbitals (FMO) are shown in Figure 4. The negative value of E_{HOMO} and E_{LUMO} indicates the stability of compounds.[23] The energy gap ($E_{HOMO}-E_{LUMO}$) provides insights into to the kinetic stability and chemical reactivity of the molecules.[24] A molecule with a lower energy gap ($E_{HOMO}-E_{LUMO}$) signifies a high degree of intramolecular transfer of an electron from the donor to the acceptor.[25] For compounds **17c** and **19b** HOMO was predominantly localized around the pyrazolone nucleus and aromatic ring attached to pyrazolone, while the LUMO was localized on the coumarin ring as well as on the pyrazolone. The theoretically calculated HOMO energies for compounds **17c** and **19b** have been identified to be −5.9536 and −5.7756 eV respec-

tively and the LUMO energies for compounds **17c** and **19b** are −2.7756 and −2.8237 eV respectively. These values indicate overall high chemical stability of compound **19b** with the HOMO-LUMO energy gap 2.952 eV as compared to that of 3.178 eV for compounds **17c**.

Energy values of HOMO and LUMO can be utilized for the calculation of important molecular properties including ionization potential (IP), electron affinity (EA), electronegativity (χ), hardness (η), softness (S), electrophilicity index (ω) and chemical potential (μ). For both the compounds, IP and EA were calculated as IP$=-E_{HOMO}$ and EA$=-E_{LUMO}$. The compound **17c** with a higher IP value as well as a lower value of EA is found to be more stable compared compound **19b** (Table 3).[26] Further stability of compounds **17c** and **19b** can be correlated with Global hardness and global softness as shown in the Table 3. Additionally, the molecular electrostatic potential (MEP) surfaces were analyzed to gain insights into the interactions and charge distribution within the compounds. The MEP surfaces, computed using the same basis set, are depicted in Figure 5. The MEP provides information about different reactivity sites available on the surfaces as well as sites for hydrogen bonding.[27,28] The MEP maps, obtained with the same basis sets Figure 5, revealed negative potential sites localized on the lactone ring of coumarin and the carbonyl group of pyrazolone. These findings further support the stability of compounds **17c** and **19b**, consistent with the previous results. DFT study showed the compound's high reactivity and stability that drug is likely to remain stable during biochemical reactions with the target and effectively interact with the biological target.

Molecular Docking

Nowadays, docking is proven to be a highly important technique, useful to predict the interaction of small ligands with biological macromolecules. The compounds were further examined by molecular docking studies in order to evaluate their binding affinity towards protein p53 (3DCY) and caspase 3 (4QTX) in the apoptosis pathway. Therefore, in the present work from all synthesized compounds, Molecular docking studies were performed on the most active compounds **17c** and **19b** to

17c

19b

Figure 4. DFT-optimized structures of compounds **17c** and **19b**.

ChemistrySelect

Research Article
doi.org/10.1002/slct.202303391

Chemistry
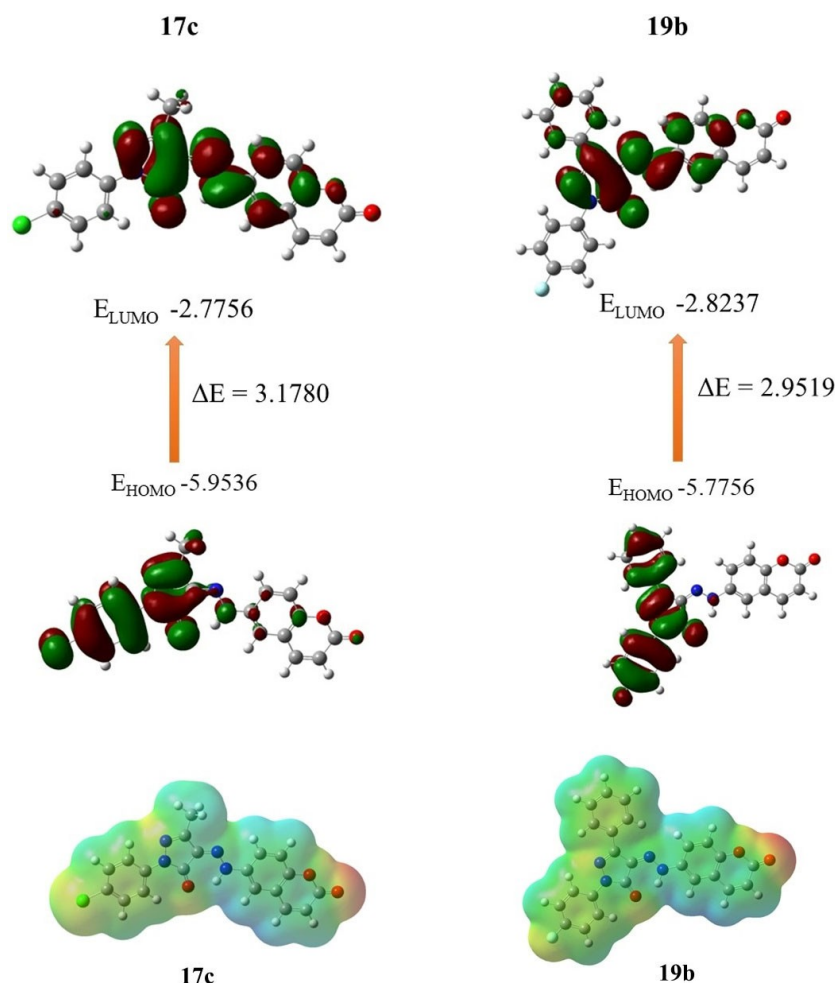**Europe**
European Chemical
Societies Publishing

Figure 5. Frontier molecular orbital surfaces of compounds (FMO) and Molecular electrostatic potential (MEP) diagram of compounds **17c** and **19b**.

highlight important binding interactions of the drug candidates with potential targets. Docking the most active compounds are summarized in Table 4. Any active compound which has capability to induce cellular stress by means of DNA damage, the guardian gene p53 activates the pathway of self-destruction in the cells.[29] However, this is highly regulated mechanism, in normal cell the low cellular level is maintained by regulators. MDM2 is one such regulator, which acts as negative regulator of p53. It physically interacts with p53 induces ubiquitination and degradation of p53 through proteasome.[30] If a drug occupies the interactive site p53 with MDM2, it can able to

overcome the negative regulation of MDM2 and induce the p53 mediated pathways responsible for anticancer activity. Caspase 3 is the effector caspase of the apoptotic pathway, which initiates the process of apoptosis upon receiving upstream activation signals.

Compound **17c** is docked with p53 (3DCY) at the active site and generated a docking score of −8.6 Kcal/mol and Caspase 3 (4QTX) at the active site and generated a docking score of −8.4 Kcal/mol, (Figure 6, Table 4). Ligand **17c** interacts with the targeted protein, p53, forming two hydrogen bonds. One hydrogen bond involves the oxygen atom of the lactone

Table 4. Molecular Docking study of compound **17c** and **19b** with PDB IDs; p53 (3DCY), Caspase 3 (4QTX) their bonding, amino acid interactions and docking score.

Comp.	PDB ID	Bond	Amino Acid Interactions	Docking Score kcal/mol
17c	p53 (3DCY)	Two H-Bond	GLN 23, ARG10	−8.6
	Caspase 3 (4QTX)	One H-bond	PHE250	−8.4
19b	p53 (3DCY)	Two H-Bond	GLN23, GLN260	−9.3
	Caspase 3 (4QTX)	Three H-Bond	Arg207, HIS121, CYS163	−9.3
Fluorouracil	p53 (3DCY)	Two H-Bond	GLN23, ASN17	−5.5
	Caspase 3 (4QTX)	Two H-Bond	PHE250, ASN208	−6.2

ChemistrySelect

Research Article
doi.org/10.1002/slct.202303391

**Chemistry
Europe**

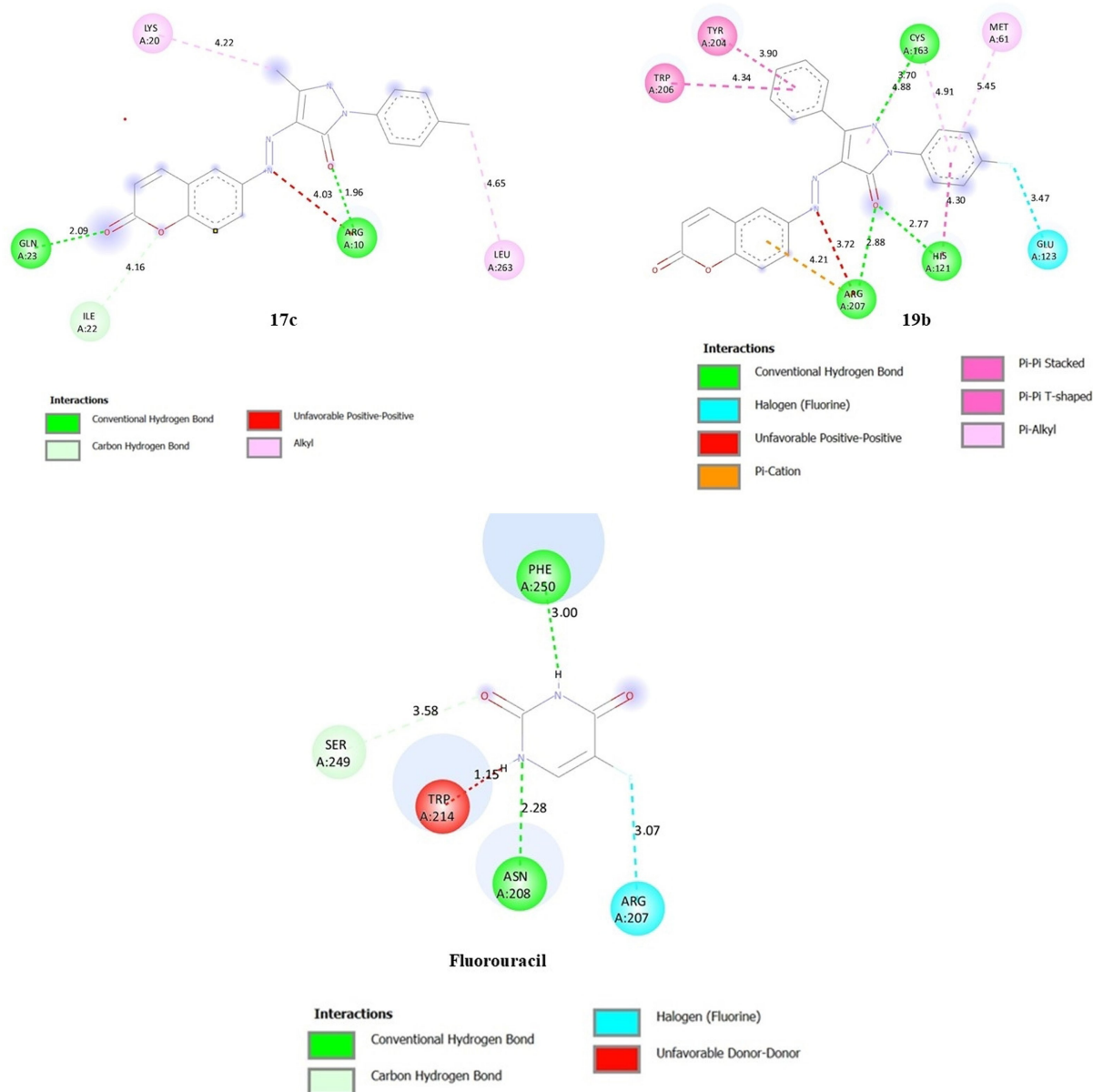European Chemical
Societies Publishing

Figure 6. 2D molecular docking structure of compound (a) **17 c** with p53(3DCY) (b) **19 b** with Caspase 3 (4QTX) (c) standard Fluorouracil with Caspase 3 (4QTX)

carbonyl with GLN 23 at a distance of 2.09 Å, and the other involves the oxygen atom of the pyrazolone with ARG10 at a distance of 1.96 Å. On the other hand, when interacting with the targeted protein caspase 3 (4QTX), a single hydrogen bond interaction was observed between the protein and the oxygen of the pyrazolone of the ligand, specifically with PHE A 250 at a distance of 2.18 Å.

Compound **19b** also docked with both proteins PDB ID p53(3DCY) and Caspase 3 (4QTX). In which p53 interacted through two hydrogen bonds (Figure 6, Table 4). The amino acid GLN A: 23 forms a hydrogen bond with the F atom of the benzene ring at a distance of 1.99 Å, and GLN A: 260 forms a hydrogen bond with the oxygen of the lactone carbonyl group of the ligand at a distance of 2.10 Å. These interactions contribute to the docking score of −9.3 kcal/mol. In Caspase 3,

the amino acids Arg207 and HIS121 form hydrogen bonds with the O atom of the pyrazolone ring at distances of 2.88 Å and 2.77 Å, respectively. Additionally, there is a hydrogen bond interaction with the N atom of the pyrazolone ring and CYS163 at a distance of 3.70 Å. These interactions result in the docking score of −9.0 kcal/mol.

Conclusions

Two series of pyrazolone derivatives containing 7-amino 4-methylcoumarin and 6-aminocoumarin were designed, synthesized and well characterized. Compounds of both the series were studied using MTT assay for anticancer activity against A549 and MCF-7 cell line. Phenyl attached to pyrazolone ring at

3rd position showed improvement in anticancer activity than methyl substituted pyrazolone derivatives. From all synthesized compounds, compound **17c** has shown excellent activity against A549 lungs cancer cell line (IC$_{50}$ 1.22 ± 0.048 μM), while compound **19b** has shown excellent activity against MCF-7 cell line (IC$_{50}$ 1.66 ± 0.015 μM). In cytotoxic investigations utilizing the EtBr/AO assay, both compounds exhibited an apoptosis pathway in the tested cell lines. The induction of apoptosis was primarily governing by reactive oxygen species (ROS) at the IC$_{50}$ value in A549 and MCF-7 cell lines for compound **17c** and **19b**, respectively. To predict the molecular mechanism, molecular docking was performed with the critical apoptotic genes p53 and caspase 3 for both compounds. Both compounds, **17c** and **19b**, exhibited docking scores of −8.6 and −8.4 kcal/mol as well as −9.3 and −9.3 kcal/mol for p53 and caspase 3, respectively. In comparison, fluorouracil displayed significantly lower docking scores of −5.5 and −6.2 kcal/mol. Consequently, it can be inferred that compounds **17c** and **19b** exhibit high reactivity, primarily activating the ROS-induced p53-dependent caspase 3-mediated apoptotic pathway in both cancer cell lines at the lowest IC$_{50}$ concentration.

Experimental

General Chemistry

All the chemicals and solvents purchased were of Reagent-grade and used after purification. TLC was carried out on silica gel F254 plates (Merck), while for column chromatographic purification Acme's silica gel (60–120 mesh) was used. All the melting points were determined using open capillary tubes. IR spectra were captured after making KBr pellet using the Perkin Elmer RX 1 spectrometer. ^{1}H-NMR and ^{13}C-NMR were recorded on Advance Bruker spectrometer (400 MHz/500 MHz) with CDCl$_3$ or DMSO-d6 as the solvent containing internal standard TMS. *J* values are given in Hz. ESI-MS was used to determine the mass spectra using a Shimadzu LCMS 2020 device. Elemental analysis was carried out on Thermo Finnigan Flash 11–12 series EA. 7-amino 4-methyl coumarin, 6-amino coumarin, and substituted pyrazolone derivatives were prepared according to literature method.[31,32,33]

General Procedure for preparation of compounds 8, 9, 16 and 18

7-Amino-4-methyl-coumarin **7**/ 6-aminocoumarin **15** (0.01 mol) was dissolved in concentrated hydrochloric acid (7.5 ml), (15 ml) acetic acid and stirred until amine was completely dissolved then the mixture cooled (external cooling) to the temperature 0–5 °C. Sodium nitrite solution (0.01 mol) in water (10 mL) was then added dropwise with vigorous stirring during 30 min. at 0–5 °C. This solution was poured into the cooled solution of sodium acetate, ethyl acetoacetate (for Compounds **8** and **16**) / ethyl benzoyl acetate (for Compound **9** and **18**) in ethanol. After addition kept the reaction mixture at room temperature for a duration 2 hours. The reaction mixture was then poured into ice cold water, filter and recrystallized from ethanol.

(Z)-ethyl 2-(2-(4-methyl-2-oxo-2H-chromen-7-yl)hydrazono)-3-oxobutanoate (8)

Yellow Solid, Yield: 76%; M.P: 158–160 °C; IR (KBr) (υ, cm^{-1}): 3054, 2982, 2925 (C–H), 1733 (lactone C=O), 1705 (ester C=O), 1617 (Ketone C=O), 1565, 1520, 1437, 1387, 1365, 1319, 1263(C–O), 1188, 1135, 1091, 1068, 1016, 979, 943, 882, 791, 749, 606 cm^{-1}; ^{1}H-NMR (400 MHz, CDCl$_3$): δ 1.43 (t, *J*=7.2 Hz, 3H), 2.44 (s, 3H), 2.62 (s, 3H), 4.36 (q, *J*=7.2 Hz, 2H), 6.22 (s, 1H), 7.26 (dd, *J*=2.0 Hz and *J*=8.8 Hz, 1H), 7.42 (d, *J*=2.0 Hz, 1H), 7.60 (d, *J*=8.4 Hz, 1H), 14.59 (s, 1H); ^{13}C-NMR (100 MHz, CDCl$_3$): δ ppm 14.31, 18.72, 30.93, 61.39, 103.74, 112.51, 113.71, 117.25, 125.95, 127.56, 144.71, 152.19, 154.80, 160.80, 164.47, 197.60.

(Z)-ethyl 2-(2-(4-methyl-2-oxo-2H-chromen-7-yl)hydrazono)-3-oxo-3-phenylpropanoate (9)

Orange solid, Yield: 85%; M.P: 143–145 °C; IR (KBr) (υ, cm^{-1}): 3436 (N–H), 3230, 3065, 2984 (C–H), 1740 (lactone C=O), 1683 (ester C=O), 1657 (ketone C=O), 1619 (C=N), 1529, 1448, 1387, 1369, 1319, 1261(C–O), 1178, 1132, 1067, 1031, 1017, 977, 904, 877, 851, 813, 779, 742, 714, 692, 670 cm^{-1}; ^{1}H-NMR (400 MHz, CDCl$_3$): δ 1.37 (t, *J*=7.2 Hz, 3H), 2.40 (s, 3H), 4.40 (q, *J*=7.0 Hz, 2H), 6.18 (s, 1H), 7.07–7.10 (m, 2H), 7.49–7.55 (m, 3H), 7.62–7.65 (m, 1H), 7.95–7.97 (m, 2H), 12.70 (s, 1H); ^{13}C-NMR (100 MHz, CDCl$_3$): δ ppm 14.00, 18.69, 61.92, 102.62, 111.54, 113.14, 116.19, 126.01, 128.25, 128.78, 130.30, 133.13, 136.89, 144.92, 152.24, 154.93, 160.89, 163.58, 189.15.

(E)-ethyl 3-oxo-2-(2-(2-oxo-2H-chromen-6-yl)hydrazono)butanoate (16)

Yellow Solid, Yield: 83%; M.P: 148–150 °C; IR (KBr) (υ, cm^{-1}): 3417 (N–H), 3147, 3001, 2926 (C–H), 1712 (lactone C=O), 1687 (ester C=O), 1651 (ketone C=O), 1572, 1526, 1492, 1375, 1357, 1311, 1255, 1214, 1263(C–O), 1181, 1122, 1102, 1066, 1016, 946, 920, 871, 827, 790, 754, 725, 618 cm^{-1}; ^{1}H-NMR (400 MHz, CDCl$_3$): δ 1.42 (t, *J*=6.8 Hz, 3H), 2.54 (s, 3H), 4.40 (q, *J*=7.0 Hz, 2H), 6.51 (d, *J*=9.6 Hz, 1H), 7.39 (d, *J*=8.8 Hz, 1H), 7.44 (d, *J*=2.4 Hz, 1H), 7.54 (dd, *J*=2.4 Hz and *J*=8.8 Hz, 1H), 7.75 (d, *J*=9.2 Hz, 1H), 12.89 (s, 1H).

(E)-ethyl 3-oxo-2-(2-(2-oxo-2H-chromen-6-yl)hydrazono)-3-phenylpropanoate (18)

Yellow Solid, Yield: 86%; M.P: 142–144 °C; IR (KBr) (υ, cm^{-1}): 3426 (N–H), 3046, 2926 (C–H), 1722 (lactone C=O), 1671(ester C=O), 1653 (ketone C=O), 1599, 1572, 1526, 1493, 1448, 1388, 1334, 1269, 1208, 1263(C–O), 1179, 1121, 1100, 1020, 942, 920, 885, 828, 786, 718, 670 cm^{-1}; ^{1}H-NMR (400 MHz, CDCl$_3$): δ 1.36 (t, *J*=7.2 Hz, 3H), 4.39 (q, *J*=7.0 Hz, 2H), 6.45 (d, *J*=9.2 Hz, 1H), 7.31–7.37 (m, 3H), 7.51 (t, *J*=7.6 Hz, 2H), 7.62 (t, *J*=8.8 Hz, 2H), 7.64 (dd, *J*=2.4 Hz, 8.8 Hz, 1H), 7.95 (d, *J*=7.6 Hz, 1H), 12.80 (s, 1H); ^{13}C-NMR (100 MHz, CDCl$_3$): δ ppm 13.99, 61.63, 112.92, 117.69, 118.01, 119.49, 119.71, 127.72, 128.10, 130.24, 132.73, 137.47, 138.65, 142.90, 150.66, 160.37, 163.82, 189.31.

General procedure for compounds 10a–c, 11a–d, 12,13,17a–d and 19a–d.

Compounds **8/9/16/18** and different substituted hydrazines/hydrazides were added in absolute ethanol (20 mL), and the reaction mixture was then refluxed for 18–20 hours. 2–3 drops of acetic acid were added to catalyze the reaction. It was then concentrated to half its original volume and reaction mixture allowed to cool down at ambient temperature. The solid separated out was filtered,

ChemistrySelect

Research Article
doi.org/10.1002/slct.202303391

Chemistry Europe
European Chemical
Societies Publishing

washed with ethanol and dried to give compounds target pyrazolone derivatives **10a–c, 11a–d, 12, 13, 17a–d** and **19a–d**.

Characterization data for compounds 10a–c, 11a–d, 12 and 13.

(Z)-3-methyl-4-(2-(4-methyl-2-oxo-2H-chromen-7-yl)hydrazono)-1-phenyl-1H-pyrazol-5(4H)-one (10a)

Yellow Solid, Yield: 79%; M.P: Above 270°C; IR (KBr) (υ, cm^{-1}): 3400 (N–H), 3075, 2922, 2854 (C–H), 1730 (lactone C=O), 1656 (Pyrazolone C=O), 1612 (C=N), 1552 (C=N), 1497, 1424, 1390, 1341, 1266 (C–O), 1159 (C–O), 1071, 1045, 995, 905, 880, 818, 772, 749, 729, 688, 668 cm^{-1}; ^{1}H-NMR (400 MHz, CDCl$_3$): δ 2.41 (S, 3H), 2.46 (s, 3H), 6.27 (s, 1H), 7.26–7.31 (m, 2H), 7.45–7.49 (m, 3H), 7.64 (d, J=8.8 Hz, 1H), 7.95–7.97 (m, 2H), 13.58 (s, 1H); ^{13}C-NMR (100 MHz, CDCl$_3$): δ ppm 11.85, 18.72, 103.15, 112.04, 113.91, 117.68, 118.58, 125.52, 126.12, 129.03, 130.58, 137.59, 144.09, 148.68, 152.00, 152.58, 154.95, 157.44; Anal. calc. for C$_{20}$H$_{16}$N$_4$O$_3$ C,66.66; H,4.48; N,15.55; found: C,66.64; H,4.44; N,15.59; ESI-MS: 361.13[M+H]$^+$.

(Z)-1-(4-fluorophenyl)-3-methyl-4-(2-(4-methyl-2-oxo-2H-chromen-7-yl)hydrazono)-1H-pyrazol-5(4H)-one (10b)

Yellow Solid; Yield = 76%; M.P: Above 270°C; IR (KBr) (υ, cm^{-1}): 3432 (N–H), 2924, 2854 (C–H), 1730 (lactone C=O), 1656 (pyrazolone C=O), 1612 (C=N), 1553 (C=N), 1504, 1428, 1389, 1342, 1266 (C–O), 1145 (C–O), 1069, 1047, 998, 908, 880, 861, 836, 772, 729, 661, 585 cm^{-1}; ^{1}H-NMR (400 MHz, CDCl$_3$): δ 2.41(s, 3H), 2.47 (s, 3H), 6.28 (s, 1H), 7.13–7.17 (m, 2H), 7.30–7.31(m, 1H) 7.47 (s, 1H), 7.65 (d, J= 8.4 Hz, 1H) 7.92–7.95 (m, 2H) 13.54 (s, 1H); Anal. Calc. for C$_{20}$H$_{15}$FN$_4$O$_3$ C,63.49; H, 4.00; N,14.81; found: C,63.53; H,3.95; N,14.83; ESI-MS: 377.7[M-H]$^+$.

(Z)-1-(4-chlorophenyl)-3-methyl-4-(2-(4-methyl-2-oxo-2H-chromen-7-yl)hydrazono)-1H-pyrazol-5(4H)-one (10c)

Orange Solid, Yield: 78%; M.P: Above 270°C; IR (KBr) (υ, cm^{-1}) 3054, 2980, 2925(C–H), 1732 (lactone C=O), 1664 (2 C=O), 1614 (C=N), 1555 (C=N), 1494, 1425, 1389, 1368, 1340, 1266 (C–O), 1245 (C–O), 1159, 1144, 1096, 1069, 1051, 1012, 1002, 907, 856, 830, 771, 731, 709, 659 cm^1; ^{1}H-NMR (400 MHz, CDCl$_3$): δ 2.40 (s, 3H), 2.46 (s, 3H), 6.27 (s, 1H), 7.27–7.30 (m, 1H), 7.40–7.45 (m, 3H), 7.64 (d, J=8.8 Hz, 1H), 7.92 –7.94 (m, 2H), 13.51 (s, 1H); Anal. calc. for C$_{20}$H$_{15}$ClN$_4$O$_3$ C, 60.84; H, 3.83; N, 14.19; found: C,60.89; H,3.78; N,14.16; ESI-MS: 393.80[M-H]$^+$.

(Z)-4-(2-(4-methyl-2-oxo-2H-chromen-7-yl)hydrazono)-1,3-diphenyl-1H-pyrazol-5(4H)-one (11a)

Yellow Solid; Yield: 76%; M.P: Above 270°C; IR (KBr) (υ, cm^{-1}): 3430 (N–H), 3057, 2883, 2764 (C–H), 1723 (lactone C=O), 1658 (pyrazolone C=O), 1614 (C=N), 1554 (C=N), 1496, 1433, 1388, 1342, 1268 (C–O), 1247, 1198 (C–O), 1171, 1133, 1067, 1013, 958, 898, 858, 812, 754, 683, 648 cm^{-1}; ^{1}H-NMR (400 MHz, CDCl$_3$): δ 2.37 (s, 3H), 6.18 (s, 1H), 7.18 (d, J=8.4 Hz, 2H), 7.23–7.29 (m, 1H), 7.36–7.56 (m, 6H), 8.00 (d, J=8.4 Hz, 2H), 8.15–8.16 (m, 2H), 13.90 (s, 1H); ^{13}C-NMR (100 MHz, CDCl$_3$): δ ppm 18.66, 103.00, 112.28, 113.87, 117.47, 118.55, 125.68, 126.17, 127.22, 128.73, 128.99, 129.27, 129.68, 130.23, 137.65, 143.86, 146.17, 152.04, 154.82, 157.59, 160.56; Anal. calc. for C$_{25}$H$_{18}$N$_4$O$_3$; C, 71.08; H, 4.29; N, 13.26; found: C, 71.10; H, 4.33; N, 13.23; ESI-MS: 422.09[M+].

(Z)-1-(4-fluorophenyl)-4-(2-(4-methyl-2-oxo-2H-chromen-7-yl)hydrazono)-3-phenyl-1H-pyrazol-5(4H)-one (11b)

Yellow Solid; Yield: 72%; M.P: Above 270°C; IR (KBr) (υ, cm^{-1}): 3425 (N–H), 3054, 2883, 2811(C–H), 1726 (lactone C=O), 1658 (pyrazolone C=O), 1617 (C=N), 1547 (C=N), 1511, 1390, 1368, 1347, 1297, 1259 (C–O), 1216, 1174 (C–O), 1136, 1111, 1066, 979, 961, 851, 833, 764, 732, 688, 651 cm^{-1}; ^{1}H-NMR (400 MHz, CDCl$_3$): δ 2.46 (s, 3H), 6.27 (s, 1H), 7.18 (d, J=8.0 Hz, 2H), 7.27 (d, J=8.0 Hz, 1H), 7.48–7.53 (m, 4H), 7.65 (d, J=8.4 Hz, 1H), 8.03–8.04 (m, 2H), 8.21 (s, 2H), 13.98 (s, 1H); ^{13}C-NMR (100 MHz, CDCl$_3$): δ ppm 18.73, 103.24, 112.42, 114.04, 115.69, 115.91, 117.65, 120.58, 126.24, 127.35, 128.81, 129.21, 129.67, 130.35, 133.88, 143.91, 146.54, 152.03, 154.94, 157.51, 160.56; C$_{25}$H$_{17}$FN$_4$O$_3$; Anal. calc. for C, 68.18; H,3.89; N,12.72; found: C,68.23; H,3.85; N, 12.71; ESI-MS: 441.13[M+H]$^+$.

(Z)-1-(4-chlorophenyl)-4-(2-(4-methyl-2-oxo-2H-chromen-7-yl)hydrazono)-3-phenyl-1H-pyrazol-5(4H)-one (11c)

Yellow Solid; Yield: 89%; M.P: Above 270°C; IR (KBr) (υ, cm^{-1}): 3436 (N–H), 2993, 2881, 2784 (C–H), 1729 (lactone C=O), 1663 (pyrazolone C=O), 1615 (C=N), 1552 (C=N), 1494, 1422, 1388, 1342, 1269(C–O), 1248, 1200, 1171 (C–O), 1135, 1089, 959, 901, 846, 771, 686, 650 cm^{-1}; ^{1}H-NMR (400 MHz, CDCl$_3$): δ 2.44 (s, 3H), 6.25 (s, 1H), 7.22 (d, J=8.4 Hz, 1H), 7.38–7.50 (m, 6H), 7.62 (d, J =8.0 Hz, 1H), 7.99 (d, J=8.4 Hz, 2H), 8.16 (s, 2H), 13.9 (s, 1H); ^{13}C-NMR (100 MHz, CDCl$_3$): δ ppm 18.73, 103.18, 112.41, 114.04, 117.70, 119.67, 126.23,, 127.32, 128.79, 129.05, 129.55, 130.40, 130.81, 136.21, 143.69, 146.66, 151.98, 154.94, 157.60, 160.57; Anal. calc. for C$_{25}$H$_{17}$ClN$_4$O$_3$; C,65.72; H,3.75; N, 12.26; found: C, 65.73; H, 3.70; N,12.23; ESI-MS: 455.10[M-H]$^+$.

(Z)-1-(2,4-dichlorophenyl)-4-(2-(4-methyl-2-oxo-2H-chromen-7-yl)hydrazono)-3-phenyl-1H-pyrazol-5(4H)-one (11d)

Yellow Solid; Yield: 78%; M.P: Above 270°C; IR (KBr) (υ, cm^{-1}): 3442 (N–H), 3081, 3052, 2883, 2813(C–H), 1732 (lactone C=O), 1659 (pyrazolone C=O), 1616 (C=N), 1551 (C=N), 1491, 1430, 1388, 1348, 1270 (C–O), 1240, 1201 (C–O), 1175, 1088, 1065, 1012, 963, 904, 851, 822, 758, 730, 686, 648 cm^{-1}; ^{1}H-NMR (400 MHz, CDCl$_3$): δ 2.45 (s, 3H), 6.27 (s, 1H), 7.28–7.30 (m, 1H), 7.39 (d, J=8.4 Hz, 1H), 7.49–7.58 (m, 6H), 7.65 (d, J=8.4 Hz, 1H), 8.16 (s, 2H) 13.8 (s, 1H); ^{13}C-NMR (100 MHz, CDCl$_3$): δ ppm 18.75, 103.34, 112.50, 114.06, 117.70, 126.24, 127.33, 128.00, 128.11, 128.83, 129.59, 129.64, 130.36, 130.45, 132.44, 132.90, 135.36, 143.86, 147.35, 152.08, 154.88, 157.93, 160.58; C$_{25}$H$_{16}$Cl$_2$N$_4$O$_3$; Anal. calc. for C,61.11; H,3.28; N,11.40; found: C,61.08; H,3.30; N,11.42; ESI-MS: 490.02[M+].

(Z)-3-methyl-4-(2-(4-methyl-2-oxo-2H-chromen-7-yl)hydrazono)-1-(2-nitrobenzoyl)-1H-pyrazol-5(4H)-one (12)

Orange solid, Yield: 85%; M.P: Above 270°C; IR (KBr) (υ, cm^{-1}): 3441 (N–H), 2961, 2934, 2869 (C–H), 1740 (lactone C=O), 1618 (pyrazolone C=O), 1531(C=N), 1354, 1304, 1262 (C–O), 1214, 1146 (C–O), 1098, 1002, 880, 849, 788, 728 cm^{-1}; ^{1}H-NMR (400 MHz, DMSO-d$_6$): δ 2.42 (s, 3H), 2.51 (s, 3H), 6.35 (s, 1H), 7.65–7.67 (m, 2H), 7.79–7.85 (m, 3H), 7.95–7.99 (m, 1H), 8.32 (d, J=8.0 Hz, 1H), 13.00 (s, 1H); Anal. calc. for C$_{21}$H$_{15}$N$_5$O$_6$; C, 58.20; H,3.49; N, 16.16; found: C,58.25; H,3.51; N,16.14; ESI-MS: 434.10[M+H]$^+$.

ChemistrySelect

Research Article
doi.org/10.1002/slct.202303391

Chemistry Europe
European Chemical
Societies Publishing

(Z)-4-(2-(4-methyl-2-oxo-2H-chromen-7-yl)hydrazono)-1-(2-nitrobenzoyl)-3-phenyl-1H-pyrazol-5(4H)-one (13)

Brown Solid; Yield: 70%; M.P: Above 270°C; IR(KBr) (υ, cm^{-1}): 3447 (N–H), 3071, 2881 (C–H), 1745 (lactone C=O), 1710 (pyrazolone C=O), 1615 (C=O), 1526 (C=N), 1388, 1351, 1297, 1264 (C–O), 1206, 1164 (C–O), 1060, 978, 932, 887, 863, 771, 731, 703, 653 cm^{-1}; ^{1}H-NMR (400 MHz, DMSO-d$_6$): δ 2.41 (s, 3H), 6.35 (s, 1H), 7.58–7.67 (m, 5H), 7.83–7.90 (m, 3H), 7.99–8.03 (m, 3H), 8.36 (d, J=8.4 Hz, 1H), 13.22 (s, 1H); Anal. calc. for C$_{26}$H$_{17}$N$_5$O$_6$; C,63.03; H,3.46; N,14.14; found: C,63.08; H, 3.50; N,14.13; ESI-MS: 496.15 [M+H]$^+$.

(Z)-3-methyl-4-(2-(2-oxo-2H-chromen-6-yl)hydrazono)-1-phenyl-1H-pyrazol-5(4H)-one (17a)

Yellow Solid, Yield: 75%; M.P: Above 270°C; IR (KBr) (υ, cm^{-1}): 3431(N–H), 2923, 2854 (C–H), 1715 (lactone C=O), 1659 (pyrazolone C=O), 1560 (C=N), 1496, 1421, 1386, 1369, 1345, 1324, 1273, 1254 (C–O), 1183 (C–O), 1158, 1104, 1049, 1002, 905, 816, 757, 715, 688 cm^{-1}; ^{1}H-NMR (400 MHz, CDCl$_3$): δ 2.41 (S, 3H), 6.53 (d, J=9.6 Hz, 1H), 7.25 (t, J=7.6 Hz, 1H), 7.41–7.48 (m, 3H), 7.55 (d, J=2.4 Hz, 1H), 7.63 (dd, J=2.4 Hz and 8.8 Hz, 1H), 7.75 (d, J=9.6 Hz, 1H), 7.95–7.97 (m, 2H), 13.69 (s, 1H); Anal. calc. for C$_{19}$H$_{14}$N$_4$O$_3$; C, 65.89; H, 4.07; N, 16.18; found: C,65.92; H,4.01; N,16.14; ESI-MS: 347.10 [M+H]$^+$.

(Z)-1-(4-fluorophenyl)-3-methyl-4-(2-(2-oxo-2H-chromen-6-yl)hydrazono)-1H-pyrazol-5(4H)-one (17b)

Yellow Solid, Yield: 70%; M.P: Above 270°C; IR (KBr) (υ, cm^{-1}): 3435 (N–H), 3065, 2924 (C–H), 1726 (lactone C=O), 1655 (pyrazolone C=O), 1557 (C=N), 1508 (C=N), 1423, 1382, 1348, 1270 (C–O), 1213 (C–O), 1178, 1151, 1122, 1100, 1049, 1002, 907, 867, 826, 772, 710, 658 cm^{-1}; 1H-NMR (400 MHz, CDCl$_3$): δ 2.40 (S, 3H), 6.53 (d, J=9.6 Hz, 1H), 7.13 (d, J=2.4 Hz, 1H), 7.16 (d, J=9.2 Hz, 1H), 7.43 (d, J=8.8 Hz, 1H), 7.56 (d, J=2.4 Hz, 1H), 7.63 (dd, J=2.4 Hz & 8.8 Hz, 1H), 7.76 (d, J=9.6 Hz, 1H), 7.91–7.95 (m, 2H), 13.66 (s, 1H); Anal. calc.for C$_{19}$H$_{13}$FN$_4$O$_3$; C, 62.64; H, 3.60; N, 15.38; found: C,62.59; H,3.58; N,15.41; ESI-MS: 365.10 [M+H]$^+$.

(Z)-1-(4-chlorophenyl)-3-methyl-4-(2-(2-oxo-2H-chromen-6-yl)hydrazono)-1H-pyrazol-5(4H)-one (17c)

Yellow Solid, Yield: 70%; M.P: Above 270°C; IR (KBr) (υ, cm^{-1}): 3438 (N–H), 3063 (C–H), 1726 (lactone C=O), 1658 (pyrazolone C=O), 1556 (C=N), 1495 (C=N), 1454, 1424, 1376, 1343, 1265 (C–O), 1181 (C–O), 1151, 1123, 1098, 1051, 1004, 904, 823, 774, 719, 620 cm^{-1}; ^{1}H-NMR (400 MHz, CDCl$_3$): δ 2.41 (S, 3H), 6.54 (d, J=9.6 Hz, 1H), 7.41–7.45 (m, 3H), 7.57 (d, J=2.4 Hz, 1H), 7.64 (dd, J=2.4 Hz and 8.8 Hz, 1H), 7.77 (d, J=9.6 Hz, 1H), 7.94–7.96 (m, 2H), 13.65 (s, 1H); ^{13}C-NMR (100 MHz, DMSO-d$_6$): δ ppm 11.56, 114.71, 117.12, 117.45, 117.58, 119.32, 120.19, 124.73, 128.07, 128.93, 137.98, 143.75, 148.45, 150.94, 156.30, 159.57; Anal. calc. for C$_{19}$H$_{13}$ClN$_4$O$_3$ C, 59.93; H, 3.44; N, 14.71; found: C,59.96; H,3.47; N,14.69; ESI-MS: 381.09 [M+H]$^+$.

(Z)-1-(2,4-dichlorophenyl)-3-methyl-4-(2-(2-oxo-2H-chromen-6-yl)hydrazono)-1H-pyrazol-5(4H)-one (17d)

Yellow Solid, Yield: 70%; M.P: Above 270°C; IR (KBr) (υ, cm^{-1}): 3434 (N–H), 3078, 2926 (C–H), 1723 (lactone C=O), 1661 (pyrazolone C=O), 1610 (C=O), 1562 (C=N), 1496, 1454, 1381, 1336, 1263 (C–O), 1182 (C–O), 1107, 1072, 1041, 1000, 911, 881, 857, 821, 774, 705 cm^{-1}; ^{1}H-NMR (400 MHz, CDCl$_3$): δ 2.40 (S, 3H), 6.53 (d, J=

9.6 Hz, 1H), 7.36–7.43 (m, 3H), 7.55–7.56 (m, 2H), 7.63 (dd, J=2.4 Hz and 8.8 Hz, 1H), 7.75 (d, J=9.6 Hz, 1H), 13.49 (s, 1H); Anal. calc. for C$_{19}$H$_{12}$Cl$_2$N$_4$O$_3$; C,54.96; H,2.91; N,13.49; found: C,54.92; H,2.95; N,13.52; 414.03; ESI-MS: 416.2 [M+H]$^+$.

(Z)-4-(2-(2-oxo-2H-chromen-6-yl)hydrazono)-1,3-diphenyl-1H-pyrazol-5(4H)-one (19a)

Yellow Solid, Yield: 70%; M.P: Above 270°C; IR (KBr) (υ, cm^{-1}): 3435 (N–H), 2925 (C–H), 1715 (lactone C=O), 1660 (pyrazolone C=O), 1597 (C=N), 1550 (C=N), 1492, 1420, 1384, 1345, 1326, 1267 (C–O), 1183 (C–O), 1165, 1119, 1099, 964, 916, 890, 819, 791, 757, 715, 688 cm^{-1}; ^{1}H-NMR (400 MHz, CDCl$_3$): δ 6.50 (d, J=9.6 Hz, 1H), 7.26–7.30 (m, 1H), 7.42 (d, J=8.8 Hz, 1H), 7.47–7.55 (m, 6H), 7.65 (dd, J=2.4 Hz, 8.8 Hz, 1H), 7.72 (d, J=9.6 Hz, 1H), 8.06 (d, J=7.6 Hz, 2H), 8.21–8.23 (m, 2H), 14.14 (s, 1H); Anal. calc. for C$_{24}$H$_{16}$N$_4$O$_3$; C, 70.58; H, 3.95; N, 13.72; found: C,70.61; H,3.93; N,13.70; ESI-MS: 407.10 [M-H]$^+$, 408.11[M+].

(Z)-1-(4-fluorophenyl)-4-(2-(2-oxo-2H-chromen-6-yl)hydrazono)-3-phenyl-1H-pyrazol-5(4H)-one (19b)

Yellow Solid, Yield: 70%; M.P: Above 270°C; IR (KBr) (υ, cm^{-1}): 3436 (N–H), 2924 (C–H), 1735 (lactone C=O), 1657 (pyrazolone C=O), 1553 (C=N), 1505 (C=N), 1453, 1383, 1344, 1275 (C–O), 1219 (C–O), 1183, 1157, 1100, 963, 920, 876, 840, 813, 766, 723, 692, 651 cm^{-1};^{1}H-NMR (400 MHz, CDCl$_3$): δ 6.55 (d, J=9.6 Hz, 1H), 7.19 (t, J=9.2 Hz, 2H), 7.46 (d, J=8.8 Hz, 1H), 7.53–7.57 (m, 4H), 7.70 (dd, J=2.6 Hz & 8.4 Hz, 1H), 7.78 (d, J=9.6 Hz, 1H), 8.05–8.08 (m, 2H), 8.22–8.24 (m, 2H), 14.16 (s, 1H);^{13}C-NMR (100 MHz, DMSO-d$_6$): δ ppm 115.37, 115.55, 115.68, 115.86, 116.36, 116.43, 117.18, 117.71, 120.27, 126.74, 127.15, 128.77, 129.73, 129.89, 141.91, 143.79, 145.99, 151.25, 156.57, 158.31; Anal. calc. for C$_{24}$H$_{15}$FN$_4$O$_3$; C, 67.60; H, 3.55; N, 13.14; found: C,67.57; H,3.58; N,13.18; ESI-MS: 427.21 [M+H]$^+$.

(Z)-1-(4-chlorophenyl)-4-(2-(2-oxo-2H-chromen-6-yl)hydrazono)-3-phenyl-1H-pyrazol-5(4H)-one (19c)

Yellow Solid, Yield: 70%; M.P: Above 270°C; IR (KBr) (υ, cm^{-1}): 3436 (N–H), 3045, 2924(C–H), 1714 (lactone C=O), 1660 (pyrazolone C=O), 1597 (C=N), 1551 (C=N), 1492, 1420, 1385, 1346, 1327, 1268 (C–O), 1183 (C–O), 1166, 1119, 1100, 964, 916, 891, 817, 790, 757, 715, 687, 668 cm^{-1}; ^{1}H-NMR (400 MHz, CDCl$_3$): 6.52 (d, J=9.6 Hz, 1H), 7.30 (t, J=7.6 Hz, 1H), 7.43 (d, J=9.2 Hz, 1H), 7.47–7.57 (m, 5H), 7.66 (dd, J=2.4 Hz and J=8.8 Hz, 1H), 7.73 (d, J=9.6 Hz, 1H), 8.07 (d, J=7.6 Hz, 2H), 8.23 (dd, J=2.4 Hz, 7.4 Hz, 2H), 14.15 (s, 1H); ^{13}C-NMR (100 MHz, CDCl$_3$): δ ppm 113.92, 118.02, 118.45, 118.73, 119.40, 119.62, 125.65, 127.39, 128.08, 128.08, 128.65, 128.99, 130.01, 130.09, 137.75, 137.83, 142.56, 146.36, 151.72, 157.94, 160.06; Anal. calc. for C$_{24}$H$_{15}$ClN$_4$O$_3$; C, 65.09; H, 3.41; N, 12.65; found: C,65.14; H,3.39; N,12.61; ESI-MS: 442.86 [M+].

(Z)-1-(2,4-dichlorophenyl)-4-(2-(2-oxo-2H-chromen-6-yl)hydrazono)-3-phenyl-1H-pyrazol-5(4H)-one (19d)

Yellow Solid, Yield: 70%; M.P: Above 270°C; IR (KBr) (υ, cm^{-1}): 3446 (N–H), 2925 (C–H), 1719 (lactone C=O), 1661 (pyrazolone C=O), 1556 (C=N), 1487 (C=N), 1425, 1385, 1349, 1279 (C–O), 1181 (C–O), 1119, 1101, 1062, 967, 918, 879, 816, 756, 686 cm^{-1}; ^{1}H-NMR (400 MHz, CDCl$_3$): 6.54 (d, J=9.6 Hz, 1H), 7.42 (dd, J=2.4 Hz & 8.8 Hz, 1H), 7.46 (d, J=8.8 Hz, 1H), 7.50 (d, J=8.4 Hz, 1H), 7.53–7.57 (m, 4H), 7.60 (d, J=2.4 Hz, 1H), 7.70 (dd, J=2.4 Hz and 8.8 Hz, 1H), 7.77 (d, J=9.6 Hz, 1H), 8.16–8.18 (m, 2H), 13.97 (s, 1H); Anal. calc.

ChemistrySelect

Research Article
doi.org/10.1002/slct.202303391

Chemistry Europe
European Chemical
Societies Publishing

for $C_{24}H_{14}Cl_2N_4O_3$ C, 60.39; H, 2.96; N, 11.74; found: C,60.43; H,3.01; N,11.72; ESI-MS: 477.09 $[M+H]^+$.

Biological activity screening

MTT assay:

According to procedure, the MTT [3-(4,5-dimethylthiazol-2-yl)-2,5-diphenyltetrazolium bromide] test was used to determine the half minimum inhibitory concentration. In DMEM medium supplemented with 10% FBS, cells were plated in a 96-well plate (1×104 cells/well) and allowed to incubate overnight. Each substance was added in concentrations of 0.5, 1, 10, 25, 50, 75, and 100 M before being further 48 hours' incubation. After adding 20 μl of MTT solution (5 mg/mL in PBS), the plate underwent a further 4-hour incubation. 100 μl of acidified isopropanol was used to dissolved the blue formazan. after the supernatant solution was removed. At 570 nm (Metertech 960), the microplate reader was used to measure the absorbance. control group yields 100% for cell viability (%). Graph Pad Prism was used to calculate the IC_{50} values.

Cell viability (%) = (average absorbance of treated groups/average absorbance of control group)×100%. IC_{50} values were calculated using Graph Pad Prism. Each experiment was performed in triplicates.

Ethidium bromide/acridine orange staining assay:

Using the EtBr/AO staining approach, morphological alterations brought on by apoptosis and necrosis were seen. For 48 hours, the IC_{50} concentrations of compounds **17c** and **19b** were applied to the appropriate cells. The positive control utilized was Triton-X 100. Following treatment, cells were stained in a 1:1 mixture of EtBr and AO solution (100 g/ml). The ratio of cells to stain was kept constant at 1:2. Using a Leica DM 2500 fluorescent microscope equipped with a Leica EZ camera, 10 μl of cell suspension was placed on a tiny slide.

DCFH-DA assay:

DCFH-DA staining was employed to measure the intracellular ROS levels subsequent to treating both cell lines (A549 and MCF-7) with derivative **17c** and **19b**. To perform ROS quantification using Fluorimetry, cells at a density of 5×10^5 cells/well were cultured in 6-well plates and allowed to adhere overnight. On the following day, the cells were treated to the IC_{50} concentration of compounds **17c** and **19b** and then incubated for 48 hours. After the incubation period, the procedure was carried out according to the previously outlined protocol in the work by Umar *et al.*[34]

Computational method:

All calculations for the examined derivatives were finished using a Pentium IV machine and Gaussian 09 software. The method selected for the calculations was DFT/B3LYP method at 6–31 G (d,p) basis set. A geometrical optimization process was done for both molecules without enforcing any molecular symmetry constraints to develop a geometrical structure of the lowest energy. All the optimized structures were stable as the imaginary frequency was not present. Gauss View has been used to show the structures of the optimized geometries. Furthermore, the frequency process was carried out for the optimized structures using the same basis set and level of theory to calculate varies parameters. All structures in the optimization processes were demonstrated by the frequency calculations to be stationary points, but none were demonstrated by the vibrational analyses.

Molecular docking:

Protein model, 2D structure and prediction of active site

The molecular docking score provides insight into the potential binding strength and affinity between a ligand and a target protein, aiding in predicting and understanding the likelihood of successful binding in a biological context. A lower docking score often suggests a more favorable and stronger binding interaction; a more negative score indicates a more stable binding. Hereby, the binding energies of the selected apoptosis protein p53 and caspase 3 with bioactive compounds **17c** and **19b** are predicted using Auto Dock Tools 4.2.2. The protein structure of p53 (PDB ID: 3DCY) were fetched from the Research Collaborator for Structural Bioinformatics Protein Data Bank (PDB) database (https://www.rcsb.org/), respectively[35] Protein data was saved in .pdb file format. after removal of water, hetatm, and ligand molecules using BIOVIA Discovery Studio 2021.[36] The structure of a protein is predicted with BIOVIA Discovery Studio 2021 predicts the active sites present in the structure of protein, which was utilized for docking. From all synthesized compounds, more potent anticancer compound **17c** and **19b** bioactive compounds were selected which possess good anti-cancer property based on literature review.[29,30,35]

Supporting Information

Full experimental detail, ^{1}H-NMR and ^{13}C-NMR spectra, this material can be found via the "Supplementary Content" section of this article's webpage.

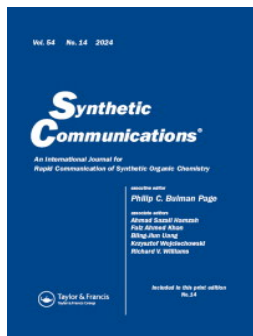## *Conflict of Interests*

The authors declare no conflict of interest.

Data Availability Statement

The data that support the findings of this study are available in the supplementary material of this article.

[1] *Cancer fact sheet*, World Health Organisation (2022) Feb **2022**.
[2] WHO, *Global Breast Cancer Initiative Implementation Framework*: Assessing, Strengthening and Scaling up of Services for the Early Detection and Management of Breast Cancer, **2023**.
[3] D. K. Lang, R. Kaur, R. Arora, B. Saini, S. Arora, *Med. Chem.* **2020**, *20*, 2150–2168.
[4] S. Pearce, *Drug Discov. World.* **2017**, *18*, 66–70.
[5] C. Kharbanda, M. S. Alam, H. Hamid, K. Javed, S. Bano, A. Dhulap, Y. Ali, S. Nazreen, S. Haider, *Bioorg. Med. Chem.* **2014**, *22*, 5804–5812.
[6] S. Viveka Dinesha, P. Shama, G. K. Nagaraja, S. Ballav, S. Kerkar, *Eur. J. Med. Chem.* **2015**, *101*, 442–451.
[7] Z. Zhao, X. Dai, C. Li, X. Wang, J. Tian, Y. Feng, J. Xie, C. Ma, Z. Nie, P. Fan, M. Qian, X. He, S. Wu, Y. Zhang, X. Zheng, *Eur. J. Med. Chem.* **2020** *186*, 111893.
[8] R. C. Kulkarni, J. M. Madar, S. L. Shastri, F. Shaikh, N. S. Naik, R. B. Chougale, L. A. Shastri, S. D. Joshi, S. R. Dixit, V. A. Sunagar, *Chem. Data Collect.* **2018**, *17–18*, 497–506.
[9] L. Zhang, Z. Xu, *Eur. J. Med. Chem.* **2019**, *181*, 111587.
[10] T. Al-Warhi, A. Sabt, E. B. Elkaeed, W. M. Eldehna, *Bioorg. Chem.* **2020**, *103*, 104163.
[11] T. K. Mohamed, R. Z. Batran, S. A. Elseginy, M. M. Ali, A. E. Mahmoud, *Bioorg. Chem.* **2019**, *85*, 253–273.
[12] G. Saidachary, K. Veera Prasad, D. Divya, A. Singh, U. Ramesh, B. Sridhar, B. China Raju, *Eur. J. Med. Chem.* **2014**, *76*, 460–469.
[13] R. Kenchappa, Y. D. Bodke, A. Chandrashekar, M. Aruna Sindhe, S. K. Peethambar, *Arab. J. Chem.* **2017**, *10*, S3895–S3906.
[14] K. K. Sivakumar, A. Rajasekaran, P. Senthilkumar, P. P. Wattamwar, *Bioorg. Med. Chem. Lett.* **2014**, *24*, 2940–2944.
[15] C. G. Naik, G. M. Malik, H. M. Parekh, *South African J. Chem.* **2019**, *72*, 248–252.
[16] R. C. Kulkarni, J. M. Madar, S. L. Shastri, F. Shaikh, N. S. Naik, R. B. Chougale, L. A. Shastri, S. D. Joshi, S. R. Dixit, V. A. Sunagar, *Chem. Data Collect.* **2018**, *17*, 497–506.
[17] R. Soni, S. S. Soman, *Bioorg. Chem.* **2018**, *79*, 277–284.
[18] S. D. Durgapal, R. Soni, S. Umar, B. Suresh, S. S. Soman, *ChemistrySelect.* **2017**, *2*, 147–153.
[19] J. V. Patil, S. Umar, R. Soni, S. S. Soman, S. Balakrishnan, *Synth. Commun.* **2023**, *53*, 217–233.
[20] H. Yang, R. M. Villani, H. Wang, M. J. Simpson, M. S. Roberts, M. Tang, X. Liang, *J. Exp. Clin. Cancer Res.* **2018**, *37*, 1–10.
[21] M. R. Ramsey, N. E. Sharpless, *Cell Biol.* **2006**, *8*, 1213–1215.
[22] T. Yanai, D. P. Tew, N. C. Handy, *Chem. Phys. Lett.* **2004**, *393*, 51–57.
[23] M. Govindarajan, M. Karabacak, A. Suvitha, S. Periandy, *Mol. Biomol. Spectrosc.* **2012**, *89*, 137–148.
[24] M. Odabasoglu, C. Albayrak, B. Kosar, O. Buyukgungor, *Mol. Biomol. Spectrosc.* **2012**, *92*, 357–364.
[25] M. N. Arshad, A. Bibi, T. Mahmood, A. M. Asiri, K. Ayub, *Molecules.* **2015**, *20*, 5851–5874.
[26] A. S. Girgis, A. F. Mabied, J. Stawinski, L. Hegazy, R. F. George, H. Farag, E. S. M. Shalaby, *New J. Chem.* **2015**, *39*, 8017–8027.
[27] T. B. Hadda, F. S. S. Deniz, I. E. Orhan, H. Zgou, A. Rauf, Y. N. Mabkhot, B. Bennani, D. R. Emam, N. A. Kheder, A. Asayari, A. B. Muhsinah, A. Maalik, *Med. Chem. (Los. Angeles)* **2020**, *17*, 834–843.
[28] N. Kerru, L. Gummidi, S. V. H. S. Bhaskaruni, S. N. Maddila, P. Singh, S. B. Jonnalagadda, *Sci. Rep.* **2019**, *9*, 1–17.
[29] J. S. Fridman, S. W. Lowe, *Oncogene* **2003**, *22*, 9030–040.
[30] J. Momand, D. Jung, S. Wilczynski, J. Niland, *J. Nucleic Acids Res.* **1998**, *26(15)*, 3453–3459.
[31] S. N. Kanchana, V. Burra, L. K. Ravindra Nath, *Orient. J. Chem.* **2014**, *30*, 1349–1360.
[32] A. P. Rajput, S. S. Rajput, *Int. J. Pharm. Pharm. Sci.* **2011**, *3*, 346–351.
[33] T. Aysha, M. Zain, M. Arief, Y. Youssef, *Heliyon.* **2019**, *5*, e02358.
[34] S. Umar, R. Soni, S. D. Durgapal, S. S. Soman, *J. Biochem. Mol. Toxicol.* **2020**, *34*, 10.
[35] S. Rath, M. Jagadeb, R. Bhuyan, *Genomics and Informatics* **2021**, *19(4)*, 1–11.
[36] URL: https://www.3dsbiovia.com/products/collaborative-science/biovia-discovery-studio/visualizationdownload.php.

Studies in synthesis and anticancer activity of 6-aminocoumarin/piperazine hybrids

Jayashree V. Patil, Shubhangi S. Soman, Anjali Singh & Suresh Balakrishanan

View supplementary material ☐

Published online: 16 Jul 2024.

Submit your article to this journal ☐

Article views: 63

View related articles ☐

View Crossmark data ☐

Taylor & Francis
Taylor & Francis Group

Check for updates

Studies in synthesis and anticancer activity of 6-aminocoumarin/piperazine hybrids

Jayashree V. Patil[a], Shubhangi S. Soman[a], Anjali Singh[b] and Suresh Balakrishanan[b]

[a]Department of Chemistry, The M.S. University of Baroda, Vadodara, India; [b]Department of Zoology, The M.S. University of Baroda, Vadodara, India

ABSTRACT

Breast cancer and lung cancer causes a high rate of mortality all over the world. Pursuing our efforts toward searching for efficient anticancer agents herein a series of coumarin/piperazine hybrids **10a-f**, **12a-d**, **14** were synthesized and subsequently assessed for their potential *In Vitro* anticancer activity, against A549 (Lung cancer) and MCF-7 (breast cancer) cell lines using MTT assay. Encouragingly, all the synthesized compounds displayed varying degrees of effectiveness, ranging from good to moderate activity against these two cancer cell lines. However, amongst all the compounds synthesized, compound **12c** exhibited notably higher potency against both A549 and MCF-7 cell lines, with an IC_{50} of **0.40 μM** and **0.51 μM,** respectively. Additionally, the study delved deeper by conducting EtBr/AO assays, unveiling the induction of apoptosis. Furthermore, investigations into Reactive Oxygen Species (ROS) were conducted by using DCFH-DA dye. To understand the behavioral patterns and selectivity of the synthesized compounds, computational techniques were employed alongside experimental analysis. Utilizing density functional theory (DFT) calculations, electronic and structural characteristics were determined for compound **12c** These calculations were then compared and associated with the observed biological effects. Additionally, molecular docking was utilized to investigate how compounds **12c** interacted with crucial apoptotic genes, specifically targeting p53 and caspase 3. Compound **12c** exhibited docking scores of −8.4 kcal/mol and −7.9 kcal/mol for p53 and caspase 3 respectively. Lastly, an *in Silico* ADME study was performed to evaluate the compounds' potential as drug candidates.

Introduction

Uncontrolled cell division causing cancer or malignancy leads to tissue deterioration and widespread abnormal cell growth, affecting individuals of all ages and genders. Globally, cancer claimed approximately 10 million lives in 2023, with breast cancer ranking as the second leading cause of female mortality and showing an upward trend.[1,2] Lung cancer also remains a critical public health concern, significantly contributing to cancer-related deaths, highlighting the urgent need for innovative treatments due to frequent therapy resistance.[3] In the last two decades, advancements in cancer treatment have seen remarkable progress, introducing more potent medications with improved safety and targeted molecular precision. However, a significant hurdle in these treatments remains drug resistance, a challenge encountered by nearly all targeted anticancer drugs during clinical use.[4] This resistance stems from various processes, such as genetic or epigenetic mutations, amplification of specific pathways, the presence of cancer stem cells (CSCs), efflux transporters expelling drugs from cells, dysregulation of apoptosis (cell death), and alterations in autophagy. These mechanisms collectively contribute to the reduced efficacy of cancer treatments, emphasizing the need for continued research and innovative approaches to combat drug resistance and enhance the effectiveness of anticancer therapies.[5] Distinct challenges exist in providing cancer care across both developed and developing nations. These encompass concerns related to healthcare funding, patient education, and the delivery of treatments, posing

significant hurdles in effective cancer management on a global scale.[6,7] Heterocyclic nuclei are the versatile moieties used by medicinal chemists for the drug design and development of potential medicinal agents.[8] Recently, a hybridized approach based on multi-target directed ligands has received considerable attention to develop therapeutic agents which act at multiple targets. Researchers are presently dedicated to synthesize novel heterocyclic hybrid molecules designed for a spectrum of biological applications, aiming to integrate distinctive properties for enhanced efficacy in various biological contexts.[9–11]

Hybrid drugs, also known as "single molecule multiple targets" or "multiple ligands," represent compounds that embody structural elements from two different original molecules.[10,12–14] These hybrid molecules integrate features from two separate biologically active compounds (pharmacophores) that individually engage with distinct pharmacological targets, demonstrating a single entity's ability to interact with multiple targets simultaneously. Hybrid drugs are classified by their connectivity, achieved through two distinct strategies in designing and preparing these molecules.[12,15] Firstly, by merging drug pharmacophores, either directly connecting two pharmacophoric groups or linking them with a spacer, forming the basis of their structural arrangement.[16,17] These strategies play a crucial role in creating hybrid molecules with varied biological activities and enhanced therapeutic potential. Scaffolds based on several heterocyclic rings or a hybrid of more than two heterocyclic rings have been employed such as pyrazolone, imidazole, thiazole, piperazine, etc. have been explored for different biological applications such as anticancer, antimicrobial, antifungal, anticonvulsant, antibacterial, etc.[18] In the literature study, several potent hybrid anti-proliferative and anti-tumor compounds have been developed using molecular hybridization methods, incorporating diverse chemical structures such as quinazoline, indole, carbazole, quinoline, imidazole, hydroxamic acid, pyrimidine, curcumin, triazole, Sisatin, chalcone, benzimidazole, coumarin, pyrazole, and pyridine.[19] One of the important compound for hybridization is coumarin which is widely explored in literature. Coumarin hybrids, formed through coupling with diverse molecular entities, hold considerable importance in biological applications.[20,21] By combining coumarin with compounds such as quinazoline, indole, carbazole, pyrimidine, pyrazole, piperazines, etc. these hybrids exhibit amplified pharmacological properties, offering enhanced bioactivity, targeted specificity, and improved pharmacokinetics. These versatile compounds demonstrate significant potential in various fields.[22,23] Among the array of coumarin hybrids, one notable compound in molecular hybridization is the coumarin/piperazine hybrid, this unique combination merges the strengths of coumarin with the attributes of piperazine, presenting potential in targeting specific diseases.[20,22,24] These hybrids exhibit diverse therapeutic benefits, holding promising biological applications. Researchers are actively investigating coumarin/piperazine hybrids for their role in developing new medications for various health concerns. Furthermore, piperazine skeleton is an important pharmacophore showing various activities therefore it is used as a linker or bridge between two active compounds.[25–27] The piperazine analogs of coumarin were reported wide range of biological activities, such as antimicrobial, antifungal, anti-inflammatory, inhibitory and anticancer.[23,28] Cheng-Shi et al.[29] and Mahmoud et al.[30] synthesized the coumarin/piperazine hybrid **1** and **2** have shown acetylcholinesterase inhibitory activity[29,30] shown in Figure 1. It was also reported that coumarin/piperazine moieties
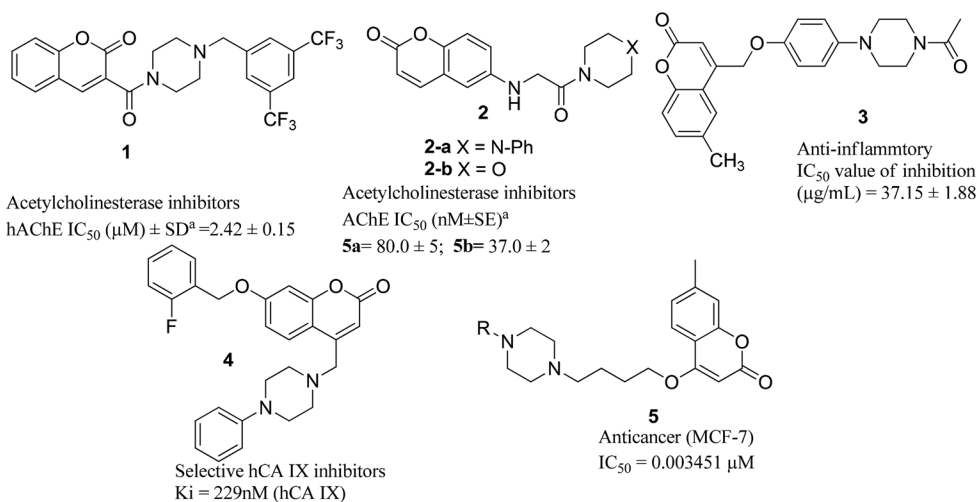
Figure 1. Coumarin/piperazine hybrids with different biological activity.

had excellent potency against different biological activities including anticancer activity in different cancer cell lines. According to the study's findings, the combination of coumarin and piperazine displayed significant biological action which some of the reports are depicted in Figure 1. Slight modification to the substitution pattern on the piperazine and coumarin nucleus facilitates a recognizable difference in the medicinal potential of the resultant molecules.[31] piperazines can be a flexible building block to discover drug-like elements and have a significant impact on the pharmacokinetics and pharmacodynamics factors of the resulting molecules. Literature studies have highlighted the potential of coumarin/piperazine derivatives as promising candidates in the fight against cancer.[24,30] These compounds exhibited cytotoxicity against various cancer cell lines and have shown promise in inhibiting tumor growth through mechanisms such as apoptosis induction, cell cycle arrest, and interference with angiogenesis. In the present scenario, coumarin-based anticancer drugs are actively exploring the therapeutic potential aiming to develop innovative treatments that could provide new hope for cancer patients soon. Very recently, Mallika Alvala et al synthesized coumarin and Piperazine Conjugates **4** as selective inhibitors of the tumor-associated carbonic anhydrase IX and XII isoforms. It was also reported that coumarin/piperazine moieties had excellent potency against several bacterial strains.[32] Also, very recently Premlata K. et al synthesized new coumarin/piperazine hybrids **5** as potential antibacterial and anticancer agents (MCF-7) in breast cancer cell line.[33] Hence, the exploration of coumarin/piperazine derivatives for the treatment of breast cancer and lung cancer has been relatively limited in the literature.
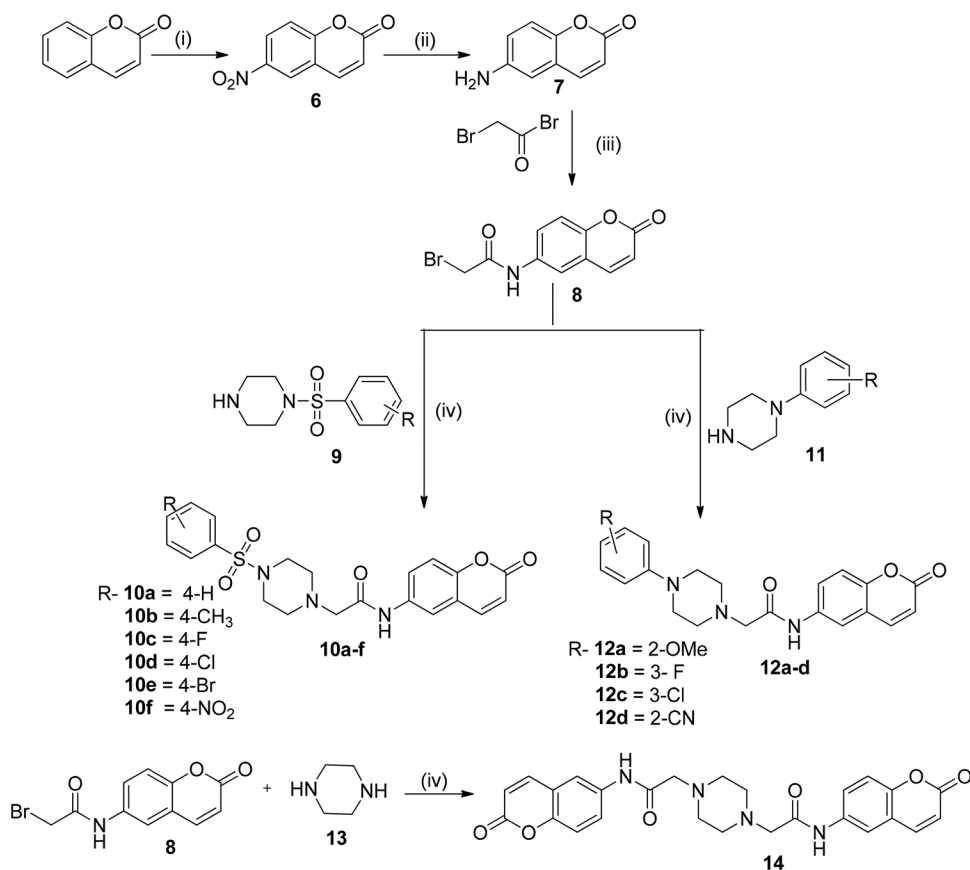
Therefore, based on existing findings in the literature, and our continuous ongoing research on synthesis and study of anticancer activity of coumarin-based derivatives[34–36] we have chosen to synthesize coumarin/piperazine derivatives as potential candidates for anticancer drugs targeting these specific types of cancers. we have designed compounds containing 6-aminocoumarin attached to different substituted phenyl sulfonyl piperazines and phenyl piperazines and studied them for *In Vitro* anticancer activity. The positioning of nitrogen in piperazine is vital, significantly contributing to the

improved water solubility of drug-like molecules and thus enhancing their bioavailability of the molecule.

Results and discussion

Chemistry

In search of some novel compounds with potent anticancer activity, initially we started from the preparation of 6-aminocoumarin via two steps, first nitration of 2*H*-chromen-2-one was carried out which is followed by reduction of 6-nitro-2*H*-chromen-2-one **6** which on reduction gave 6-amino-2*H*-chromen-2-one **7** by using iron powder and NH_4Cl in water which on further reaction with bromo acetyl bromide gave 6-bromoacetamide coumarin **8** (Scheme 1). Further reaction of 6-bromoacetamide coumarin **8** with different phenyl sulfonyl piperazines and phenyl piperazines using base in DMF gave desired 6-substituted aminocoumarin based acetamide derivatives **10a-f and 12a-d** and **14** (Scheme 1). All the synthesized compounds were characterized by ^{1}H-NMR, ^{13}C-NMR, ESI-MS, IR.

Reagents and Conditions:(i) HNO_3:H_2SO_4 (1:3)Conc. H_2SO_4, RT, 2hr (ii) Fe (powder), NH_4Cl, H_2O Reflux,80°C,6hrs (iii) TEA, DCM,RT, 2hrs. (iv)TEA, DMF, RT, 4-6hrs.

Scheme 1. Synthesis of compounds **10a-f, 12a-d** and **14**.

IR spectra of compounds **10a-f** exhibited one band for N-H stretching frequency of amide range from $3215 - 3288 \, cm^{-1}$, -CH stretching observed in the range of 2830-3092. The stretching band for lactone carbonyl group of coumarin ranges from 1701 to $1737 \, cm^{-1}$ and the stretching band for amide was observed in the range of 1615 to $1678 \, cm^{-1}$. The ^1H-NMR spectrum of compounds **10a-f** showed piperazine protons in the range of δ 2.73 to 3.07 as a broad singlet. Methylene protons adjacent to amide carbonyl were observed in the range of δ 3.21 to δ 3.28 and all aromatic protons were observed in the range of δ 6.41 to 7.99 ppm. The -NH protons appeared in the range of δ 8.84-9.87 ppm. In ^{13}C-NMR of compounds **10a-f** showed peaks of aliphatic carbons in the region of δ 45.36–61.58 ppm of piperazine carbons and methylene carbon and all aromatic carbons appeared from δ 116.57 to 150.00 ppm. Amide carbonyl carbon was observed in the range of δ 159.84 to 160.61 ppm. while carbonyl carbon of coumarin lactone ring at 167.67–168.26 ppm.

For compound **12a-d,** and **14** IR spectrum exhibited one strong band for -NH proton in the range of 3288-to $3539 \, cm^{-1}$. Band for lactone carbonyl group of coumarin was observed in the rage of 1719 to $1730 \, cm^{-1}$ and the band for amide carbonyl was observed in the range of δ 1618 to δ $1684 \, cm^{-1}$. In ^1H-NMR of compounds **12a-d** and **14** aliphatic protons were observed from δ 2.82- δ3.90 of piperazine and methylene protons respectively. All aromatic protons for compounds observed in the range of δ 6.47 to δ 7.73, along with –NH protons around δ 9.26 ppm. In ^{13}C-NMR of compounds **12a-d** and **14**, aliphatic carbons were observed in the range of δ 48.99–61.95 ppm for piperazine and methylene carbon. All aromatic carbons were observed in the range of δ 106.29–151.96. Amide carbonyl carbon observed in the range of δ 159.86-160.68, while lactone carbonyl carbon of the coumarin ring appeared in the range of δ 168.26–168.68 ppm.

Biological evaluation
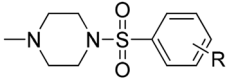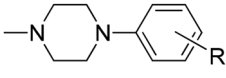
Anticancer activity by MTT assay

The anticancer activity of coumarin/piperazine hybrids **10a-f**, **12a-d** and **14** on reaction with substituted phenyl piperazine sulfonamide and phenyl piperazine was investigated through MTT assay against A549 (lung cancer cell line) and MCF-7 (breast cancer cell line), and the findings were compared with the results obtained from the standard drug Fluorouracil. (Table 1).

Structure activity relationship (SAR) for anticancer activity

Compound **10a** without any substituent on the phenyl ring showed good activity against A549 cell line with IC_{50} value 3.93 ± 0.15 μM whereas it showed moderate activity against MCF-7 cell line with IC_{50} value 8.14 ± 0.033 μM. When electron donating –CH$_3$ group was attached on phenyl ring in compound **10b** drops its anticancer activity against both tested cell lines and showed poor activity against both cell lines whereas –CH$_3$ is replaced by –fluoro group as in compound **10c** showed improvement in the activity against A549 cell line but for MCF-7 cell line it resulted in loss of activity (Table 1).

When -fluoro is replaced by -chloro substituent then it was observed that there is improvement in the activity and compound **10d** showed good activity against both cell

Table 1. Anticancer activity against A549 (Lungs cancer cell line), MCF-7 (Breast cancer cell line) for compounds **10a-f**, **12a-d and 14**.

Compounds	Compounds	R	IC$_{50}$ μM[a]	
			A549 μM	MCF-7 μM
(piperazine sulfonyl phenyl structure)	10a	4-H	3.93 ± 0.150	8.14 ± 0.033
	10b	4-CH$_3$	460 ± 5.660	50.41 ± 1.710
	10c	4-F	5.62 ± 0.053	338.1 ± 2.520
	10d	4-Cl	2.06 ± 0.057	4.93 ± 0.029
	10e	4-Br	92.62 ± 1.23	0.85 ± 0.030
	10f	4-NO$_2$	3.50 ± 0.045	3.95 ± 0.027
(piperazine phenyl structure)	12a	2-OMe	1.70 ± 0.059	39.17 ± 1.60
	12b	3-F	7.74 ± 0.038	4.74 ± 0.042
	12c	3-Cl	0.40 ± 0.032	0.51 ± 0.031
	12d	2-CN	14.5 ± 0.120	11.15 ± 0.019
	14		5.04 ± 0.071	11.43 ± 0.014
Fluorouracil	Fluorouracil		11.13 ± 0.083	45.04 ± 1.020

[a]IC$_{50}$ values were determined based on MTT assay using GraphPad Prism software.

lines, for A549 with IC$_{50}$ value 2.06 ± 0.057 μM and in MCF-7 with IC$_{50}$ value 4.93 ± 0.029 μM. In compound **10e** where –fluoro is replaced by –bromo drops its activity against A549 cell line and showed poor activity whereas improvement in the anticancer activity against MCF-7 cell line and showed excellent activity against breast cancer cell line MCF-7 with IC$_{50}$ value 0.85 ± 0.030 μM However, when -fluoro in **10e** was replaced by strong electron withdrawing -NO$_2$ compound **10f** showed improvements in the anti-cancer activity against A549 cell line having moderate activity with IC$_{50}$ value 3.50 ± 0.045 μM and drops activity against MCF-7 with IC$_{50}$ value 3.95 ± 0.027 μM.

In another variation when different phenyl piperazines attached to compound **8** i.e., **12a-d**, compound **12a** with –OMe group attached to phenyl group showed good activity against A549 cell line with IC$_{50}$ value 1.70 ± 0.059 μM and dropped the anticancer activity against MCF-7 cell line. When methoxy was replaced by –fluoro group in compound **12b** showed the loss of anticancer activity against A549 cell line whereas showed improvement in the activity against MCF-7 cell line with IC$_{50}$ value 4.74 ± 0.042 μM. On replacing -fluoro by -chloro in compound **12c** showed very good improvement in the anticancer activity and showed excellent activity against both tested cell lines i.e., IC$_{50}$ value 0.40 ± 0.032 μM for A549 cell line and 0.51 ± 0.031 μM for MCF-7 cell line respectively. However, when -Cl is replaced by –CN in compound **12d** showed drop in anticancer activity having moderate activity against both tested cell lines with IC$_{50}$ values 14.5 ± 0.120 μM and 11.15 ± 0.019 μM against A549 cell line and MCF-7 cell line respectively. Compound **14** coumarin dimer with piperazine showed improvement in anticancer activity against A549 cell line with IC$_{50}$ value 5.04 ± 0.071 μM and remains moderate for MCF-7 cell line with IC$_{50}$ value 11.43 ± 0.014 μM. Compound **12c**, exhibiting significantly lower IC$_{50}$ values of 0.40 ± 0.032 μM against the A549 cell line and 0.51 ± 0.031 μM against the MCF-7 cell line, therefore effect of compound **12c** on the noncancer cell line NIH3T3 was studied by using MTT assay and the IC$_{50}$ value was found to be 85.04 ± 6.24 μM. However, the **12c** could effectively curb viability of A549 and MCF-7 at a very low concentration of 0.40 μM and 0.51 μM. It is therefore, prudent to presume that at the selected dose, compound **12c** will not cause any deleterious effect to neighboring noncancer cells or the cells remained refractory even at the highest concentration tested for the cancer

cell line. In continuation of our study, compound **12c** was subsequently chosen for additional analysis employing the Ethidium bromide/acridine orange staining assay and assessment of Reactive Oxygen Species (ROS) activity.

Ethidium bromide/acridine orange staining assay

The EtBr/AO staining assay was conducted for compound **12c** for the A549 cell line and MCF-7 cell line, respectively, serving as vital experimental validations to comprehend the impact of these compounds on distinct cancer cell lines. Ethidium bromide selectively stains cells that have lost membrane integrity, while the essential dye acridine orange stains both live and dead cells.[37]

In the EtBr/AO dye staining, necrotic cells exhibit red fluorescence, live cells appear green, early apoptotic cells with evident condensation also exhibit green fluorescence, and late apoptotic cells with condensation and fragmentation display an orange fluorescence. Upon treating cells with IC_{50} concentrations of compound **12c**, predominant early apoptotic characteristics were observed in the A549 cell line (Figure 2a–c) and MCF-7 cell line (Figure 2d–f), and in positive control notably late apoptosis and necrosis were observed.

DCFH-DA assay

The majority of chemotherapy drugs stimulate an excessive generation of Reactive Oxygen Species (ROS) beyond the necessary threshold, leading to cytotoxic effects in cancer cells. These heightened ROS levels play a pivotal role in initiating apoptosis
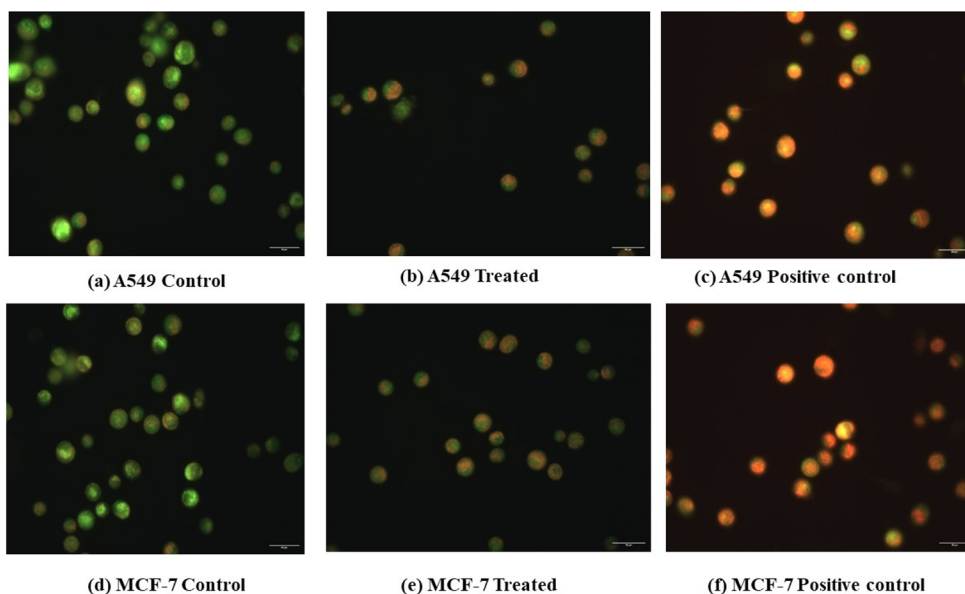

(a) A549 Control   (b) A549 Treated   (c) A549 Positive control

(d) MCF-7 Control   (e) MCF-7 Treated   (f) MCF-7 Positive control

Figure 2. EtBr/AO assay: Performed with (i)A549 Lung cancer cell line for **12c** (a, b, c) images represent control, treated, positive control (ii) MCF-7 breast cancer cell line (d, e, f). For compound **12c** (d, e, f) Images represent control, IC_{50} conc. of compound **12c** treated and positive control in MCF-7 cell line.
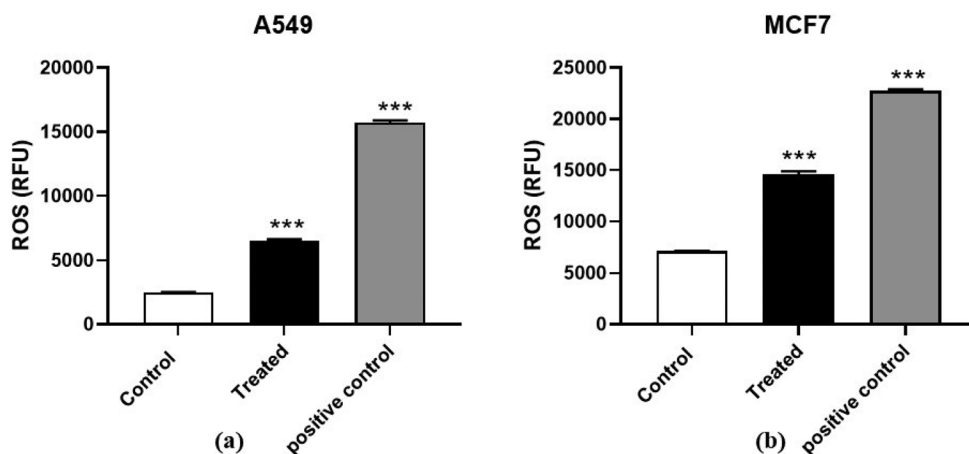
Figure 3. DCFH-DA assay to Estimate the intracellular reactive oxygen species (ROS) level by for compound **12c** in A549 and in MCF-7 respectively. (***p ≤.001).

pathways involving key factors like p53, caspase-8, and Fas-associated cell death.[38] As per the findings by Ramsey and Sharpless, p53, acting as a redox-sensitive transcription factor, detects increased ROS levels, subsequently initiating apoptosis in cancerous cells. Therefore, this study focused on assessing ROS levels in compounds **12c** within the A549 and MCF-7 cell lines (as depicted in Figure 3).

The marked elevation of ROS levels observed in both cell lines upon exposure to the IC_{50} concentration of compound **12c** strongly corroborates the study's findings. Monitoring ROS levels serves as a critical indicator of cellular stress and oxidative damage. This elevation in ROS beyond the threshold might be indicative of the mechanisms underlying the cytotoxic effects induced by compounds **12c** in the A549 and MCF-7 cell lines, shedding light on their potential as agents targeting ROS-mediated pathways in cancer treatment.

DFT study

The Gaussian 09 software employing the B3LYP/6-31G level of theory under (d, p) basis set was utilized to optimize the geometrical structure of active compound **12c**. Figure 4 displays the estimated optimized structure of compound **12c** with a true minimum energy. Assessments regarding the kinetic and chemical stability of compound **12c** variants were made by calculating the energy difference between the highest occupied molecular orbital (HOMO) and the lowest unoccupied molecular orbital (LUMO).[39]

The frontier molecular orbitals (FMO) for compound **12c** displayed in Figure 4. Negative E_{HOMO} and E_{LUMO} values signify compound's stability and the E_{HOMO}-E_{LUMO} energy gap offers insights into both kinetic stability and chemical reactivity.[40] For compound **12c,** the HOMO was mainly localized around the coumarin ring and the carbonyl nucleus of the acetamide linked to coumarin, while the LUMO was localized only on the coumarin ring. The theoretically calculated HOMO energies for compound **12c** were found to be −8.355799 eV, and the LUMO energies for compound **12c** were −1.814999 eV, indicating an overall high chemical stability with HOMO-LUMO energy

gap of 6.5408 eV. These energy values were used to calculate essential molecular properties such as ionization potential (IP), electron affinity (EA), electronegativity (χ), hardness (η), softness (S), electrophilicity index (ω), and chemical potential (μ). IP and EA were derived as IP = $-E_{HOMO}$ and EA = $-E_{LUMO}$. Comparing the IP and EA values, compound **12c** with a higher IP and a lower EA demonstrated increased stability (Table 2).[41]

Additionally, the stability of compound **12c** was correlated with global hardness and softness, as outlined in Table 2. Molecular electrostatic potential (MEP) surfaces, computed using the same basis set, are depicted in Figure 5 The MEP provides information about different reactivity sites available on the surfaces as well as sites for hydrogen bonding. The MEP surfaces in Figure 5 revealed negative potential sites localized on the carbonyl carbon of coumarin and the carbonyl group of acetamide, indicating stability, consistent with the previous findings (Figure 5). DFT study showed the compound's high stability and low reactivity for compounds **12a** and **12c** as
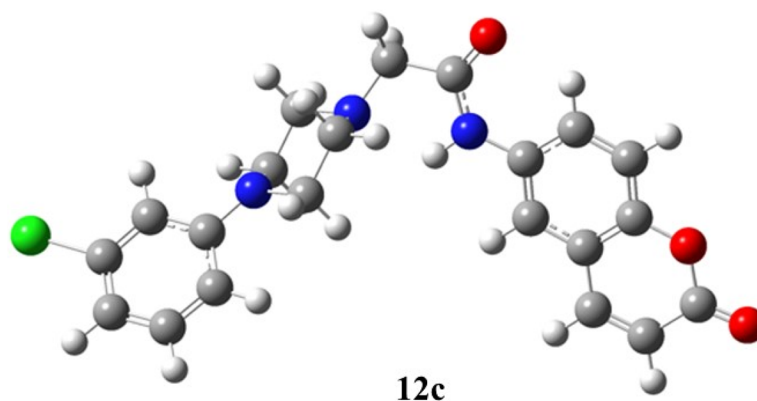

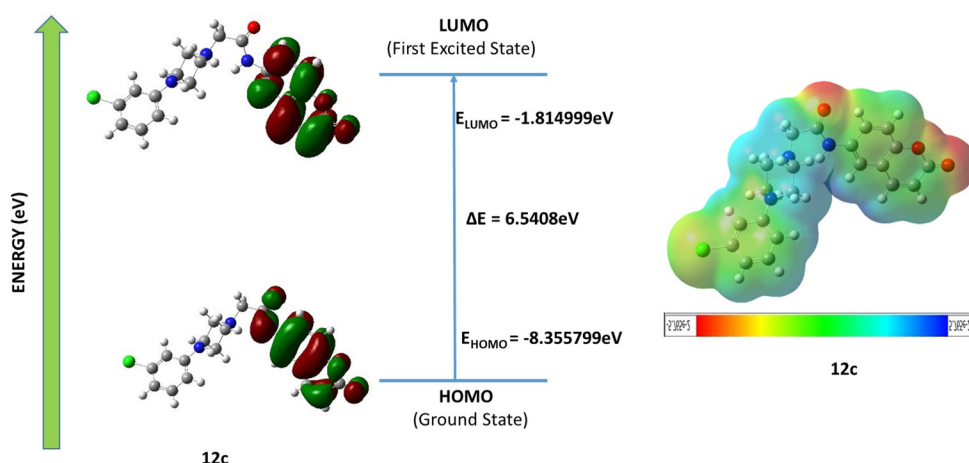**Figure 4.** DFT-optimized structure of compounds **12c**.

Figure 5. Frontier molecular orbital surfaces of compounds (FMO) and Molecular electrostatic potential (MEP) diagram of compounds **12c**.

Table 2. Molecular properties (in eV) compound **12c**.

Parameters	Compound **12c**
E_{HOMO} (eV)	−8.355799
E_{LUMO} (eV)	−1.814999
E_{HOMO} -E_{LUMO} gap ΔE (eV)	6.5408
Ionization potential (*I*) (eV)	8.355799
Electron affinity (EA) (eV)	1.814999
Global hardness (η)	4.5408
Global softness (*S*)	0.1101
Electronegativity (χ)	3.27040
Electrophilicity index (*ω*)	1.011993
Chemical potential (μ)	−5.0854

compared to that observed for compounds **10b** and **10e**. Hence compounds **12a** and **12c** are more likely to remain stable during biochemical reactions with the target and effectively interact with the biological target to give good activity.

Following the completion of the DFT study, our study extended for molecular docking for the active compound. This study allowed to delve deeper into understanding the interactions and potential binding affinities of the compound within biological macromolecules.

Molecular docking

Molecular Docking an essential technique, is now widely recognized for its ability to predict how small ligands interact with biological macromolecules. The compound further examined by molecular docking studies which was employed to assess the binding affinity of compounds with proteins involved in the apoptosis pathway: protein p53 (3DCY) and caspase 3 (4QTX). This investigation focused on compounds **12c**, the most active among those synthesized, revealing their binding interactions with potential targets in Table 3. The guardian gene p53 triggers a self-destructive pathway

Table 3. Molecular docking study of compound **10e** and **12c** PDB IDs; p53 (3DCY), Caspase 3 (4QTX) their bonding, amino acid interactions and docking score.

Compound	PDB ID	Bond	Amino acid interactions	Docking score kcal/mol
10e	p53 (3DCY)	Hydrogen Bond	HIS11, ARG10,ARG203	−8.6
		Carbon Hydrogen Bond	SER228	
		Pi-Anion	GLU89	
	Caspase 3 (4QTX)	Hydrogen Bond	PHE250, ASN208	−8.4
		Carbon Hydrogen Bond	ASP211	
		Pi-Sulfur	TRP214	
12c	p53 (3DCY)	Hydrogen Bond	GLN23, ARG10, ASN17	−8.4
		Carbon Hydrogen Bond	ASN232, ILE22	
		Pi-Alkyl	PRO231	
	Caspase 3 (4QTX)	Hydrogen Bond	ASN208, TRP214	−7.9
		Carbon Hydrogen	PHE250, GLU248	
		Pi-Anion	ASP211	
		Pi-Pi	PHE247	
Fluorouracil	p53 (3DCY)	Hydrogen Bond	GLN23, ASN17	−5.5
		Carbon hydrogen bond	LYS20	
		Hydrogen (Fluorine)	ASN17	
	Caspase 3 (4QTX)	Hydrogen Bond	PHE250, ASN208	−6.2
		Carbon Hydrogen Bond	TRP206	
		Halogen (Fluorine)	ARG207	

in cells when a compound induces cellular stress and causes DNA damage.[42] Yet, this mechanism is tightly regulated to maintain low cellular levels in normal cells, regulated by entities like MDM2, a negative regulator of p53. MDM2 physically interacts with p53, leading to p53's ubiquitination and degradation via proteasomes.[43] If a drug occupies the interaction site between p53 and MDM2, it can potentially counteract MDM2's negative regulation, enabling the activation of p53-mediated pathways responsible for anticancer activity.

Caspase 3 serves as the effector caspase in the apoptotic pathway, initiating apoptosis upon receiving activation signals from upstream sources. Compound **12c** is docked with p53 (3DCY) at the active site and generated a docking score of −8.4 Kcal/mol and Caspase 3 (4QTX) at the active site and generated a docking score of −7.9 Kcal/mol, (Figure 6, Table 3). Ligand **12c** interacts with the targeted protein, p53, forming three hydrogen bonds. One hydrogen bond involves the oxygen atom of the lactone carbonyl with GLN 23 at a distance of 1.99 Å, one involves the oxygen atom of carbonyl of amide with ARG10 at a distance of 6.11 Å and one involves hydrogen atom of amide attached to coumarin with ASN 17 at a distance of 3.02 Å. Also form carbon hydrogen interactions one with piperazine nucleus and other with oxygen of pyrone with ASN 232 and ILE 22 at 3.64 Å and 4.20 Å respectively. Benzene nucleus attached to piperazine shows Pi-alkyl interaction with PRO at 4.19 Å.

On the other hand, when interacting with the targeted protein caspase 3 (4QTX), two hydrogen bond interactions were observed between the protein and the ligand. The protonated nitrogen atom in the piperazine ring could form H-bond interaction with ASN 208 at a distance of 2.64 Å and another hydrogen interaction with oxygen of carbonyl of amide with TRP 214 at a distance of 2.90 Å two carbon hydrogen interactions with PHE 250 and GLU 248 at a distance 3.50 Å, 3.69 Å, 3.73 Å and Pi anion and Pi-Pi interaction of coumarin nucleus with ASP 211 at distance 3.38, 4.32 and PHE 247 at a distance 4.63 Å and 4.74 Å. Compound **10e** is also docked with p53 (3DCY) at the active site and generated a docking score of −8.6 Kcal/mol and Caspase 3 (4QTX) at the active site and generated a docking score of −8.4 Kcal/mol. Ligand **10e** interacts with the targeted protein, p53, forming three hydrogen bonds with HIS11, ARG10, ARG203, carbon hydrogen bond with SER228 and Pi-Anion bonds with GLU89 (Fig. S1). On the other hand, when interacting with the targeted protein caspase 3 (4QTX), two hydrogen bonds interactions were observed between the protein and the ligand. Two hydrogen bonds with PHE250, ASN208 and carbon hydrogen bond with ASP211 and Pi-Sulfur with TRP214 were found.

In-silico based ADME and toxicity study

The *in-silico* study conducted on compound **12c** involved an exhaustive analysis of its Absorption, Distribution, Metabolism, Excretion (ADME), and toxicity profiles.[44] The drug-likeliness of compound was predicted using SwissADME. (Table 4) To be a drug-like candidate, the compound should follow Lipinski's Rule of Five (clogP ≤ 5, molecular weight ≤ 500, the number of hydrogen bond acceptors ≤ 10 and donor ≤ 5) which predict lipophilicity, critical molecular weight and chemical structure. The compound violating more than one of these rules will be poor in terms of bioavailability and not be orally active, hence, cannot be used as a drug without modification.[38] The
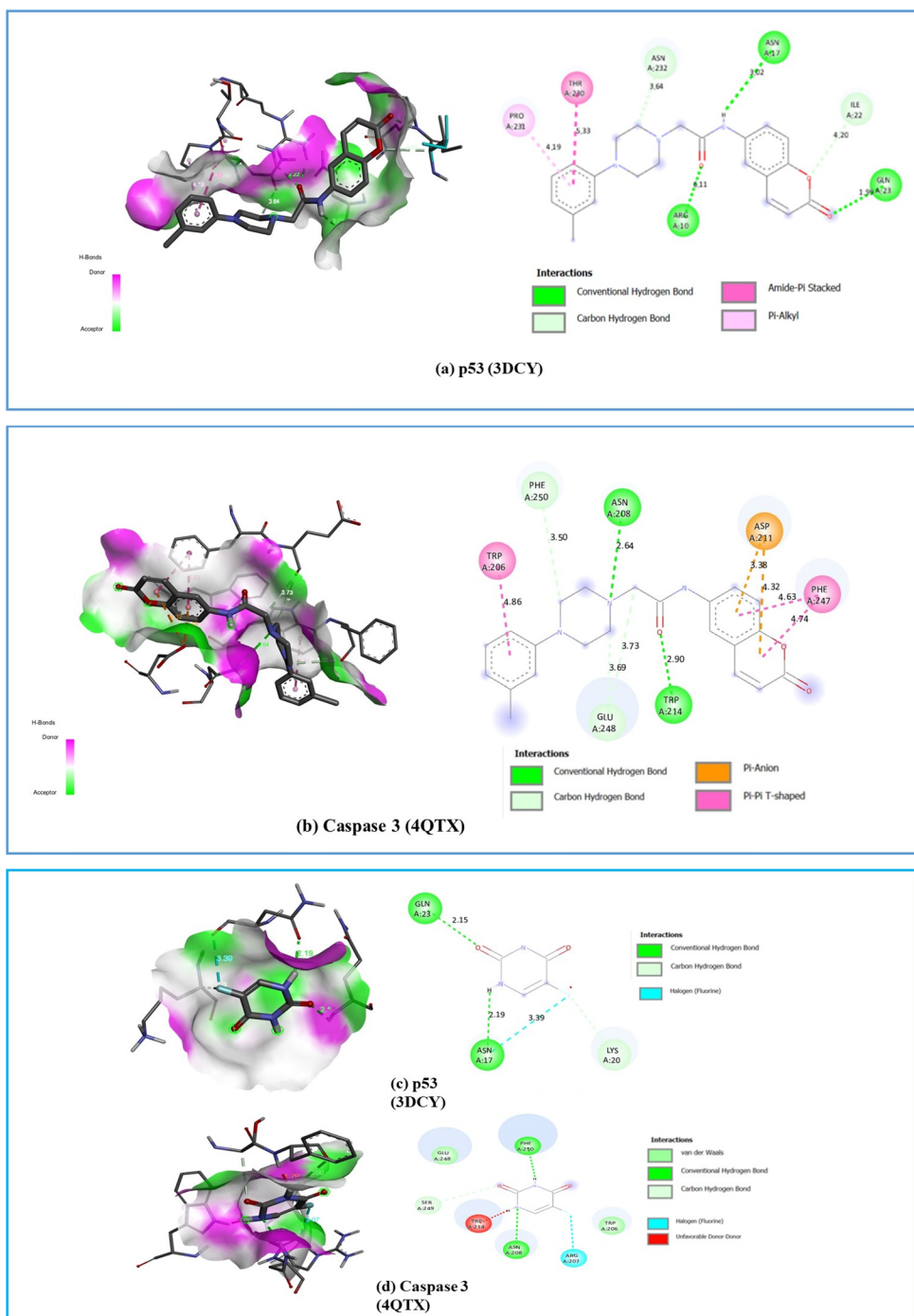
Figure 6. 3D and 2D molecular docking structure of compound **12c** with (a) p53(3DCY) (b) Caspase 3 (4QTX) (c) standard Fluorouracil with p53 (3DCY) and (d) with Caspase 3 (4QTX).

compound **12c** satisfied all four criteria of good drug candidate *viz.,* Molecular weight 397.85 g/mol; octanol/water partition coefficient *viz.,* 2.88 (logP$_{o/w}$ less than 5), the number of hydrogen donor *viz.,* 1 and the number of hydrogen acceptor *viz.,* 4. In

Table 4. ADMET properties of compound **12c**.

ADMET Properties	Compound 12c
M.W(g/mol)	397.85
No. of H-donor group	1
No. of H-acceptor	4
$logP_{o/w}$	2.88
GI absorption	High
BBB permeability	Yes
Log S	Moderately soluble
LD_{50}	617mg/kg
Hepatotoxicity(dili)	Inactive
Carcinogenicity	Inactive
Immunotoxicity	Inactive
Mutagenicity	Inactive

addition, gastrointestinal (GI) absorption of a drug molecule in Swiss ADME is indicated as high predicted which are again under acceptable limit, it suggests that the drug is likely to be absorbed effectively in the gastrointestinal tract when taken orally. This high GI absorption implies that the drug has a favorable ability to pass through the intestinal membrane and enter the bloodstream, potentially leading to better systemic availability and effectiveness of the drug. The allowed violation of rule of five is one, hence the compound was still a good drug candidate for further study. The compounds' toxicity was anticipated using the ProTox-II webserver, developed by Drwal et al.[45]

The forecast encompassed various parameters such as rat oral acute toxicity, focusing on median lethal dose (LD_{50}) measured in mg/kg, organ toxicity particularly hepatotoxicity, immunotoxicity, genetic toxicity including cytotoxicity, mutagenicity, and carcinogenicity endpoints, all of which were predicted specifically for compound **12c**. The LD_{50} for compound **12c** was 617 mg/kg hence, classified as class IV ($300 \leq LD50 \leq 2000$). According to GHS class I is the most toxic and class VI is nontoxic. However, the IC_{50} concentration of compounds was found to be much less than LD_{50} hence, it will not pose any toxicity if given orally. The derivative **12c** hepatotoxicity, carcinogenicity, immunotoxicity, and mutagenicity were not observed. Hence, the compound **12c** can be taken further as anticancer drug candidate for detail analysis.

Conclusion

In this work different coumarin/piperazine hybrids were synthesized and their *in-Vitro* anticancer activity were studied against two cancer cell lines A549-Lungs cancer cell line and MCF-7 breast cancer cell lines. For phenyl sulfonyl piperazine derivatives of coumarin **10a-f**, compound **10e** showed very good activity against the MCF-7 breast cancer cell line and other compounds showed good to moderate activity against the A549 cell line and MCF-7 cell line. From compounds **12a-d** phenyl piperazines attached to coumarin, compound **12c** showed excellent activity against both lung cancer cell line (A549) and breast cancer (MCF-7) cell line. However, compounds **12a, 12b, 12d** and **14** showed good to moderate activity against both lung cancer A549 and MCF-7 breast cancer cell lines. From all synthesized compounds, compound **12c** has shown excellent activity against both A549 lung cancer cell line (IC_{50} 0.40 μM) and MCF-7 cell line (IC_{50} 0.51 μM) and was selected for further evaluation. In cytotoxic investigations utilizing the EtBr/AO assay, compound **12c** exhibited an apoptosis pathway in

the tested cell lines. The induction of apoptosis was primarily governed by reactive oxygen species (ROS) at the IC_{50} value in A549 and MCF-7 cell lines for compound **12c.** To predict the molecular mechanism, molecular docking was performed with the critical apoptotic genes p53 and caspase 3 for **12c**. Compound **12c**, exhibited docking scores of −8.4 kcal/mol as well as −7.9 kcal/mol for p53 and caspase 3, respectively. In comparison, fluorouracil displayed significantly higher docking scores of −5.5 kcal/mol. in p53 and −6.2 kcal/mol in Caspase 3. Consequently, it can be inferred that compound **12c** as potent anticancer agent, primarily activating the ROS-induced p53-dependent caspase 3-mediated apoptotic pathway in both cancer cell lines at the lowest IC_{50} concentration. The *in-silico* based ADME and toxicity studies of compound **12c** indicated drug-likeliness of it and can be studied further in detail as anticancer drug.

Experimental

General chemistry

Reagent-grade chemicals and solvents purchased from commercial supplier are used after purification. TLC was done on silica gel F254 plates from Merck. For column chromatographic purification, Acme's silica gel (60–120 mesh) was used. The melting points of open capillary tubes were calculated using a Rolex melting point instrument. KBr pellet IR spectra were recorded on the Perkin Elmer RX 1 spectrometer. Spectral data for ^{1}H NMR and ^{13}C NMR were gathered on an Advance Bruker 400 spectrometer (400 MHz/500 MHz) using $CDCl_3$ or DMSO-d6 as the solvent and TMS as the internal standard. *J* values are in Hz. A Shimadzu LCMS 2020 equipment was utilized to determine the mass spectra using ESI-MS. The findings of the elemental analysis were recorded using a Thermosinnigan Flash 11–12 series EA. 6-amino coumarin, different phenyl sulfonyl piperazines were prepared according to the literature method.[31,46]

Synthesis of 6-nitrocoumarin (6)

To a cold solution of coumarin (10.0 g, 68.5 mmol) in concentrated H_2SO_4 (50 mL), was added 20 ml of mixed acid (HNO_3: H_2SO_4 = 1:3, v/v). The resulting mixture was stirred at 0 °C for 15 minutes and then at room temperature for 2 hours. The reaction mixture was poured into ice-cold water to give white solid. The solid was filtered washed with cold water and recrystallized using acetic acid. M.P184-186 °C.

Synthesis of 6-amino coumarin (7)

To a suspension of 6-Nitrocoumarin (10.0 g, 52.38 mmol) and Fe powder (20 g) in water (170 mL) was added ammonium chloride (3.25 g, 60.75 mmol) in several portions over a period of 10 mins. The resulting mixture was heated at 80 °C for 6 hours. The completion of reaction was checked by TLC. After completion of reaction, the reaction mixture was filtered and brown solid was dissolved in ethyl acetate. The organic layer was filtered to remove insoluble solid and filtrate was concentrated on a rotavapor to give the compound as silky golden crystals. M.P.162 °C-164 °C.

2-bromo-N-(2-oxo-2H-chromen-6-yl)acetamide (8). To a solution of 6-aminocoumarin **7** (10.0 mmol) in dichloromethane (DCM) (25 mL) was added triethylamine (TEA)

(15.0 mmol) and stirred for 5–10 min. To this bromoacetyl bromide (12.0 mmol) was added dropwise over a period of 10 min. The resulting solution was stirred at room temperature for 2 hours. The reaction mixture filtered, washed with DCM, water and acetone to give compound **8** as a pale white solid. The substituted bromoacetamide **8** thus obtained, used directly for next step without any purification.

White Solid; Yield: 70%; M.P: 174-176°C; IR (KBr) 3291, 3108, 1739, 1651, 1622, 1575, 1490, 1438, 1378, 1340, 1299, 1261, 1180, 1111, 918, 884, 826, 751, 714 cm-1; ^{1}H-NMR (400 MHz, DMSO-d_6): δ 4.07 (s, 2H), 6.50 (d, $J = 9.6$ Hz, 1H), 7.39 (d, $J = 8.8$ Hz, 1H), 7.66 (dd, $J = 2.4$ Hz, 8.8 Hz, 1H), 8.05 (d, $J = 2.8$ Hz, 1H), 8.10 (d, $J = 9.6$ Hz, 1H), 10.65 (s, 1H); ^{13}C-NMR (400 MHz, DMSO-d_6): δ ppm 30.65, 117.11, 117.28, 118.44, 119.23, 123.82, 135.40, 144.71, 150.16, 160.41, 165.46.

General procedure for the synthesis of compounds 10a-f and 12a-d, 14

To a Solution of 2-bromo-N-(2-oxo-2H-chromen-6-yl)acetamide **8** (**1.1 eq**) and phenyl sulfonyl piperazines **9**/phenyl piperazines **11**/piperazine **13 (1 eq)** in DMF (20 mL) was added triethylamine (1.5 eq). The resulting mixture was stirred at room temperature for 16 hr and then poured into cold water. The aqueous layer thus obtained was extracted using ethyl acetate and/or dichloromethane (checked by TLC) and solvent evaporated to give crude product. The crude compound was purified by column chromatography.

Characteristics data of compounds 10a-f and 12a-d, 14:

N-(2-oxo-2H-chromen-6-yl)-2-(4-(phenylsulfonyl)piperazin-1-yl)acetamide (10a). White Solid; Yield: 72%; M.P: 184-186°C; IR (KBr) 3289, 3089, 2959, 2923, 2855, 2805, 1698, 1615, 1571, 1484, 1435, 1344, 1257, 1163, 1129, 1101, 1071, 950, 924, 900, 819, 746, 691 cm^{-1}; ^{1}H-NMR (400 MHz, CDCl$_3$): δ 2.73 (broad s, 4H), 3.15 (broad s, 4H), 3.19 (s, 2H), 6.42 (d, $J = 9.2$ Hz, 1H), 7.23 (d, $J = 8.4$ Hz, 1H), 7.35 (d, $J = 8.4$ Hz, 1H), 7.58-7.68 (m, 5H), 7.80 (d, $J = 7.2$, 1H), 7.99 (s, 1H), 8.84 (s, 1H); ^{13}C-NMR (100 MHz, CDCl$_3$): δ ppm 45.36, 45.86, 52.65, 61.58, 116.57, 116.75, 117.20, 117.30, 118.20, 119.20, 123.28, 130.31,131.97, 143.23, 150.50, 160.52, 164.37, 166.40, 167.67 Anal. calc. for C$_{21}$H$_{21}$N$_3$O$_5$S; C,59.00; H,4.95; N,9.83; found: C,59.03; H,5.60; N,6.25; ESI-MS: 428.3 [M + H]$^+$.

N-(2-oxo-2H-chromen-6-yl)-2-(4-tosylpiperazin-1-yl)acetamide (10b). White Solid; Yield: 84%; M.P: 200-202°C; IR (KBr) 3271, 3040, 2901, 2840, 1737, 1675, 1571, 1528, 1438, 1374, 1345, 1322, 1163, 1132, 1098, 984, 927, 829, 722, 654 cm^{-1}; ^{1}H-NMR (400 MHz, CDCl$_3$): 2.49 (S,3H), 2.74 (t, $J = 4.8$ Hz, 4H), 3.14 (S, 4H), 3.20 (S, 2H), 6.44 (d, $J = 9.6$ Hz, 1H), 7.25 (d, $J = 8.8$ Hz, 1H), 7.35 (dd, $J = 2.4$ Hz & 8.8 Hz, 1H), 7.39 (d, $J = 8.4$ Hz, 2H), 7.68-7.70 (m, 3H), 8.00 (d, $J = 2.4$ Hz, 1H), 8.84 (S, 1H); ^{13}C-NMR (100 MHz, DMSO-d_6): 20.94, 45.56, 51.63, 60.98, 116.25, 116.37, 118.42, 118.49, 124.03, 127.53, 129.73, 131.99, 134.77, 143.53, 144.12, 149.45, 159.88, 168.08; Anal. calc. for C$_{22}$H$_{23}$N$_3$O$_5$S; C,59.85; H,5.25; N,9.52; found: C,59.87; H,5.28; N,9.55; ESI-MS:442.4 [M + H]$^+$.

2-(4-((4Fluorophenyl)sulfonyl)piperazin-1-yl)-N-(2-oxo-2H-chromen-6-yl)acetamide (10c). White Solid; Yield: 80%; M.P: 194-196°C; IR (KBr) 3255, 3045, 2959, 2928, 2856,

1732, 1678, 1592, 1574, 1529, 1492, 1440, 1381, 1349, 1291, 1234, 1171, 1126, 1099, 1073, 1014, 989, 950, 911, 832, 734, 655 cm^{-1}; ^{1}H-NMR (400 MHz, CDCl$_3$): δ 2.74 (t, $J=4.8$ Hz, 4H), 3.12-3.15 (m,4H), 3.20 (S, 2H), 6.42 (d, $J=9.6$ Hz, 1H), 7.23-7.30 (m, 3H), 7.35 (dd, $J=2.4$ Hz & 8.8 Hz, 1H), 7.67 (d, $J=9.6$ Hz, 1H), 7.80-7.84 (m, 2H), 7.99 (d, $J=2.4$ Hz, 1H), 8.83 (s, 1H); ^{13}C-NMR (100 MHz, CDCl$_3$): δ ppm 45.86, 52.69, 61.58, 117.19, 117.29, 118.20, 119.02, 123.29, 127.77, 129.27, 129.31, 133.13, 133.77, 135.80, 150.49, 160.54, 167.73; Anal. calc. for C$_{21}$H$_{20}$FN$_3$O$_5$S C,56.62; H,4.53; N,9.43; found: C,56.60; H,4.52; N,9.40; ESI-MS: 446.4 [M + H]$^+$.

2-(4-((4-Chlorophenyl)sulfonyl)piperazin-1-yl)-N-(2-oxo-2H-chromen-6-yl)acetamide (10d).

White Solid; Yield: 75%; M.P: 186-188 °C; IR (KBr) 3288, 3092, 3042, 2920, 2852, 1732, 1680, 1573, 1529, 1477, 1440, 1381, 1348, 1304, 1279, 1258, 1167, 1099, 1013, 987, 952, 911, 826, 761, 718, 656, 607 cm^{-1}; ^{1}H-NMR (400 MHz, CDCl$_3$): δ 2.75 (t, $J=4.8$ Hz, 4H), 3.15 (broad s, 4H), 3.21 (s, 2H), 6.44 (d, $J=9.6$ Hz, 1H), 7.26 (d, $J=8.8$ Hz, 1H), 7.37 (dd, $J=2.4$ Hz, 8.8 Hz, 1H), 7.58 (d, $J=8.8$ Hz, 2H), 7.69 (d, $J=9.6$ Hz, 1H), 7.75 (d, $J=8.4$ Hz, 2H), 8.00 (d, $J=2.4$ Hz, 1H), 8.81 (s, 1H); ^{13}C-NMR (100 MHz, DMSO-$d6$): δ ppm 45.53, 51.53, 60.83, 116.31, 116.37, 118.42, 118.47, 124.02, 129.39, 129.49, 133.83, 134.75, 138.21, 144.13, 149.44, 159.87, 168.03; Anal. calc. for C$_{21}$H$_{20}$ClN$_3$O$_5$S C,54.60; H,4.36; N,9.10; O,17.96; S,6.94; Anal. calc. for C$_{21}$H$_{20}$ClN$_3$O$_5$S C,54.60; H,4.36; N,9.10; found: C,54.58; H,4.34; N,9.13; O,17.96; S,6.94; ESI-MS: 462.3 [M + H]$^+$.

2-(4-((4-Bromophenyl)sulfonyl)piperazin-1-yl)-N-(2-oxo-2H-chromen-6-yl)acetamide (10e).

White Solid; Yield: 88%; M.P: 222-224 °C; IR (KBr) 3294, 3089, 2853, 1730, 1681, 1573, 1528, 1439, 1384, 1349, 1278, 1167, 1135, 1102, 1067, 1010, 951, 912, 822, 752, 711, 656 cm^{-1}; ^{1}H-NMR (400 MHz, CDCl$_3$): δ 2.75 (t $J=4.8$ Hz, 4H), 3.15 (broad s, 4H), 3.21 (s, 2H), 6.44 (d, $J=9.6$ Hz, 1H), 7.26 (d, $J=8.8$ Hz, 1H), 7.37 (dd, $J=2.4$ Hz, 8.8 Hz, 1H), 7.66-7.70 (m, 3H), 7.74 (d, $J=8.4$ Hz, 2H), 8.00 (d, $J=2.4$ Hz, 1H), 8.82 (s, 1H); ^{13}C-NMR (100 MHz, CDCl$_3$): δ ppm 45.86, 52.65, 61.60, 117.21, 117.30, 118.21, 123.32, 128.23, 129.21, 129.26, 132.59, 133.74, 134.85, 143.23, 150.51, 160.52, 167.64 Anal. calc. for C$_{21}$H$_{20}$BrN$_3$O$_5$S C,49.81; H,3.98; N,8.30; found: C,49.84; H,3.95; N,8.280; ESI-MS: 506.37, 508.04 [M + H]$^+$.

2-(4-((4-Nitrophenyl)sulfonyl)piperazin-1-yl)-N-(2-oxo-2H-chromen-6-yl)acetamide (10f).

White Solid; Yield: 88%; M.P: Above 250-252 °C; IR (KBr) 3278, 3104, 3043, 2923, 2857, 1726, 1681, 1605, 1574, 1529, 1440, 1379, 1350, 1310, 1257, 1172, 1130, 1103, 1065, 1011, 956, 915, 881, 854, 828, 749, 712, 685 cm^{-1}; ^{1}H-NMR (400 MHz, DMSO-d_6): δ 2.51 (broad s, 4H), 3.07 (broad s, 4H), 3.18 (s, 2H), 6.48 (d, $J=9.6$ Hz, 1H), 7.35 (d, $J=8.8$ Hz, 1H), 7.68 (dd, $J=2.4$ Hz, 8.8 Hz, 1H), 8.01-8.06 (m, 4H), 8.48 (d, $J=8.8$ Hz, 2H), 9.87 (s, 1H); ^{13}C-NMR (100 MHz, DMSO-d_6): δ ppm 45.54, 51.43, 60.72, 116.35, 116.39, 118.36, 118.43, 123.93, 124.62, 129.04, 134.74, 140.79, 144.14, 149.40, 150.00, 159.84, 168.03; Anal. calc. for C$_{21}$H$_{20}$N$_4$O$_7$S C,53.38; H,4.27; N,11.86; found: C,53.40; H,4.25; N,11.89; ESI-MS: 473.3 [M + H]$^+$.

2-(4-(2-Methoxyphenyl)piperazin-1-yl)-N-(2-oxo-2H-chromen-6-yl)acetamide (12a).

White Solid; Yield: 88%; M.P: 234-236 °C; IR (KBr) 3539, 3213, 3077, 2988, 2821,

1719, 1622, 1574, 1499, 1441, 1379, 1340, 1302, 1242, 1214, 1185, 1133, 1105, 1061, 1023, 921, 881, 821, 751 cm^{-1}; ^{1}H-NMR (400 MHz, CDCl$_3$): δ 2.87 (t, J = 4.6 Hz, 4H), 3.19 (broad s, 4H), 3.27 (s, 2H), 3.90 (s, 3H), 6.47 (d, J = 9.6 Hz, 1H), 6.91 (d, J = 8.0 Hz, 1H), 6.97-7.00 (m, 2H), 7.05-7.09 (m, 1H), 7.32 (d, J = 8.8 Hz, 1H), 7.50 (dd, J = 2.4 Hz & 8.8 Hz, 1H), 7.73 (d, 9.6 Hz, 1H), 8.09 (d, J = 2.4 Hz, 1H), 9.37 (s, 1H); δ NMR (100 MHz, CDCl$_3$): δ ppm 50.85, 53.83, 55.46, 61.95, 111.44, 117.26, 117.28, 117.90, 118.23, 119.08, 121.04, 123.20, 123.37, 134.16, 140.79, 143.35, 150.43, 152.30, 160.68, 168.68; Anal. calc. for C$_{22}$H$_{23}$N$_3$O$_4$ C,67.16; H,5.89; N,10.68; found: C,67.19; H,5.85; N,10.65; ESI-MS: 394.4 [M + H]$^+$.

2-(4-(3-fluorophenyl)piperazin-1-yl)-N-(2-oxo-2H-chromen-6-yl)acetamide (12b).

White Solid; Yield: 88%; M.P: 244-247 °C; IR (KBr) 3527, 3215, 3085, 2828, 1720, 1618, 1572, 1530, 1499, 1445, 1381, 1341, 1300, 1215, 1137, 1103, 1018, 927, 879, 818, 756 cm^{-1}; ^{1}H-NMR (400 MHz, CDCl$_3$): δ 2.86 (t, J = 4.8 Hz, 4H), 3.22 (s, 4H), 3.28 (s, 2H), 6.47 (d, J = 9.6 Hz, 1H), 6.98-7.13 (m, 4H), 7.32 (d, J = 8.8 Hz, 1H), 7.50 (dd, J = 2.4 Hz, 8.8 Hz, 1H), 7.73 (d, J = 9.6 Hz, 1H), 8.09 (d, J = 2.4 Hz, 1H), 9.32 (s, 1H); ^{13}C-NMR (100 MHz, CDCl$_3$): δ ppm 45.86, 52.65, 61.60, 117.21, 117.30, 118.21, 119.03, 123.32, 128.23, 129.21, 129.26, 132.37, 132.59, 133.74, 134.85, 143.23, 150.51, 160.52,167.64 Anal. calc. for C$_{21}$H$_{20}$FN$_3$O$_3$; C,66.13; H,5.29; N,11.02; found: C,66.15; H,5.32; N,11.04; ESI-MS: 382.3 [M + H]$^+$.

2-(4-(3-Chlorophenyl)piperazin-1-yl)-N-(2-oxo-2H-chromen-6-yl)acetamide (12c).

White Solid; Yield: 88%; M.P: 250-252 °C; IR (KBr) 3288, 3074, 2942, 2830, 1724, 1679, 1595, 1574, 1539, 1488, 1437, 1381, 1335, 1307, 1283, 1247, 1223, 1171, 1143, 1104, 1013, 986, 949, 918, 829, 764, 680 cm^{-1}; ^{1}H-NMR (400 MHz, CDCl$_3$):): δ 2.82 (t, J = 4.8 Hz, 4H), 3.26 (s, 2H), 3.29 (t, J = 4.8 Hz, 4H), 6.45 (d, J = 9.6 Hz, 1H), 6.83 (dd, J = 2.4 Hz, 8.0 Hz, 1H), 6.86 (d, J = 8.0 Hz, 1H), 6.90 (d, J = 1.6 Hz, 1H), 7.20 (t, J = 8.0 Hz, 1H), 7.29 (d, J = 9.6 Hz, 1H), 7.50 (dd, J = 8.8 Hz, 2.4 Hz, 1H), 7.71 (d, J = 9.6 Hz, 1H), 8.06 (d, J = 2.4 Hz, 1H), 9.26 (s, 1H); ^{13}C-NMR (100 MHz, CDCl$_3$): δ ppm 48.99, 53.37, 61.85, 114.19, 116.00, 117.29, 117.93, 119.08, 119.87, 123.18, 130.16, 134.05, 135.02, 143.29, 150.46, 151.96, 160.61, 168.26; Anal. calc. for C$_{21}$H$_{20}$ClN$_3$O$_3$ C,63.40; H,5.07; N,10.56; found C,63.43; H,5.10; N,10.58; ESI-MS: 398.3 [M + H]$^+$.

2-(4-(2-Cyanophenyl)piperazin-1-yl)-N-(2-oxo-2H-chromen-6-yl)acetamide (12d).

White Solid; Yield: 88%; M.P: 284-286 °C; IR (KBr) 3256, 2939, 2889, 2829, 2217, 1728, 1684,1575, 1527, 1490, 1442, 1378, 1341, 1288, 1233, 1175, 1137, 1102, 1014, 929, 885, 820, 763 cm^{-1}; ^{1}H-NMR (400 MHz, CDCl$_3$): δ 2.90 (t, J = 4.4 Hz, 4H), 3.30 (s, 2H), 3.34 (t, J = 4.4 Hz, 4H), 6.47 (d, J = 9.6 Hz, 1H), 7.06-7.11 (m, 2H), 7.31 (d, J = 8.8 Hz, 1H), 7.48 (dd, J = 2.4 Hz & 8.8 Hz, 1H), 7.52-7.56 (m, 1H), 7.61 (dd, J = 1.2 Hz & 8.8 Hz, 1H), 7.73 (d, J = 9.6 Hz, 1H), 8.10 (d, J = 2.4 Hz, 1H), 9.27 (s, 1H); ^{13}C-NMR (100 MHz, CDCl$_3$): δ ppm 51.65, 53.55, 61.76, 106.29, 117.25, 118.00, 118.25, 118.83, 119.07, 122.34, 123.22, 133.90, 134.09, 134.41, 143.34, 150.44, 155.18, 160.62, 168.33 Anal. calc. for C$_{22}$H$_{20}$N$_4$O$_3$; C,68.03; H,5.19; N,14.42; found: C,68.05; H,5.21; N,14.45 ESI-MS: 389.3 [M + H]$^+$.

2,2'-(Piperazine-1,4-diyl)bis(N-(2-oxo-2H-chromen-6-yl)acetamide) (14).

White Solid; Yield: 88%; M.P: 216-218 °C; IR (KBr) 3276, 3064, 2945, 2883, 2829, 1717, 1572, 1525,

1492, 1431, 1379, 1330, 1278, 1178, 1129, 1014, 920, 878, 824, 748, 641 cm^{-1}; ^{1}H-NMR (400 MHz, CDCl$_3$): δ 2.50 (broad s, 4H), 3.20 (s, 4H), 3.39 (s, 2H), 6.50 (d, $J = 9.6$ Hz, 1H), 7.38 (d, $J = 8.8$ Hz, 1H), 7.76 (dd, $J = 2.0$ Hz & 8.8 Hz, 1H), 8.07-8.09 (m, 2H), 9.97 (s, 1H); ^{13}C-NMR (100 MHz, CDCl$_3$): δ ppm 52.48, 61.61, 116.42, 118.09, 118.50, 123.66, 134.90, 144.17, 149.37, 159.86, 168. 34 Anal. calc. for C$_{26}$H$_{24}$N$_4$O$_6$; C,63.93; H,4.95; N,11.47; found: C,63.95; H,4.93; N,11.51; ESI-MS: 489.4 [M + H]$^+$.

Biological activity screening

MTT assay

The half-minimum inhibitory concentration (IC$_{50}$) was determined utilizing the MTT (3-(4,5-dimethylthiazol-2-yl)-2,5-diphenyltetrazolium bromide) assay as per the established protocol. Initially, cells were seeded onto a 96-well plate at a density of 1×104 cells per well and were allowed to incubate overnight in DMEM medium supplemented with 10% FBS. Subsequently, various concentrations of each chemical (0.5, 1, 10, 25, 50, 75, and 100 M) were added to the cells, followed by a further 48-hour incubation period.

Afterward, the plate underwent an additional 4-hour incubation with the addition of 20 μl of MTT solution (5 mg/mL in PBS). Following the removal of the supernatant solution, 100 μl of acidified isopropanol was employed to dissolve the resulting blue formazan crystals. The absorbance at 570 nm was then measured using a microplate reader (Metertech 960). The cell viability results are expressed as percentages relative to the control group, which is set at 100%. For the determination of IC$_{50}$ values, Graph Pad Prism software was utilized. The formula used to calculate cell viability (%) is as follows: Cell viability (%) = (average absorbance of treated groups/average absorbance of control group) × 100%.

The IC$_{50}$ values were subsequently calculated using Graph Pad Prism, allowing for a comprehensive analysis of the inhibitory concentration of the chemicals. Each experiment was performed in triplicate.

Ethidium bromide/acridine orange staining assay

The Ethidium bromide/acridine orange staining technique was employed to observe cellular changes associated with apoptosis and necrosis. Cells were exposed to IC$_{50}$ concentrations of compound **12c** for 48 hours, alongside a positive control, Triton-X 100. Post-treatment, cells were stained with a mixture of EtBr and AO solution (100 g/ml) in a 1:1 ratio, maintaining a consistent cell-to-stain ratio of 1:2. Subsequently, 10 μl of the cell suspension was applied onto a small slide for examination using a Leica DM 2500 fluorescent microscope equipped with a Leica EZ camera.

DCFH-DA assay

The DCFH-DA assay was employed to assess the levels of intracellular Reactive Oxygen Species (ROS) after the treatment of both A549 and MCF-7 cell lines with compound **12c**. For ROS quantification via Fluorimetry, cells were cultured in 6-well plates at a density of 5×105 cells/well and allowed to adhere overnight. Upon reaching adequate confluence, the cells were exposed to the IC$_{50}$ concentration of compound **12c**, followed by an incubation period of 48 hours. Subsequently, the procedure

was executed following the prescribed protocol for ROS quantification as previously outlined.[38,42]

Computational method

The calculations for the investigated derivative were conducted using Gaussian 09 software on a Pentium IV machine. The chosen method for these calculations was the DFT/B3LYP method with a 6–31 G (d,p) basis set. Geometrical optimization of the molecule was performed without imposing any molecular symmetry constraints to attain the lowest energy geometrical structure. Optimized structure of compound was deemed stable, indicating the absence of imaginary frequency. Visualization of optimized geometries was facilitated using Gauss View. Additionally, frequency calculations employing the same basis set and level of theory were carried out for the optimized structure to compute various parameters. Throughout the optimization processes, structure was confirmed as stationary points based on the frequency calculations, although none were validated through vibrational analyses.

Molecular docking

Protein model, 2D and 3D structure and prediction of active site

The docking score in molecular studies serves as a crucial indicator, offering valuable insights into the potential strength and affinity of binding interactions between a ligand and its target protein. It aids in predicting and comprehending the probability of successful binding within a biological context. Typically, a lower docking score signifies a more favorable and stronger binding interaction, with a more negative score indicating increased stability in binding. In this study, Auto Dock Tools 4.2.2 was utilized to predict the binding energies of the bioactive compound **12c** with the selected apoptosis proteins p53 and caspase 3.[42,43] The protein structures of p53 (PDB ID: 3DCY) were obtained from the Research Collaborator for Structural Bioinformatics Protein Data Bank (PDB) database. Subsequently, the protein data was formatted in PDB files after eliminating water, hetatm, and ligand molecules using BIOVIA Discovery Studio 2021.[47] Furthermore, BIOVIA Discovery Studio 2021 was employed to predict the protein structure and identify active sites crucial for docking studies. From an array of synthesized compounds, compound **12c** bioactive compound was selected which possesses good anti-cancer properties based on literature.[37,38]

In-silico-based ADME and toxicity study

The assessment of the compound for drug-likeness was carried out using Lipinski's rule of five or criteria of four, as stipulated by reference utilizing the SwissADME webserver tool. Structure of compound **12c** converted into canonical SMILES format and input into the SwissADME prediction tool (http://www.swissadme.ch) for drug-likeness evaluation. Furthermore, the toxicity prediction of compound **12c** was done using ProTox-II18, employing its chemical structure. ProTox-II was utilized to predict various toxicity endpoints, including oral toxicity, organ toxicity, hepatotoxicity, cytotoxicity, carcinogenicity, mutagenicity, and immunotoxicity.[44] The toxicity classes assigned to the compounds are based on their LD_{50} (mg/kg), categorized according to the globally harmonized system of classification in labeling of chemicals (GHS).

Acknowledgements

Disclosure statement

No potential conflict of interest was reported by the author(s).

References

[1] Cancer fact sheet, World Health Organisation. **2022** Feb 2022.
[2] WHO. *Global Breast Cancer Initiative Implementation Framework: Assessing, Strengthening and Scaling up of Services for the Early Detection and Management of Breast Cancer*, **2023**. WHO, Geneva.
[3] Arruebo, M.; Vilaboa, N.; Sáez-Gutierrez, B.; Lambea, J.; Tres, A.; Valladares, M.; González-Fernández, Á. Assessment of the Evolution of Cancer Treatment Therapies. *Cancers. (Basel)* **2011**, *3*, 3279–3330. DOI: 10.3390/cancers3033279.
[4] Zugazagoitia, J.; Guedes, C.; Ponce, S.; Ferrer, I.; Molina-Pinelo, S.; Paz-Ares, L. Current Challenges in Cancer Treatment. *Clin. Ther.* **2016**, *38*, 1551–1566. DOI: 10.1016/j.clinthera.2016.03.026.
[5] Waks, A. G.; Winer, E. P. Breast Cancer Treatment: A Review. *JAMA - J. Am. Med. Assoc* **2019**, *321*, 288–300. DOI: 10.1001/jama.2018.19323.
[6] Pucci, C.; Martinelli, C.; Ciofani, G. Innovative Approaches for Cancer Treatment: Current Perspectives and New Challenges. *Ecancermedicalscience* **2019**, *13*, 961. DOI: 10.3332/ecancer.2019.961.
[7] Mokgautsi, N.; Kuo, Y. C.; Tang, S. L.; Liu, F. C.; Chen, S. J.; Wu, T. H.; Huang, H. S. Anticancer Activities of 9-Chloro-6-(Piperazin-1-yl)-11Hindeno[1,2-c] Quinolin-11-One (SJ10) in GlioblastomMultiforme (GBM) Chemoradioresistant Cell Cycle-RelatedOncogenic Signatures. *Cancers* **2022**, *14*, 262. DOI: 10.3390/cancers14010262.
[8] Qadir, T.; Amin, A.; Sharma, P. K.; Jeelani, I.; Abe, H. A Review on Medicinally Important Heterocyclic Compounds. *TOMCJ.* **2022**, *16*, e187410452202280. DOI: 10.2174/18741045-v16-e2202280.
[9] Taylor, A. P.; Robinson, R. P.; Fobian, Y. M.; Blakemore, D. C.; Jones, L. H.; Fadeyi, O. Modern Advances in Heterocyclic Chemistry in Drug Discovery. *Org. Biomol. Chem.* **2016**, *14*, 6611–6637. DOI: 10.1039/c6ob00936k.
[10] Kerru, N.; Gummidi, L.; Maddila, S.; Gangu, K. K.; Jonnalagadda, S. B. A Review on Recent Advances in Nitrogen-Containing Molecules and Their Biological Applications. *Molecules* **2020**, *25*, 1909. DOI: 10.3390/molecules25081909.
[11] Fortin, S.; Bérubé, G. Advances in the Development of Hybrid Anticancer Drugs. *Expert Opin. Drug Discov.* **2013**, *8*, 1029–1047. DOI: 10.1517/17460441.2013.798296.
[12] Ceylan, S.; Bektas, H.; Bayrak, H.; Demirbas, N.; Alpay-Karaoglu, S.; Ulker, S. Syntheses and Biological Activities of New Hybrid Molecules Containing Different Heterocyclic Moieties. *Arch. Pharm.* **2013**, *346*, 743–756. DOI: 10.1002/ardp.201300161.
[13] Singh, A. K.; Kumar, A.; Singh, H.; Sonawane, P.; Paliwal, H.; Thareja, S.; Pathak, P.; Grishina, M.; Jaremko, M.; Emwas, A. H.; et al. Concept of Hybrid Drugs and Recent Advancements in Anticancer Hybrids. *Pharmaceuticals* **2022**, *15*, 1071. DOI: 10.3390/ph15091071.
[14] Decker, M. Hybrid Molecules Incorporating Natural Products: Applications in Cancer Therapy, Neurodegenerative Disorders and Beyond. *Curr. Med. Chem.* **2011**, *18*, 1464–1475. DOI: 10.2174/092986711795328355.

[15] Meunier, B. Hybrid Molecules with a Dual Mode of Action: Dream or Reality? *Acc. Chem. Res.* **2008**, *41*, 69–77. DOI: 10.1021/ar7000843.

[16] Ali, M. I.; Naseer, M. M. Recent Biological Applications of Heterocyclic Hybrids Containing s-Triazine Scaffold. *RSC Adv.* **2023**, *13*, 30462–30490. DOI: 10.1039/d3ra05953g.

[17] Zhong, Y.; Liu, J.; Cheng, X.; Zhang, H.; Zhang, C.; Xia, Z.; Wu, Z.; Zhang, L.; Zheng, Y.; Gao, Z.; et al. Design, Synthesis and Biological Evaluations of Diverse Michael Acceptor-Based Phenazine Hybrid Molecules as TrxR1 Inhibitors. *Bioorg. Chem.* **2021**, *109*, 104736. DOI: 10.1016/j.bioorg.2021.104736.

[18] Raiguru, B. P.; Panda, J.; Mohapatra, S.; Nayak, S. Recent Developments in the Synthesis of Hybrid Antimalarial Drug Discovery. *Bioorg. Chem.* **2023**, *139*, 106706. DOI: 10.1016/j.bioorg.2023.106706.

[19] Kaur, G.; Silakari, O. *Benzimidazole Scaffold Based Hybrid Molecules for Various Inflammatory Targets: Synthesis and Evaluation* **2018**, *80*, 24–35. DOI: 10.1016/j.bioorg.2018.05.014.

[20] Wei, H.; Ruan, J.; Zhang, X. Coumarin-Chalcone Hybrids: Promising Agents with Diverse Pharmacological Properties. *RSC Adv.* **2016**, *6*, 10846–10860. DOI: 10.1039/C5RA26294A.

[21] Sandhu, S.; Bansal, Y.; Silakari, O.; Bansal, G. Coumarin Hybrids as Novel Therapeutic Agents. *Bioorg. Med. Chem.* **2014**, *22*, 3806–3814. DOI: 10.1016/j.bmc.2014.05.032.

[22] Salehian, F.; Nadri, H.; Jalili-Baleh, L.; Youseftabar-Miri, L.; Abbas Bukhari, S. N.; Foroumadi, A.; Tüylü Küçükkilinç, T.; Sharifzadeh, M.; Khoobi, M. A Review: Biologically Active 3,4-Heterocycle-Fused Coumarins. *Eur. J. Med. Chem.* **2021**, *212*, 113034. DOI: 10.1016/j.ejmech.2020.113034.

[23] Yildirim, M.; Poyraz, S.; Ersatir, M. Recent Advances on Biologically Active Coumarin-Based Hybrid Compounds. *Med. Chem. Res.* **2023**, *32*, 617–642. DOI: 10.1007/s00044-023-03025-x.

[24] Zeng, C.; Avula, S. R.; Meng, J.; Zhou, C. Synthesis and Biological Evaluation of Piperazine Hybridized Coumarin Indolylcyanoenones with Antibacterial Potential. *Molecules* **2023**, *28*, 2511. DOI: 10.3390/molecules28062511.

[25] Husain, A.; Balushi, A.; Akhtar, M. J.; Khan, S. A. Coumarin Linked Heterocyclic Hybrids: A Promising Approach to Develop Multi Target Drugs for Alzheimer's Disease. *J. Mol. Struct.* **2021**, *1241*, 130618. DOI: 10.1016/j.molstruc.2021.130618.

[26] Jadala, C.; Sathish, M.; Anchi, P.; Tokala, R.; Lakshmi, U. J.; Reddy, V. G.; Shankaraiah, N.; Godugu, C.; Kamal, A. Synthesis of Combretastatin-A4 Carboxamidest That Mimic Sulfonyl Piperazines by a Molecular Hybridization Approach: In Vitro Cytotoxicity Evaluation and Inhibition of Tubulin Polymerization. *ChemMedChem* **2019**, *14*, 2052–2060. DOI: 10.1002/cmdc.201900541.

[27] Kamal, A.; Sreekanth, K.; Shankaraiah, N.; Sathish, M.; Nekkanti, S.; Srinivasulu, V. Dithiocarbamate/Piperazine Bridged Pyrrolobenzodiazepines as DNA-Minor Groove Binders: Synthesis, DNA-Binding Affinity and Cytotoxic Activity. *Bioorg. Chem.* **2015**, *59*, 23–30. DOI: 10.1016/j.bioorg.2015.01.002.

[28] Sana, S.; Reddy, V. G.; Srinivasa Reddy, T.; Tokala, R.; Kumar, R.; Bhargava, S. K.; Shankaraiah, N. Cinnamide Derived Pyrimidine-Benzimidazole Hybrids as Tubulin Inhibitors: Synthesis, in Silico and Cell Growth Inhibition Studies. *Bioorg. Chem.* **2021**, *110*, 104765. DOI: 10.1016/j.bioorg.2021.104765.

[29] Mahmoud, W. R.; Nissan, Y. M.; Elsawah, M. M.; Refaey, R. H.; Ragab, M. F.; Amin, K. M. Neurobehavioral Investigation and Acetylcholinesterase Inhibitory Activity Study for Some New Coumarin Derivatives. *Eur. J. Med. Chem.* **2019**, *182*, 111651. DOI: 10.1016/j.ejmech.2019.111651.

[30] Zhang, J.; Jiang, C. S. Synthesis and Evaluation of Coumarin/Piperazine Hybrids as Acetylcholinesterase Inhibitors. *Med. Chem. Res.* **2018**, *27*, 1717–1727. DOI: 10.1007/s00044-018-2185-x.

[31] Koparde, S.; Hosamani, K. M.; Kulkarni, V.; Joshi, S. D. Synthesis of Coumarin-Piperazine Derivatives as Potent anti-Microbial and anti-Inflammatory Agents, and Molecular Docking Studies. *Chem. Data Collect.* **2018**, *15-16*, 197–206. DOI: 10.1016/j.cdc.2018.06.001.

[32] Sethi, A.; Munagalasetty, S.; Arifuddin, M.; Carradori, S.; Supuran, C. T.; Alvala, R.; Alvala, M. Coumarin and Piperazine Conjugates as Selective Inhibitors of the Tumor-Associated

Carbonic Anhydrase IX and XII Isoforms. *Anticancer. Agents Med. Chem.* **2023**, *23*, 1184–1191. DOI: 10.2174/1871520623666230202123535.

[33] Patel, K. B.; Mukherjee, S.; Bhatt, H.; Rajani, D.; Ahmad, I.; Patel, H.; Kumari, P. Synthesis, Docking, and Biological Investigations of New Coumarin-Piperazine Hybrids as Potential Antibacterial and Anticancer Agents. *J. Mol. Struct.* **2023**, *1276*, 134755. DOI: 10.1016/j.molstruc.2022.134755.

[34] Soni, R.; Soman, S. S. Design and Synthesis of Aminocoumarin Derivatives as DPP-IV Inhibitors and Anticancer Agents. *Bioorg. Chem.* **2018**, *79*, 277–284. DOI: 10.1016/j.bioorg.2018.05.008.

[35] Patil, J. V.; Umar, S.; Soni, R.; Soman, S. S.; Balakrishnan, S. Design, Synthesis and Anticancer Activity of Amide Derivatives of Substituted 3-Methyl-Benzofuran-2-Carboxylic Acid. *Synth. Commun.* **2023**, *53*, 217–233. DOI: 10.1080/00397911.2022.2160648.

[36] Durgapal, S. D.; Soni, R.; Umar, S.; Suresh, B.; Soman, S. S. Anticancer Activity and DNA Binding Studies of Novel 3,7-Disubstituted Benzopyrones. *ChemistrySelect* **2017**, *2*, 147–153. DOI: 10.1002/slct.201601361.

[37] Liu, K.; Liu, P. c.; Liu, R.; Wu, X. Dual AO/EB Staining to Detect Apoptosis in Osteosarcoma Cells Compared with Flow Cytometry. *Med. Sci. Monit. Basic Res.* **2015**, *21*, 15–20. DOI: 10.12659/MSMBR.893327.

[38] Umar, S.; Soni, R.; Durgapal, S. D.; Soman, S.; Balakrishnan, S. Synthetic Coumarin Derivative (4-Flourophenylacetamide-Acetyl Coumarin) Impedes Cell Cycle at G0/G1 Stage, Induces Apoptosis, and Inhibits Metastasis via ROS-Mediated P53 and AKT Signaling Pathways in A549 Cells. *J. Biochem. Mol. Toxicol.* **2020**, *34*, e22553. DOI: 10.1002/jbt.22553.

[39] Agwupuye, J. A.; Gber, T. E.; Edet, H. O.; Zeeshan, M.; Batool, S.; Duke, O. E.; Adah, P. O.; Odey, J. O.; Egbung, G. E. Molecular Modeling, DFT Studies and Biological Evaluation of Methyl 2,8-Dichloro-1,2-Dihydroquinoline-3-Carboxylate. *Chem. Phys. Impact* **2023**, *6*, 100146. DOI: 10.1016/j.chphi.2022.100146.

[40] Dhaduk, M. P.; Dabhi, R. A.; Bhatt, B. S.; Bhatt, V. D.; Patel, M. N. Molecular Modeling, DFT Studies, and Biological Evaluation of Pyrazine-Based Platinum(II) Complexes. *Chem. Phys. Impact* **2023**, *7*, 100261. : DOI: 10.1016/j.chphi.2023.100261.

[41] Khanna, L.; Singhal, S.; Jain, S. C.; Khanna, P. Spiro-Indole-Coumarin Hybrids: Synthesis, ADME, DFT, NBO Studies and in Silico Screening through Molecular Docking on DNA G-Quadruplex. *ChemistrySelect* **2020**, *5*, 3420–3433. DOI: 10.1002/slct.201904783.

[42] Oren, M. Decision Making by p53: Life, Death and Cancer. *Cell Death Differ.* **2003**, *10*, 431–442. DOI: 10.1038/sj.cdd.4401183.

[43] Momand, J.; Jung, D.; Wilczynski, S.; Niland, J. The MDM2 Gene Amplification Database. *Nucleic Acids Res.* **1998**, *26*, 3453–3459. DOI: 10.1093/nar/26.15.3453.

[44] Wang, Y.; Xing, J.; Xu, Y.; Zhou, N.; Peng, J.; Xiong, Z.; Liu, X.; Luo, X.; Luo, C.; Chen, K.; et al. In Silico ADME/T Modelling for Rational Drug Design. *Q Rev. Biophys.* **2015**, *48*, 488–515. DOI: 10.1017/S0033583515000190.

[45] Drwal, M. N.; Banerjee, P.; Dunkel, M.; Wettig, M. R.; Preissner, R. ProTox: A Web Server for the in Silico Prediction of Rodent Oral Toxicity. *Nucleic Acids Res.* **2014**, *42*, W53–8. DOI: 10.1093/nar/gku401.

[46] Guha, S.; Lohar, S.; Bolte, M.; Safin, D. A.; Das, D. Crystal Structure and Interaction of 6-Amino Coumarin with Nitrite Ion for Its Selective Fluorescence Detection. *Spectrosc. Lett.* **2012**, *45*, 225–235. DOI: 10.1080/00387010.2011.605416.

[47] https://www.3dsbiovia.com/products/collaborative-science/biovia-discovery-studio/visualizationdownload.php.